University of Alberta

Thin-Film Pyrolysis of Asphaltenes and Catalytic Gasification of Bitumen Coke

by

Arash Karimi

A thesis submitted to the Faculty of Graduate Studies and Research
in partial fulfillment of the requirements for the degree of

Doctor of Philosophy
in
Chemical Engineering

Department of Chemical and Materials Engineering

©Arash Karimi

Spring 2011
Edmonton, Alberta

Permission is hereby granted to the University of Alberta Libraries to reproduce single copies of this thesis and to lend or sell such copies for private, scholarly or scientific research purposes only. Where the thesis is converted to, or otherwise made available in digital form, the University of Alberta will advise potential users of the thesis of these terms.

The author reserves all other publication and other rights in association with the copyright in the thesis and, except as herein before provided, neither the thesis nor any substantial portion thereof may be printed or otherwise reproduced in any material form whatsoever without the author's prior written permission.

Examining Committee

Dr. Murray R. Gray, Department of Chemical and Materials Engineering

Dr. Rajender Gupta, Department of Chemical and Materials Engineering

Dr. David Mitlin, Department of Chemical and Materials Engineering

Dr. Charles Lucy, Department of Chemistry

Dr Jorge Ancheyta, Mexican Institute of Petroleum (IMP)

Abstract

Thin film pyrolysis was used to thermally crack the pendant groups from asphaltene molecules. The cracked products were rapidly quenched to minimize further decomposition. The liquid products were condensed and collected, with over 91% material balance on the recovery of gas, liquid and coke product. Simulated distillation of the condensed liquid products showed a wide range of compounds with boiling points up to more than 700°C produced in various stages of the reaction. The liquid components boiling below 538°C comprised 15-20% of the initial asphaltenes, and contained a wide range of chemical structures including paraffins, olefins, naphthenes, aromatics, thiophenes and sulfides, and nitrogen-containing compounds, by mass spectrometry. The ring groups were substituted with a range of alkyl side chains. Asphaltenes from a range of different crude oils gave similar results. The recovery of the pendant groups was limited by the reaction conditions, because re-reaction of the heavy products generated more light fragments. The diverse pendant groups, with paraffins accounting for a small fraction of the total mass, are consistent with a high concentration of complex bridged structures in the asphaltene fraction.

The compounds K_2CO_3, KCl, Na_2CO_3, $CaCO_3$, CaO, and MgO were tested as catalysts for steam gasification of coke from oil sands bitumen at atmospheric pressure and 600-800°C. K_2CO_3 and Na_2CO_3 were most effective, consistent with their high mobility within the coke phase. K_2CO_3 and Na_2CO_3 reduced the activation energy of the reaction to 1.2×10^5 $J\cdot mol^{-1}$ and

1.3×10^5 J·mol^{-1}, respectively, down from 2.1×10^5 J·mol^{-1} for the uncatalyzed reaction. The reaction rates varied with the partial pressure of steam between 60 kPa and 85 kPa consistent with a Langmuir-Hinshelwood model. The initial rate of gasification increased with increasing the catalyst loading up to 2.4 (mol potassium) / kg. A portion of the catalyst penetrated into the coke, where it could not promote the reaction with steam. A successful prediction of the rates at higher conversions from the initial rate data with a shrinking core model ruled out the possibility of a shift in the reaction mechanism.

Acknowledgement

I would like to thank Dr. Murray R. Gray for his exceptional support, understanding, and mentorship throughout my PhD program. He has been much more than a supervisor for me during these years. I am very fortunate to have had such an excellent supervisor, who is a brilliant teacher, researcher, and communicator. Any success I have earned is directly linked to your extensive knowledge, patience, diligence, and encouragement. Thank you so much.

I am deeply indebted for all of the advice, assistance, and encouragement provided to me over these years by so many different people. I do not have the space to thank you all by name, but I appreciate all of your contributions. In particular, I would like to thank Tuyet Le, Dr. Kavithaa Loganathan, and Alison Salmon for their outstanding assistance at the various stages of the research. I would also wish to acknowledge the support and assistance I received from Dr. Natalia Semagina, especially during the catalytic gasification kinetic study. I thank our wonderful collaborators at ExxonMobil Research and Engineering, Dr. Howard Freund, Dr. Kuangnan Qian, Dr. William Olmstead, and Cathleen Yung who worked attentively in parallel on the analysis of the samples and the data of the asphaltenes pyrolysis study.

The financial support from the Center for Oil Sands Innovation at the University of Alberta, the NSERC-Imperial Oil Chair in Oil Sands Upgrading, and the ExxonMobil Research and Engineering Corp. is gratefully acknowledged.

During my time in Edmonton I was surrounded by such great friends and colleagues whom I will certainly miss. Thank you all for being there for me!

My family's love and support has been invaluable, and I couldn't have done this without them. Thank you so much mom, dad, sisters and brother; you are the greatest! I especially need to acknowledge my amazing wife Forough, who was not only a constant source of love and moral support, but also made every moment of my life enjoyable with her generosity of spirit, cheerfulness, and patience.

Table of Contents

List of Tables

List of Figures

List of Symbols

A	Original hydrocarbon molecule undergoing thermal cracking
$A^{\bullet}$	Free radical formed by hydrogen abstraction from molecule A
A	Total area of the particles at any conversion (m^2)
A_0	Initial total area of the particles in the sample (m^2)
B	Olefin molecule formed as a result of the β-scission of a radical
B'	Rearranged olefin molecule from the isomerization of molecule B
d	Average diameter of the particles at any conversion (m)
d_0	Initial average diameter of the particles (m)
k_1	Specific rate constant of the reaction ($Pa^{-1} \cdot s^{-1}$)
K_2	Specific rate constants of water adsorption on carbon matrix (Pa^{-1})
m	Total mass of the particles at any conversion (mg)
m_0	Initial total mass of the particles (mg)
p_{H_2O}	Partial pressure of steam (Pa)
r	Specific gasification rate (min^{-1})
r_a	Absolute gasification rate (mg min^{-1}), $r_a = r\ m$

r_0	Initial specific gasification rate (min^{-1})
$R^{\bullet}$, $R_1^{\bullet}$, $R_2^{\bullet}$	Free radical
V	Total volume of the particles at any conversion (m^3)
V_0	Initial total volume of the particles (m^3)
w	Catalyst surface loading at any conversion, (mol cation·m^{-2})
w'	Catalyst surface loading at any conversion corrected for penetration, (mol cation·m^{-2})
w_0	Initial catalyst surface loading, (mol cation·m^{-2})
w'_0	Initial catalyst surface loading corrected for penetration, (mol cation·m^{-2})
w_{p0}	Initial catalyst surface loading lost due to penetration into coke, (mol cation·m^{-2})
X	Conversion of coke
y	Correction factor for the change in the surface area at any conversion
δ	Hildebrand solubility parameter ($MPa^{-0.5}$)
ρ	Density of coke (kg·m^{-3})

1 Introduction

This chapter contains an overall introduction to the thesis and literature review. The objectives and motivations of the research, as well as the outline of the thesis will be explained.

1.1 Molecular structure of asphaltenes

Fouling in petroleum crude and products pipelines and process equipment is a major problem in this industry. Among other causes, coke formation and precipitation of asphaltenes are of notable significance. Petroleum coke, defined as an organic solid residue insoluble in solvents as strong as toluene and benzene, generally forms as a result of thermal reactions of heavy petroleum fraction that cause these molecules to join together by addition and polymerization to form a highly condensed structure.

The fraction of petroleum molecules defined as asphaltenes have the highest propensity to contribute to coke formation upon exposure to high temperatures. Coke formation tendency is measured by different standard methods. The Conradson carbon residue measurement was first proposed by Conradson (1). An improved version of the method was later introduced as the standard test method ASTM D189. Carbon residue measurement – micro method according to ASTM D4530, also known as micro carbon residue (MCR), is currently the most widely employed standardized technique. Ramsbottom carbon

residue is also another standardized method (ASTM D524). While the MCR content of Canadian bitumens is in the range of 10-15%, asphaltenes from these sources have MCR contents of circa 50%.

On the other hand, as noted above, asphaltenes also tend to precipitate out of petroleum mixtures. In fact, asphaltenes are defined based on their solubility behavior. The precipitation tendency of these molecules is attributed to their size and chemical structure. Asphaltenes are often referred to as petroleum macromolecules, in reference to their dimensions. They are also known to form aggregates (2). The high viscosity of heavy oils is partly due to the asphaltene content (3). Deasphalting, therefore, is a common process to reduce the viscosity of the oils for transportation through pipelines.

Due to the complicated properties of these molecules, many aspects of their nature have been subject to much debate for the past several decades. A better understanding of asphaltenes is still needed in order to address the problems they cause in the petroleum industry.

1.1.1 Definition of asphaltenes

Asphaltenes are defined based on their solubility as the petroleum fraction that is soluble in toluene but precipitates in *n*-alkanes (4). The most widely used solvent for the precipitation of asphaltenes is *n*-heptane (nC_7). Propane and *n*-pentane (nC_5) are also common, especially for industrial scale applications. The solvents with lower solubility parameters will cause more asphaltenes to precipitate, i.e. propane (δ = 13.1 $MPa^{0.5}$) (5) can separate more asphaltenes than

n-pentane (δ = 14.4 $MPa^{0.5}$) and n-pentane precipitates more than *n*-heptane (δ = 15.3 $MPa^{0.5}$).

Precipitation of asphaltenes from the solution is time dependent. The solvent to oil ratio is the other factor that affects the amount of asphaltenes precipitation. Alboudwarej et al. (6) observed little change in the amount of precipitation from Athabasca bitumen dissolved in *n*-heptane after 24h and with solvent to bitumen ratios in excess of 30 cm^3/g at room temperature. At higher temperatures the asphaltenes will tend to remain in the solution and the amount of precipitation will be lower. Standard methods ASTM D3279 (*n*-heptane) and D4055 (*n*-pentane) recommend a solvent to oil ratio of 100 to be used. Agitation in an ultrasound bath will help to flocculate the asphaltenes in shorter times (6).

The identification of asphaltenes as a solubility class rather than by their chemical characteristics has caused ambiguity and uncertainty around their molecular structure. Their tendency to form aggregates exacerbates the situation by making analyses difficult. Their average molecular weight, for example, obtained by different methods including laser desorption mass spectroscopy (LDMS), field ionization mass spectroscopy (FIMS), vapor pressure osmometry (VPO), and size exclusion chromatography varies over a range of 1 to 2 orders of magnitude from 400 to 10,000 Da (7). The highest molecular weights in this range are believed to belong to asphaltene aggregates rather than individual molecules. On the other hand, the molecular weights at the lower end of this range may have been from fragmented molecules (8) or the heavier molecules being left out of the measurement. There are also other controversies around asphaltenes,

especially in regards to structural issues such as the number of aromatic and saturated ring systems per asphaltene molecule and the number of rings in each cluster. We will review these in the subsequent sections.

1.1.2 Self-association of asphaltenes

As mentioned before, an important property of asphaltenes is their self-association to form aggregates. Asphaltenes not only form aggregates in the liquid phase and solutions, their association in gas phase has also been reported (9). The latter observation causes problems for some mass spectrometry techniques in identification of these molecules.

Asphaltene aggregate sizes have been shown to reduce as the temperature is raised (8, 10). There is no consensus, however, on the size of aggregates and their formation mechanisms. Early studies by Pfeiffer and Saal (11) suggested that the asphaltenes are peptized as micelles in the oil by resins to form colloid particles (Figure 1-1). More recently, Yarranton and coworkers observed an increase in the degree of association of asphaltenes, as the resinous material was removed (6).

Yen and coworkers proposed that individual asphaltene molecules aggregated by forming stacks of the large aromatic sheets in their structure (12). They later proposed that these particles consisting of asphaltene aggregates could flocculate to form large micelles 100-300 Å in diameter (13). In this model, resins were considered to be similar to asphaltenes in structure with different aromaticities. Therefore, they could aggregate separately into particles, rather than surrounding the asphaltene molecules. However, Agrawala and Yarranton (14)

hypothesized that, unlike asphaltenes, resins cannot self-associate due to the lack of multiple active sites. They further stated that they act as termintors in the association of asphaltenes by linking to their active sites.

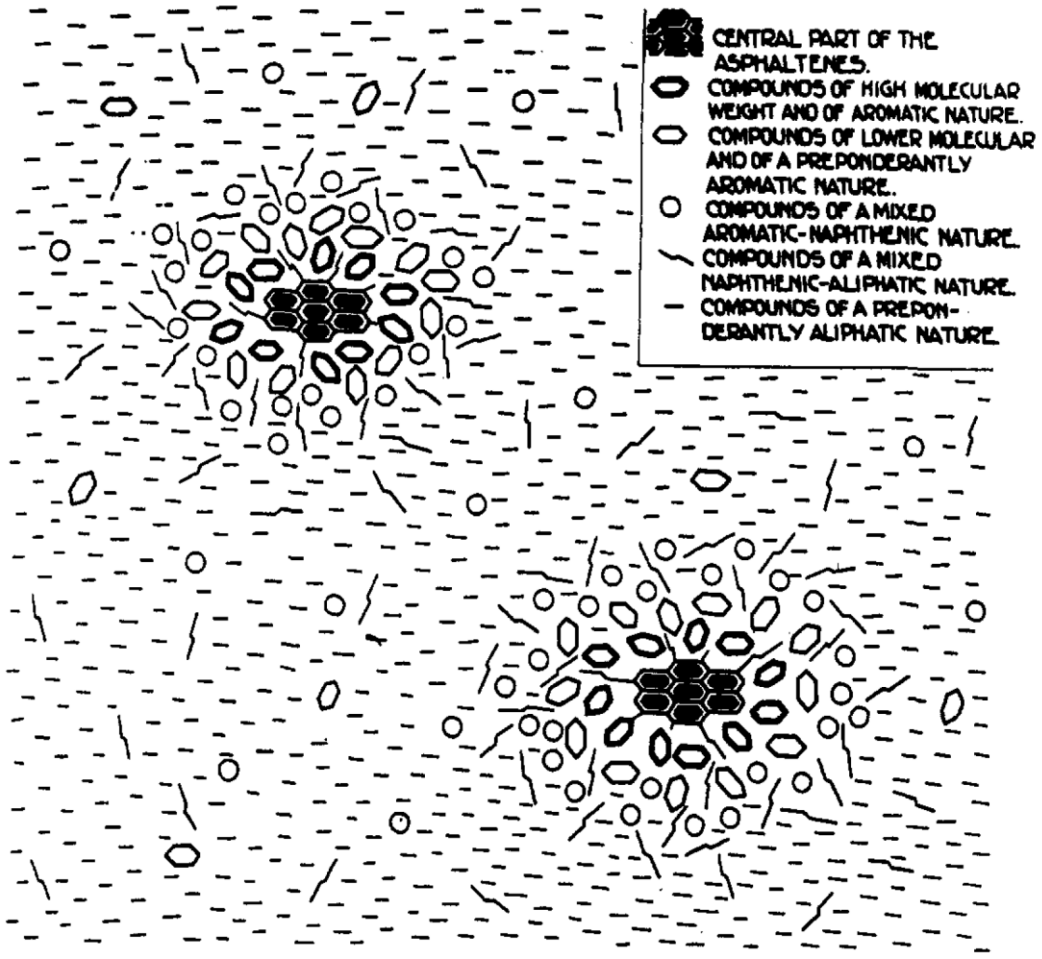

Figure 1-1. The original drawing by Pfeiffer and Saal (11) suggesting the dispersion of asphaltenes in the oils by the aid of resins.

The Yen model also portrays metal-bearing and porphyrin groups associated with the aromatic sheet stack of asphaltenes in the aggregate, suggesting them as an aid for the micelle formation. However, Gray and coworkers did not observe any interaction between porphyrins and multiring aromatic compounds using UV-vis and fluorescence spectroscopy (15).

In addition to π-π stacking interactions, other forces and mechanisms have been suggested to participate in the aggregation of asphaltenes. Moschopedis and Speight (16) suggested that the oxygen groups in asphaltenes can facilitate the interaction of these molecules with the resins. Gray and coworkers detected an enhancement in the self-association of asphaltene model compounds by water unsing ^{1}H-NMR spectroscopy (17). They did not use oxygenated model compounds. Rather, the compounds used in this study contained nitrogen groups that acted as hydrogen bonding sites. Rogel (18) using molecular mechanics and dynamics calculations suggested that the interaction between asphaltenes and resins was mainly due to van der Waals forces. Acid-base interactions has been proposed as another mechanism taking part in the aggregation of asphaltenes (19).

The mechanism of aggregate formation is the subject of several on-going researches. A better understanding of the chemical structure of asphaltenes is a crucial for the elucidation of their complex aggregation behavior.

1.1.3 Structure of asphaltenes

Asphaltenes are commonly identified as heavy molecules (hence the term macromolecules) with high aromaticity. They typically have aromaticities in excess of 40% (See Chapter 2). Therefore, the earliest proposed structural models pictured asphaltenes as large pericondensed sheets of aromatic and saturated rings substituted with a few alkyl side chains to account for the saturated portion (Figure 1-2).

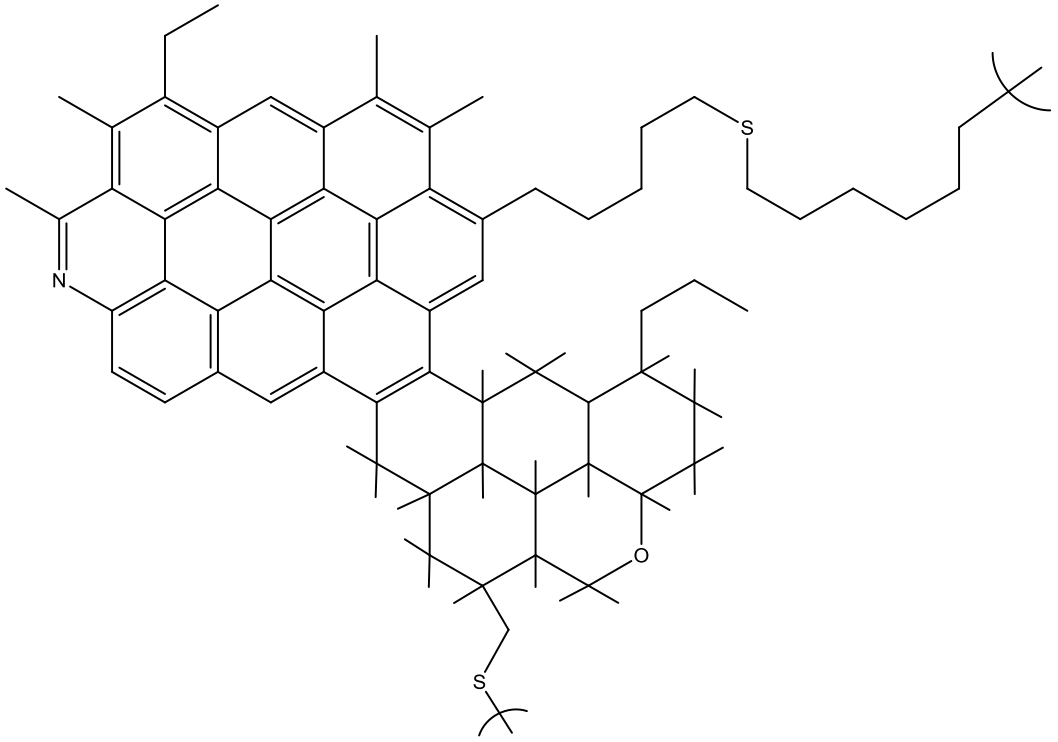

Figure 1-2. Representation of an asphaltene molecule adapted from Yen (20).

This kind of unrealistic chicken-wire models for asphaltenes are no longer supported widely (10). The number of rings per cluster is, however, still a matter of debate. Earlier studies by Speight using ^{1}H-NMR, electron spin resonance (ESR) and X-ray diffraction showed a maximum of 16 rings per fused aromatic ring cluster in asphaltenes (10). More recently, he reported that clusters with more than ten rings are unlikely to exist in asphaltenes (21). Such smaller ring systems appear to be more widely accepted (7). However, there is less agreement on the minimum number of aromatic or saturated rings per cluster. Many studies showed that single rings exist in the structure of asphaltenes attached to the molecule by alkyl or thioether chains (22, 23, 24). The separation of small ring groups from asphaltenes by thermolysis prompted some researchers to suggest alternative

structures for asphaltenes consisting of a multitude of these smaller aromatic and saturated rings (23, 25).

The proponents of the Yen model still believe in structures consisting solely of a single large sheet of polycondensed aromatic and saturated rings substituted with alkyl chains (although with a more limited number of rings than the original model), also known as *the island model*. The more recent model which includes smaller ring groups, commonly referred to as *the archipelago model*, is typically illustrated with one or more large ring groups. This is to account for the portion of the molecules that end up as a solid residue (coke) in the thermal reactions that have been used for the identification of the building blocks of asphaltene molecules.

Coke is generally believed to form as a result of oligomerization and aromatization during thermal cracking reactions. In an attempt to describe the thermal cracking behavior of petroleum residua, a structural model dubbed *the pendant-core model* was proposed by Wiehe (24). Wiehe's pendant-core model has been successfully used to predict the coking kinetics of asphaltenes (26 and 27). Wiehe (28) suggests that the coke starts to form when asphaltene "cores" crack off and form a separate phase once their concentration exceeds a certain limit. They then recombine into coke. While a solid definition has not been provided, the term "core" has been loosely used to describe the non-volatile portions of heavy hydrocarbons such as asphaltenes that will remain in the liquid phase during the thermal cracking reactions until eventually form the coke. In

contrast, portions of these molecules that will readily separate as volatile fragments upon thermal cracking have been termed "pendants" (24).

While the definitions mentioned above do not include sizes, cores are commonly considered as heavy polycondensed aromatic groups whereas pendants are apparently meant to be small groups consisting of few rings. However, Wiehe maintains that even a single ring group – that would normally be considered a pendant group – may end up in coke if bound by multiple bonds, and hence lies under the definition of cores (24). Therefore, the size of asphaltene "cores", i.e. fragments that form the coke during thermal cracking, is in fact unknown and the existence of large pericondensed groups (5+ rings) as a part of the asphaltene molecules in significant quantities is yet to be confirmed.

1.1.4 Thermal cracking of heavy hydrocarbons

Spontaneous homolytic dissociation of the chemical bonds in hydrocarbons by thermal stimulation at elevated temperatures (Equation (1.2-4)) is believed to initiate the thermal cracking reactions by forming highly reactive free radicals (29).

$$M \rightarrow R_1^{\bullet} + R_2^{\bullet} \qquad (1.1\text{-}1)$$

Table 1-1 shows the bond dissociation energies for several hydrocarbon and heteroatom bonds. These bond energies suggest high activation energies for the homolytic dissociation of these bonds, thus the high temperatures required for thermal cracking of hydrocarbons to start.

Table 1-1. Typical bond dissociation energies (BDEs) (Adapted from McMillen and Golden (30))

Type	Chemical bond	BDE, kJ/mol
Primary C–H	C_2H_5–H	410 ± 4
Secondary C–H	*i*-C_3H_7–H	397 ± 4
Tertiary C–H	*t*-C_4H_9–H	389 ± 4
Aromatic C–H	C_6H_5–H	464 ± 8
Aliphatic C–C	CH_3–CH_3	359 ± 4
Aromatic C≡C	(C_6H_6)	508 †
α-aromatic C–C	C_6H_5–CH_3	426 ± 8
β-aromatic C–C	$C_6H_5CH_2$–CH_3	317 ± 4
Thioether C–S	CH_3S–CH_3	323 ± 8
Amine C–N	CH_3–$NHCH_3$	344 ± 10
Ether C–O	CH_3O–CH_3	348 ± 4

† Sanderson (31).

Measured apparent activation energies of thermal cracking reactions, however, are significantly lower than these values (e.g. 206 kJ mol^{-1} for *n*-heptane (32) and 217 kJ mol^{-1} for Athabasca vacuum residue (35)). The advancement of thermal cracking as a chain reaction through propagation of the free radicals is the underlying reason for the lower overall activation energy. Once the free radicals form as a result of the homolytic dissociation (chain initiation) reactions, they can attack other molecules in a series of hydrogen abstraction

(Equation (1.1-2)), radical addition (Equation (1.1-3)) and decomposition (scission) (Equation (1.1-4)), and isomerization (Equation (1.1-5)) reactions (34):

$$A + R^{\bullet} \rightarrow A^{\bullet} + RH \quad (1.1\text{-}2)$$

$$A + R^{\bullet} \rightarrow AR^{\bullet} \quad (1.1\text{-}3)$$

$$A^{\bullet} \rightarrow R^{\bullet} + B \quad (1.1\text{-}4)$$

$$B \rightarrow B' \quad (1.1\text{-}5)$$

The chain will terminate upon the recombination of two radicals:

$$R_1^{\bullet} + R_2^{\bullet} \rightarrow R_1R_2 \quad (1.1\text{-}6)$$

These reactions have much lower activation energies than the homolytic dissociation reactions, thus the activation energy of the overall thermal cracking reactions will be lower (35).

Loeff and Stein (36) studied the ring opening reactions of benzene using high energy α-rays, neutron, X-rays, and UV light irradiation. They concluded the ring opening required molecular oxygen to take place, despite the high concentration of radicals. Commercial aromatic ring opening processes are chiefly based on the hydrogenation of the aromatic rings to cycloalkanes followed by the ring opening of the cycloalkanes. Both steps are carried out catalytically, either in two separate processes or using a bifunctional catalyst. The latter method, however, requires a higher ratio of hydrogen to feed (37).

Evidence for the occurrence of aromatic ring opening by thermal cracking was reported in a study of geological evolution of petroleum compounds using prolonged reaction times (38). As Table 1-1 suggests, the C–C bonds in aromatic rings are highly stable due to the high bond dissociation energy. Therefore, under

mild thermal cracking conditions, aromatic ring opening is not favorable. Khorasheh and Gray (39) did not report any non-aromatic compounds among the major products of the thermal cracking of tetralin, as would be expected if aromatic ring opening occurred at an appreciable rate. The prevalent reaction pathways in the thermal cracking of tetralin are: contraction, dehydrogenation, and ring-opening hydrogenolysis of the saturated ring, and the loss of two carbons and cracking yielding benzocyclobutene, styrene, and alkylbenzene (29). None of these reactions include aromatic ring opening. This is consistent with other studies on the pyrolysis of aromatic compounds at relatively mild conditions, which did not find any evidence for aromatic ring opening (40, 41).

Aromatic rings even stabilize the immediate C–C bond (α-position) of a substituted alkyl group. The cleavage of such a bond requires more energy than farther bonds (Table 1-1). Larger aromatic clusters consisting of more rings make the C–C bond in an α-position even stronger (30).

The above discussion demonstrates that in the thermal cracking of asphaltenes at mild conditions, the abundantly formed product molecules containing small number of rings (i.e. 1-3 rings) per cluster (e.g. ref. 42) are not likely to have been separated from larger aromatic clusters. These products, therefore, provide an evidence for the existence of asphaltene molecules with the archipelago structure.

1.1.5 Significance of the present study on the structure of asphaltenes

Previous studies on the structure of asphaltenes by pyrolysis suffered from one or more of the following limitations:

- Lack of controlled pyrolysis conditions (i.e. short residence time) allowing for secondary reactions and excessive dehydrogenation.
- Low yield of products, thus restricting analyses.
- Lack of reliable material balance, therefore weakening the interpretations that support the archipelago structure in terms of the extent of representativeness of the products of the reaction towards the asphaltene sample.
- Use of solvents such as toluene, thus incorporating uncertainties regarding the origin of the identified product groups (especially for the small ring aromatic groups).

In contrast, the present study (Chapter 2) has avoided this limitation by performing the experiments using thin films of asphaltenes with sufficient quantities for several analyses on each sample (viz. mass spectroscopy, simulated distillation, and ^{13}C-NMR). The use of thin-films made it feasible for the products of the cracking to escape the reaction zone with minimal mass transfer limitation, therefore, restraining further cracking. For the same reason, any solvent used in the preparation of the samples was allowed to evaporate before the reaction started. Low volatility solvents such as toluene were not used in the preparation of the samples at all. The achievement of reasonable material balances was another important feature of the present study.

The employment of the state-of-the-art mass spectrometry technique developed at ExxonMobil Research and Engineering Co. allowed for reliable identification and quantification of the broad range of the products of the reaction, with minimal chances of decomposition of the product molecules in the ionization step.

Furthermore, aromatic carbon balances performed using ^{13}C-NMR spectroscopy were presented to confirm that extensive structural changes of the products due to dehydrogenation and aromatization did not occur.

1.2 Gasification

Gasification is the general term applied to the reaction of (often solid) carbonaceous compounds with a gaseous agent to produce energy or valuable gases. Various gasifying agents such as H_2, H_2O, O_2, and CO_2 may be employed for this reaction, which will result in different products. For commercial applications, however, steam gasification (equation (1.2-1)) has received the most widespread attention.

$$C + H_2O_{(g)} \rightarrow CO_{(g)} + H_{2(g)} \qquad (1.2\text{-}1)$$

The products of this reaction can be used for a variety of applications such as the production of Fischer-Tropsch liquids, synthetic fuels such as dimethyl ether (via methanol production), and several other chemicals, as well as the use of hydrogen in iron reduction, fuel cells, and ammonia production. The latter applications can be boosted by shifting the carbon monoxide to hydrogen:

$$CO + H_2O \rightarrow CO_2 + H_2 \quad (1.2\text{-}2)$$

Nevertheless, an important application of gasification is in energy production in lieu of combustion. Modern gasification processes have higher efficiencies than direct combustion (43, 44). In addition, with gasification more efficient energy conversion systems such as the combined cycle gas turbine (CCGT) are available, which provide higher electrical generation efficiencies, thus, better overall system performances (44). On the other hand, in comparison to combustion which releases the energy into a high temperature flue gas stream, gasification invests the energy into chemical bonds of the products; hence, the energy does not have to be used locally. The other advantage of gasification over combustion is the opportunity for CO_2 capture which has been successfully performed in commercial integrated gasification combined-cycle (IGCC) plants, whereas it is practically impossible to do with combustion as the volume of the gas to be treated is 150-200 times higher (45). Gasification plants, however, require higher capital cost per unit output (46).

1.2.1 Catalytic gasification

Very high temperatures employed in the entrained flow gasifiers make the heat recovery from the product stream difficult, so that additional quenching of the gas will be necessary as a requirement of the existing gas treatment technologies. Therefore, the thermal efficiency of the process will be affected. Catalytic gasification offers the opportunity to operate at significantly lower temperatures compared to conventional gasification technologies. Low

temperature operation results in higher process efficiency (45). Lower energy consumption for heating, less NO_x emissions due to the introduction of less air for combustion to provide the required heat or decreased load of the air separation unit for oxygen purification, as well as less robust equipment required for the reduced severity conditions are some of the other benefits of catalytic gasification.

The most effective catalysts for gasification are alkali and alkaline earth metal salts. Transition metals such as iron, cobalt, and nickel are active for gasification mainly in their reduced form (47). They are deactivated by oxidation or poisoning by sulfur, which is usually present in the feedstock. The degree of dispersion of the catalyst plays a major role in the reactivity. Calcium requires near-atomic dispersal (i.e. less than 1-5 nm particle sizes) for high activity (48, 49).

The composition of the product gas is affected by equilibrium reactions such as (47):

$$CO + 3H_2 \leftrightarrows CH_4 + H_2O \qquad (1.2\text{-}3)$$

$$CO + H_2O \leftrightarrows CO_2 + H_2 \qquad (1.2\text{-}4)$$

The possibility of methane production by catalytic gasification of coal (in the same reactor without an additional catalyst for methanation) as suggested by equation (1.2-3) was first explored by Exxon (50). Low-temperature operation favors methane production (51, 45). Relatively high pressures (3-6 MPa) are required to avoid the steam reforming reaction (i.e. equation (1.2-3) in the reverse direction) so as to promote methane formation at notable concentrations (52).

The mechanism of the catalyst action in the catalytic gasification reactions has been widely studied and several mechanisms have been proposed (47, 51). A well-known mechanism is the oxygen spill-over (51) or the oxygen transfer mechanisms (47). These mechanisms explain the gasification reaction by the abstraction of an oxygen atom from the oxidizing gas agent (e.g. steam or CO_2) upon adsorption on the metal and releasing the rest of the molecule (i.e. H_2 or CO in the case of steam and CO_2, respectively). An active form of the oxygen is then shifted to the surrounding carbon matrix. A variation of this mechanism was proposed by Moulijn and Kapteijn (53) for alkali metal catalyzed gasification, which considers clusters of the metal bound to the carbon matrix by oxygen links as the main form of the active sites in this reaction. This was based on the studies by Yang and coworkers (54) who concluded that single metal phenolate groups (denoted as C-O-M) did not show high activity towards gasification. They postulated that the very low catalytic activity of alkali metal compounds at low catalyst loadings is because of the dispersion of the catalyst as C-O-M groups rather than clusters. Higher catalyst loadings are, therefore, required to allow for the formation of clustered metal species on the surface of the carbon material to reach high reaction rates. In order to measure the turn-over frequency of the C-O-K groups by time-resolved TEM microscopy, they prepared samples of low catalyst loading and assumed that the catalyst will disperse on the sample as single-metal C-O-K complexes with the reasoning mentioned above. No direct evidence of the formation of such complexes in their experiments was provided. In an earlier publication, they related the length and width of monolayer channels

on the basal planes of graphite to the turn-over frequencies of clustered (particle) K species and single-metal C-O-K complexes, respectively (55). They hypothesized that as the particle proceeds through the graphite layer by gasification, it leaves behind single-metal C-O-K complexes on the walls of the formed channel. They postulated that the latter complexes are responsible for the further widening of the channel, thus the low ratio of the turn-over frequencies. Nonetheless, a quantitative comparison of the activities of the clustered and single metal species per potassium atom was not provided.

The oxygen transfer mechanism has also been proposed in a number of forms of redox cycles such as (56):

$$M_2CO_3 + C \rightarrow 2M + CO + CO_2 \quad (1.2\text{-}5)$$

$$2M + 2H_2O \rightarrow 2MOH + H_2 \quad (1.2\text{-}6)$$

$$2MOH + CO_2 \rightarrow M_2CO_3 + H_2O \quad (1.2\text{-}7)$$

$$C + H_2O \rightarrow CO + H_2 \quad (1.2\text{-}1)$$

In addition, other mechanisms including electrochemical mechanisms and mechanisms involving free radical formation have been considered (47).

Kinetics of catalytic gasification has been another area of study. The effect of various parameters including: temperature, partial pressure of the reactant gas, catalyst loading, and surface area on the rate of the reaction have been extensively investigated. Kinetic observations have often been used in justification of mechanistic theories, and vice versa. The activation energy of the reaction was not altered in the Ca-catalyzed gasification by CO_2 suggesting a similar reaction pathway in both the catalyzed and uncatalyzed reactions (57). However, it was

shown that the number of active sites was increased in the catalytic reaction, which justifies the higher rate over the uncatalyzed reaction.

Many kinetic studies have commonly used mass or atomic ratios to the entire sample (or to the carbon content of the entire sample) for catalyst loading rather than surface loading, i.e. the amount of catalyst per unit area of the sample, in kinetic measurements (e.g. 58, 59, 60, 61, 62, 63). The use of high surface area porous materials for kinetic studies results in complications caused by the changes in surface area and pore diffusion limitations, which make the analysis difficult.

McKee et al. (61) tested each sample in repeated cycles of reaction with increasing temperatures followed by cooling to room temperature. The purpose of performing the experiments in this fashion was stated as to test for reproducibility. It was concluded that the rate increased in the subsequent cycles. They clearly did not consider the aforementioned change in the surface area of the particles with conversion, which may have also affected the temperature dependence of the rates measured in this manner, hence the activation energies. With the relatively high surface area chars used in that study (198 - 280 m^2/g), the changes in the microstructure of the samples upon the consumption of carbon could alter the total surface area substantially. Moreover, the reported dependence of the rates on the particle sizes in that study suggests significant internal mass transfer limitation occuring likely caused by clogging of the pores by the catalyst, which is another evidence for the surface area dependence of the rates.

Moulijn and coworkers observed variations in the reaction rates of the potassium carbonate-catalyzed gasification at different conversions (62). They

related these variations to changes in the mechanism of the reaction in terms of the catalyst action. For instance, higher rates at high conversions were postulated to be due to the break-up of K-O-C complexes that hindered the catalyst mobility. Although surface enlargement due to gasification was reported in that work, the effect of surface area on the rates of gasification was not discussed. It should be noted that a very high surface area activated carbon (750 m^2/g) was used in this study.

More recently, Zhang et al. (58) used a random pore model (RPM) to describe the variations in the rate of the potassium- and calcium-catalyzed gasification of high surface area (308-1055 m^2/g) char and activated carbon samples by CO_2. The model accounted for the changes in the surface area and pore structure of the porous materials studied. The theoretically derived model did not fit the experimental data reasonably. Therefore, they devised an empirical variable factor to make a better fit. Variations in the catalyst loading during the course of the reaction were presumed to be the source of the disagreement between the theoretically derived model and the experimental data, as the model only considered geometrical factors.

Thomson and Sy (50) did not see an appreciable increase in the rate of gasification by potassium carbonate at a low catalyst loading of 5%. They related this to the loss of catalyst by carry-over in the gas stream. A similar observation by Moulijn and coworkers was justified by formation of intercalate type compounds making the catalyst inaccessible to the reactant gas (62). No direct evidence for the intercalation of potassium was provided. It was speculated that

an observed increase in the specific surface area was due to the intercalation of potassium (64). However, an alkali metal- catalyzed gasification mechanism proposed by Wen (65) involved steps that required the formation of (intercalate-like) electron donor-acceptor complexes to catalyze the gasification reactions.

1.2.2 Bitumen coke

The increasing energy demand in North America, as well as high prices of energy carriers in the recent years, despite the challenges in its upgrading and utilization, have made the heavy hydrocarbons reserves of Alberta more attractive than ever. However, the upgrading processes of Alberta's bitumen yield in excessive amounts of low value and less usable solid coke residue stockpiled near the upgraders. The high asphaltenes content of these bitumens plays an important role in the coke yield from upgrading processes. Gasification of the coke, as well as the asphaltenes from solvent deasphalting processes, has been considered an attractive solution to make use of these carbon-rich residues.

Catalytic gasification is, therefore, a worthwhile technology in this regard. A major obstacle toward the commercialization of catalytic gasification has been the high amount of mineral impurities in most of the carbonaceous materials traditionally considered for the application with this technology. These impurities (especially of coals), which will normally end up as fly ash in the process upon the consumption of the carbon, react irreversibly with the catalyst resulting in its deactivation and catalyst recovery problems (66). In fact, most of the existing conventional (non-catalytic) gasification processes have to increase the

temperature of the reactor beyond the optimum temperature dictated by the kinetics of the reaction. This is in order to handle the fly ash emission and the deposition of the ash in the equipment by fusing the ash into a manageable liquid slag stream (slagging gasifiers) or heavier agglomerates that would settle (fluidized bed gasifiers). The choice of technology and the operating conditions, therefore, depends highly on the characteristics of the feed and the mineral constituents.

In contrast, oil sands bitumen cokes can be lean in minerals or even essentially ash-free depending on the feedstock and the extraction/upgrading technologies. Therefore, both problems (i.e. catalyst deactivation due to interactions with the minerals, and the fly ash emissions) are, in principle, minimal and controllable in the case of bitumen coke. Therefore, catalytic gasification for bitumen cokes faces less technical problems than coals in that sense. Their relatively high sulfur content, nevertheless, is still an issue that poses some challenges in terms of emission remission requirements.

1.2.3 Significance of the present study on the catalytic gasification of coke

Few published studies have addressed the catalytic gasification of bitumen coke. Although the underlying fundamentals of catalytic gasification of various carbon-containing substances are expected to be the same, there are still differences in various aspects of the process which depend on the feed material. Chemical composition in terms of heteroatom content and functional groups, the amount and composition of the mineral impurities, and the physical

microstructure of the materials in terms of the porosity and surface area are the main differences of the different carbon containing compounds. While coal and coal chars have been by far the most frequently used materials for the catalytic gasification researches, many studies on the mechanism of the catalytic action of the catalysts have deliberately avoided these feeds. Instead, simpler substances such as amorphous carbon black and graphite have been used for these studies (47). Nevertheless, the materials used for kinetic studies (mainly coals, coal chars, and activated carbons) often have relatively high surface areas and porous structures, which make the analysis complicated.

A number of contradicting data on some aspects of the kinetics of the catalytic gasification reactions have been presented in the literature, which render the outcomes of further research in the field less than obvious. An example is the activation energy of the reaction, which is suggested to be the same for the catalytic and the uncatalyzed reactions by some researchers, while other studies show significant differences.

The mechanism of the reaction has remained uncertain to this date, in spite of the large volume of research concentrated on the matter. The present work was able to shed light on some of the mechanistic aspects of the reaction, leading to confirmation and rejection of some of the previous findings.

1.3 Outline of the thesis

Chapter 1 of the thesis serves as the overall introduction to the thesis and elaborates the significance of the works done towards this thesis. Chapters 2, 3,

and 4 present the experimental methods and the results of the research in detail. These chapters have been prepared in journal paper format. Therefore, each of them contains *Introduction*, *Materials and methods*, *Results and discussions*, *Conclusions*, and *References* sections independently.

Chapter 2 showcases the research done on the identification of the structure of asphaltenes which confirmed the existence of bridged structures (archipelago) in asphaltenes in considerable quantities. This study was carried out in collaboration with the ExxonMobil Research and Engineering Co.

Chapters 3 and 4 deal with the study done on the catalytic gasification of bitumen coke. Chapter 3 includes the initial screening of the various materials tested for catalytic activity toward gasification of bitumen coke as well as the investigation of the underlying factors in the catalytic activity of these materials, particularly mobility at the reaction conditions. The subsequent portion of the work devoted to the evaluation of the kinetics of the catalytic gasification of bitumen coke will be discussed in Chapter 4.

In Chapter 5 the general conclusions of the different parts of this work are summarized. Some results from the pyrolysis of Gudao asphaltenes which were not included in Chapter 2 are presented and discussed in Appendix 1. Appendix 2 introduces a modification to the shrinking core model presented in Chapter 4, which accounts for the penetration of the catalyst into the coke particles. The modified model can predict the temporal rate of the reaction at lower initial catalyst loadings more accurately. Some additional data on the interactions of the

coke and catalyst in the case of potassium carbonate are presented and discussed in Appendix 3.

1.4 References

1. Conradson, P. H. *J. Ind. Eng. Chem.* **1912**, *4*, 903-905.
2. Wiehe, I. Process Chemistry of Petroleum Macromolecules, Boca Raton, FL: CRC Press, Taylor & Francis Group, **2008**.
3. Meyer, V.; Pilliez, J.; Habas, J.; Montel, F.; Creux, P. *Energy & Fuels* **2008,** *22*, 3154–3159.
4. Gray, M. R. Upgrading Petroleum Residues and Heavy Oils. New York: Marcel Dekker, **1994**.
5. Brandrup, J.; Immergut, Edmund H.; Grulke, Eric A.; Abe, Akihiro; Bloch, Daniel R. (1999; 2005). Polymer Handbook (4th Edition). John Wiley & Sons.
6. Alboudwarej, H.; Beck, J.; Svrcek, W.Y.; Yarranton, H.W.; Akbarzedeh, K. *Energy Fuels* **2002**, *16*, 462-469.
7. Groenzin, H.; Mullins, O. C. *Energy Fuels* **2000**, *14*, 677-684.
8. Tanaka, R.; Hunt, J. E.; Winans, R. E.; Thiyagarajan, P.; Sato, S.; Takanohashi, T. *Energy Fuels* **2003**, *17*, 127-134.
9. Qian, K.; Edwards, K. E.; Siskin, M.; Olmstead, W. N.; Mennito, A. S.; Dechert, G. J.; Hoosain, N. E. *Energy Fuels* **2007**, *21*, 1042-1047.
10. Speight, J.G. Handbook of Petroleum Analysis, John Wiley & Sons Inc., New York, **2001**.

11. Pfeiffer, J. P.; Saal., R. N. J. *J. Phys. Chem.* **1940**, *44*, 139–149.
12. Yen, T. F.; Erdman, J. G.; Pollack, S. S. *Anal. Chem.*, **1961**, *33*, 1587–1594.
13. Dickie, J. P.; T. F. Yen, *Anal. Chem.*, **1967**, 39, 1847–1852.
14. Agrawala M.; Yarranton, H. W. *Ind. Eng. Chem. Res.* **2001**, *40*, 4664-4672.
15. Yin, C.; Tan, X.; Müllen, K.; Stryker, J. M.; Gray, M. R. *Energy & Fuels* **2008,** *22*, 2465–2469.
16. Moschopedis, S. E.; Speight, J. G. *Fuel* **1976**, *55*, 187-192.
17. Tan, X.; Fenniri, H.; Gray M. R. *Energy & Fuels* **2009,** *23*, 3687–3693.
18. Rogel, E. *Energy & Fuels* **2000**, *14*, 566-574.
19. Maruska, H. P.; Rao, B. M. L. *Fuel Sci. Technol. Int.* **1987**, *5*, 119.
20. Yen, T. F. *Energy Sources, Part A: Recovery, Utilization, and Environmental Effects*, **1974**, *1*, 447– 463.
21. Speight, J.G. *Oil & Gas Science and Technology – Rev. IFP* **2004**, *59*, 467-477.
22. Speight, J.G.; Pancirov, R. J. *Liquid Fuels Technology*, **1984**, *2*, 287-305.
23. Strausz, O. P.; Mojelsky, T. W.; Lown, E. M. *Fuel* **1992**, *71*, 1355-1363.
24. Wiehe, I. A. *Energy & Fuels* **1994**, *8*, 536-544.

25. Speight, J.G. Proceedings of the National Science Foundation workshop on the fundamental organic chemistry of coal, Knoxville, Tennessee, **1975**, 125-147.
26. Rahmani, S.; McCaffrey, W. C.; Gray, M. R. *Energy & Fuels* **2002,** *16*, 148-154.
27. Rahmani, S.; McCaffrey, W. C.; Dettman, H. D.; Gray, M. R. *Energy & Fuels* **2003,** *17*, 1048-1056.
28. Wiehe, I. A. *Ind. Eng. Chem. Res*. **1993**, *32*, 2447-2456.
29. Poutsma, M. L. *Energy Fuels* **1990**, *4*, 113-131.
30. McMillen, D. F.; Golden, D. M. *Annu. Rev. Phys. Chem.* **1982**, *33*, 493-532.
31. Sanderson, R. T., Polar covalence. New York: Academic Press, **1983**.
32. Aribike, D. S.; Susu, A. A. *Thermochimica Acta* **1988**, *127*, 247-258.
33. Gray, M.R.; McCaffrey, W.C.; Huq I.; Le, T. *Ind. Eng. Chem. Res.* **2004**, *43*, 5438–5445.
34. Willems, P. A.; Froment, G. F. *Ind. Eng. Chem. Res.* **1988**, *27*, 1966-1971.
35. Gray, M. R.; McCaffrey, W. C. *Energy Fuels* **2002**, *16*, 756-766.
36. Loeff, I.; Stein, G. *Nature* **1959**, *184*, 901.
37. Weitkamp, j.; Raichle, A.; Traa, Y. *Applied Catalysis A: General* **2001**, *222*, 277–297.
38. Lorant, F.; Behar, F.; Vandenbroucke, M.; McKinney, D. E.; Tang, Y. *Energy Fuels*, **2000**, *14*, 1143—1155.

39. Khorasheh, F.; Gray, M. R. *Energy Fuels* **1993**, *7*, 960-967.

40. Smith, C. M.; Savage P. E. *AIChE Journal* **1991**, *37*, 1613-1624.

41. Lannuzel, F.; Bounaceur, R.; Michels, R.; Scacchi, G.; Marquaire, P. *J. Anal. Appl. Pyrolysis* **2010**, *87*, 236–247.

42. Payzant J. D.; Lown, E. M.; Strausz, O. P. *Energy Fuels* **1991**, *5* , 445-453.

43. Kumar, A.; Flynn, P.; Sokhansanj, S. *Renewable Energy* **2008**, *33*, 1354–1363.

44. Yassin, L.; Lettieri, P.; Simonsa, S. J. R.; Germanà, A. *Chemical Engineering Journal* **2009**, *146*, 315–327.

45. Higman, C.; van der Burgt, M. Gasification. 2nd ed., Amsterdam: Elsevier, **2008**.

46. Cameron, J. B.; Kumar, A.; Flynn, P. C. *Biomass and Bioenergy* **2007**, *31*, 137–144.

47. Wood, B. J.; Sancier, K. M. *Cat. Rev. Sci. Eng.* **1984**, *26*, 233-279.

48. Cazorla-Amorós, D.; Linares-Solano, A.; Salinas-Martínez de Lecea, C.; Joly, J.P. *Carbon* **1991**, *29*, 361–369.

49. Ginter, D. M.; Somorjai, G. A.; Heinemann, H. *Energy Fuels* **1993**, *7*, 393-398.

50. Thomson, W. J.; Sy, L. Y. *Fuel* **1987**, *66*, 223-227

51. Tomita A. *Cat. Surv. Jap.* **2001**, *5*, 17-24.

52. Hippo, E. J.; Tandon. D. *Am. Chem. Soc., Fuel Chem. Div. Prepr.* **1996**, *41*, 216-220.

53. Moulijn, J.A.; Kapteijn, F. *Carbon* **1995**, *33*, 1155-1165.

54. Chen, S. G.; Yang, R. T. *J. Catal*. **1993**, *141*, 102-113.

55. Chen, S. G.; Yang, R. T. *J. Catal*. **1992**, *138*, 12-23.

56. Veraa, M. J.; Bell, A. T. *Fuel* **1978**, *57*, 194-200.

57. Freund, H. *Fuel* **1986**, *65*, 63.

58. Zhang, Y.; Hara, S.; Kajitani, S.; Ashizawa M. *Fuel* **2010**, *89*, 152–157.

59. Sheth, A. C.; Yeboah, Y. D.; Godavarty, A.; Xu, Y.; Agarwal, P.K. *Fuel* **2003**, *82*, 305–317.

60. Schumacher, W.; Mühlen, H. -j.; van Heek, K. H.; Jüntgen, H. *Fuel* **1986**, *65*, 1360–1363.

61. McKee, D. W.; Spiro, C. L.; Kosky, P. G.; Lamby, E. J. *Fuel* **1985**, *64*, 805–809.

62. Wigmans, T.; Elfring, R.; Moulijn, J. A. *Carbon* **1983**, *21*, 1–12.

63. Mims, C. A.; Pabst, J. K. *Am. Chem. Soc., Fuel Chem. Div. Prepr.* **1980**, *25*(3), 258-262.

64. Wigmans, T.; Elfring, R.; Hoogland, A.; Moulijn, J. A. *Proceedings of the internation conference on coal science*, Düsseldorf: Glückauf Verlag, **1981**, 301-306.

65. Wen WY. *Cataly Rev* **1980**, *22*, 1–28.

66. Wang, J.; Yao, Y.; Cao, J.; Jiang, M. *Fuel* **2010**, *89*, 310–317.

2 Quantitative evidence for bridged structures in asphaltenes by thin film pyrolysis

2.1 Introduction

The largest molecules in petroleum, in the vacuum residue fraction, constitute an extraordinarily complex mixture of components with a range of functional groups and molecular weight. The asphaltenes, defined as the heptane-insoluble fraction of this material, are a convenient target for studies of the molecular architecture. Petroleum asphaltenes tend to self associate, and are polydisperse in molecular weight, functional groups, and possibly in basic molecular architecture. This complexity, and the difficulties associated with quantitative analysis of such a mixture, has led to considerable controversy regarding the basic molecular motifs. Resolution of the molecular structure of these compounds is essential in order to explain and model a range of phenomena, from phase behavior during production to refinery processing. Asphaltenes are identified by a physical behavior, i.e. solubility, rather than chemical characteristics; therefore, a variety of molecular morphologies can in principle fit into this category. As such, the assumption of a single “representative” or “average” chemical structure or even a limited class of chemical structures for all of these molecules is not valid.

Chapter 2 Quantitative evidence for bridged structures in asphaltenes by thin film pyrolysis

Two aspects of molecular structure of asphaltenes require better definition: the distribution of the size of the aromatic, heteroaromatic, and naphthenoaromatic ring groups, and the architecture of the linkages or bridges between these groups. Yen (1972) proposed alkyl aromatic structures consisting of a large cluster of several fused aromatic and naphthenic rings as the core substituted with a few alkyl branches to represent asphaltene molecules (1). Later researchers suggested that the number of rings in the cluster cannot exceed a certain limit. Speight (2001) set the maximum number of rings per cluster at 16 (2). More recent work showed that large polynuclear aromatic systems with more than 10 rings are unlikely to exist in asphaltenes (3) with the average being around 7 rings per cluster (4). Based on these constraints, a model of asphaltene molecules was proposed consisting of an "island" of aromatic and saturated rings substituted with alkyl branches. The minimum size of aromatic groups in the asphaltene fraction is also controversial. Groenzin and Mullins (2000) claimed that monoaromatic groups could not be significant on the basis of fluorescence spectroscopy (5), but their claims were not verified by suitable reference compounds, and the lack of a quantitative basis in this work has been pointed out by Strausz et al. (6). Pyrolysis studies have detected monoaromatics in cracked products from asphaltenes, under conditions that would not generate such compounds from alkyl groups (7, 8). Consequently, the size of ring groups in asphaltenes credibly ranges from 1 to 7, but better data on this distribution are highly desirable.

Chapter 2 Quantitative evidence for bridged structures in asphaltenes by thin film pyrolysis

The significance of bridges between ring groups in petroleum asphaltenes has been the second controversy in the literature. If the only significant pendant groups in the asphaltenes were alkyl side chains, as suggested by Groenzin and Mullins (5), then thermal cracking of the asphaltenes would give predominantly light naphtha-range alkanes and alkenes and heavy vacuum residue as liquid products, which is contrary to experimental observations (9). Studies of model compounds (e.g. Smith and Savage (10)) confirm the stability of aromatic ring groups under such thermal cracking conditions; therefore, the behavior of the large molecules in refinery processing can only be adequately represented by complex bridged structures (11, 12). The presence of covalent bridges is further supported by a range of specific chemical studies, including studies of biomarkers (13, 14, 15, 16), oxidative characterization of carbon-carbon bridges (14, 17), and detection of sulfides and esters (18). Wiehe (11) suggested structures consisting of smaller pendant groups attached to larger aromatic "cores" to analyze yields from coking of vacuum residues. While this terminology is attractive, coke can arise not only from large refractory groups, but also from condensation of smaller bridged structures and from trapping of much smaller fragments (19). Consequently, we use the term "building block" in this paper to describe the structural elements of the asphaltenes, without presuming a maximum or minimum size.

Given the abundant evidence for bridged components in the asphaltene fraction, can we use thermal cracking, or pyrolysis, as an analytical method to quantitatively characterize the distribution of building blocks, and the numbers of

bridges between the groups? Significant yields of small aromatic fragments can be produced by thermal cracking under conditions that would break one or two single bonds without disrupting condensed aromatic clusters (7, 20). The challenge is to conduct the thermal cracking under conditions that minimize secondary reactions of the cracked fragments, and at the same time enable quantitative analysis of the products. Gray et al. (2001) demonstrated that thermal cracking of thin films of vacuum residue gave maximal yields of liquid products under conditions that minimized secondary reactions in the liquid and the vapor phase (21). Reaction of thin film of circa 20 μm enables the release of cracked products from the liquid phase with minimal opportunity for recombination, then quenching in the vapor phase minimizes secondary cracking. Here we report the analysis of products from the thermal cracking of thin films of asphaltenes. A sufficient quantity of products was collected to enable material balances on the reactions, and to apply gas chromatography-field ionization time-of-flight high-resolution mass spectrometry analysis to the liquid products (22). Analysis of the liquid and solid products by ^{13}C-NMR enabled a balance on the aromatic carbon.

2.2 Materials and Methods

2.2.1 Characteristics of the raw materials

Asphaltenes from various sources, as listed in Table 2-1, were prepared by precipitation in heptane. A 40:1 solvent to crude (or vacuum residue) ratio by volume solution was sonicated in ultrasound bath for 1 h, followed by vacuum

filtration using 0.22 μm membrane filter papers (Millipore). The asphaltenes were subsequently dried at room temperature overnight. The vacuum residues were taken from vacuum distillation tower bottoms and had not undergone significance chemical alteration. In the case of Athabasca asphaltenes, the asphaltenes were precipitated using pentane in an industry pilot plant. This sample (referred to as industrial asphaltenes hereafter when used as received) contained 28.2% by weight pentane-solubles. Athabasca asphaltenes were also prepared by washing the industrial asphaltenes with extra pentane to remove the pentane-soluble fraction (labelled as Athabasca C_5 insolubles), as well as precipitation in heptane (Athabasca C_7 insolubles).

2.2.2 Pyrolysis technique

The asphaltene molecules were thermally cracked in an induction furnace. In order to control the extent of the reaction (i.e. to minimize further cracking of the formed fragments), the samples were coated as thin films on metal strips (a Ni-Fe alloy) with a Curie point of 500°C. A 3% solution of asphaltenes in dichloromethane (Fisher Scientific) was sprayed on the metal strips followed by drying overnight at room temperature. The measured mass of the coating was then used to estimate the film thickness. The film thickness was controlled not to exceed 20 μm in order to minimize the mass transfer limitation in the liquid film at reaction conditions, so that the lighter products of cracking do not get trapped in the film and evaporate readily (21). The vaporized asphaltene fragments were rapidly quenched in a 7.5 L/min flow of nitrogen gas so as to inhibit the cracking reactions in the gas phase.

The condensed liquid products of the reaction formed aerosols which either coalesced on the walls of the reaction chamber and tubing or were collected in a U-shaped tube immersed in liquid nitrogen with glass fiber packing acting as a trap. Light gases, chiefly consisting of methane and ethane, which passed through the trap were collected in a gas bag and subsequently analyzed by a refinery gas chromatograph (SRI Instruments 8610C GC equipped with two 6 ft silica gel and 13X molecular sieve columns and a thermal conductivity detector). The column temperature was held constant at 50°C for 4 min followed by ramping to 220°C at 10°C/min. The column sequence was switched after 7 min to allow for the elution of CO_2, ethane, and heavier organic gases.

The reaction chamber, tubing, and the cold trap were rinsed with dichloromethane to collect the liquid products after the reaction. The solution was subsequently filtered under vacuum using Millipore 0.22 μm cellulose membranes to remove any solids including glass fibers from the packing. The solvent was evaporated at room temperature afterwards and the mass of the remaining liquid was reported as the yield of liquid product. The metal strips were sonicated in toluene to remove the coke followed by vacuum filtration using Millipore 0.22 μm membranes to collect the coke. Subsequently the toluene was removed from the filtrate in a rotary evaporator and the remaining liquids were collected for the sake of mass balance.

In order to analyze the heavier components of the cracked products, the liquid products of the pyrolysis of Athabasca industrial asphaltenes were distilled under high vacuum (3×10^{-4} Torr absolute pressure) at circa 160°C using a Welch

8920 Direct-Drive high vacuum pump. The vacuum distillation residue was then re-pyrolyzed in the induction furnace by the same method as described for the pyrolysis of asphaltenes.

2.2.3 Characterization of the asphaltenes and products

The tendency of each asphaltene sample to form coke was determined using thermogravimetic analysis by heating the samples up to 500°C under an argon flow in a Thermo Cahn Thermax 300 thermogravimetric analyzer (TGA). The gas flow was then switched to air to burn off the coke and measure the ash content of the asphaltenes. The difference in mass between the residual solid at 500°C and the ash was recorded as the "TGA residue", which approximates the ASTM D4530 test for micro carbon residue (MCR). The elemental composition of the samples were determined using a Vario MICRO cube elemental analyzer (Elementar Analysensysteme, GmbH, Hanau, Germany).

Raw asphaltenes and the products of the reaction were analyzed by simulated distillation (SimDis) using a Varian 450-GC (Varian BV, the Netherlands) according to ASTM D5307 standard. The temperature profile used for the GC column (UltiMetal® capillary) consisted of an isothermal stage of 1 min at 35°C followed by ramping up to 400°C at 20°C/min with a total heating time of 45 min. Samples were injected as 2% by weight solutions in carbon disulfide (CS_2). An ASTM D5307 internal standard mixture was used as received (Supelco Analytical, Bellefonte, PA).

Volatile products of the reaction were analyzed by thermal desorption gas chromatography with a flame ionization detector (TD-GC-FID; Agilent Technologies 7890A GC-FID system equipped with a TD-5 Short Path Thermal Desorption System; Scientific Instrument Services, Inc., Ringoes, NJ). A piece of the glass fiber packing from the liquid nitrogen trap used to capture the products of the pyrolysis was placed into the thermal desorption unit immediately after the reaction. The sample was then heated at 150°C for 4 min. The resulting vapors were then injected into the GC. The temperature profile of the GC's oven consisted of an initial isothermal period of 3 min at 35°C followed by ramping at 5 °C/min to 200°C. The temperature was then held constant for 60 min.

Nuclear magnetic resonance (NMR) spectra were collected on a JEOL ECS400 at 50°C. The ^{13}C-NMR spectra were collected at 125 MHz. A relaxation agent was added to the solvent (7 mg CrAcAc/ 1 mL of $CDCl_3$) and the sample concentrations were ~30 to 50 wt%. A relaxation delay of 4.5 s was used, the data were recorded using a flip angle of 45° and 2400 scans were recorded. Solid-state ^{13}C MAS NMR spectra of the coke samples were recorded on a 9.4 T Varian InfinityPlus-400 spectrometer corresponding to Larmor frequencies of 399.42 and 100.44 MHz for ^{1}H and ^{13}C, respectively. The samples were loaded in 4 mm (o.d.) MAS rotors and spun at the magic angle at a rate of 14 kHz. The spectra were obtained with a 90º pulse, a recycle delay of 60 s, and about 62 kHz decoupling during data acquisition. The chemical shift was referenced with respect to an external secondary standard (using hexamethyl benzene and setting

the methyl peak at 17.36 ppm). All solid-state NMR measurements were performed at room temperature.

Mass spectra of the liquid products were obtained using the gas chromatrography-field ionization time of flight high resolution mass spectrometry (GC-FI-TOF-HRMS) technique as described elsewhere (22). The method can reliably identify compounds of boiling points up to 538°C with a high precision; therefore, the method gave quantitative analysis of the components with lower boiling points.

2.3 Results and Discussions

2.3.1 Characteristics of the feed materials

The estimated MCR contents of the samples (Table 2-1) show an increasing trend of coke formation propensities among the three Athabasca asphaltenes samples ranging from the industrial C_5 asphaltenes (which contained 28.2% pentane-solubles) to C_7 insolubles. The Cold Lake and Venezuelan samples had markedly lower MCR contents among the C_7 asphaltenes, while the Safaniya sample had the highest value.

Elemental compositions of these asphaltenes are shown in Table 2-2, revealing a remarkable similarity between the samples. The low carbon content of the Cold Lake sample was due to the high ash content (Table 2-1). The samples show significant differences in nitrogen and sulfur content, but the range of values was relatively narrow (1.1-2.0% for nitrogen and 5.6 to 8.2% for sulfur).

Table 2-1. Sources and characteristics of the asphaltenes

	C_7 insoluble, wt%	TGA residue[a], %	Ash, %	Source type
Athabasca industrial C_5	54.5	32.1	1.0	Vacuum residue
Athabasca C_5	75.9	40.7	1.6	Industrial asphaltenes
Athabasca C_7	100	47.2	2.0	Industrial asphaltenes
Cold Lake C_7	100	42.0	6.4	Vacuum Residue
Maya C_7	100	46.1	2.1	Heavy crude
Safaniya C_7	100	48.1	1.9	Vacuum residue
Venezuelan C_7	100	42.8	1.6	Vacuum residue

[a] The TGA residue content approximates the microcarbon residue (MCR) as determined by ASTM D4530

Table 2-2. Elemental composition of the asphaltene samples.

	C	H	N	S
Athabasca (Canada) industrial C_5 insolubles	82.1	7.9	1.1	5.6
Athabasca C_5 insolubles	82.0	7.6	1.4	7.6
Athabasca C_7 insolubles	81.5	7.5	1.5	8.1
Cold Lake (Canada) C_7 insolubles	77.9	7.5	1.5	8.2
Maya (Mexico) C_7 insolubles	82.1	7.7	1.4	7.4
Safaniya (Saudi Arabia) C_7 insolubles	82.4	7.3	1.2	7.7
Venezuelan C_7 insolubles	81.5	7.6	2.0	5.6

2.3.2 Mass balances and characterization of the products

A key objective of this work was the demonstration of accurate mass balances. As shown in Figure 2-1, the recovery of materials after the reaction with respect to the mass of the feed was over 95% in the case of Athabasca C_5 asphaltenes and 91% or higher in all cases of C_7 asphaltenes. The lower recovery of the materials in the case of C_7 asphaltenes was likely due to the higher yield of light liquids which are inevitably lost during the solvent evaporation step. Pyrolysis-GC MS studies (e.g. Speight and Pancirov (23) and Philp et al. (24)) have detected unquantified amounts of low boiling materials (<200°C). However, as the data of Figure 2-2 illustrate, volatile compounds below the boiling point of C_{14} were not observed in the chromatogram of the condensed liquids from the pyrolysis of Cold Lake C_7 asphaltenes heated at 150°C for 4 min. Consequently, we attribute the lack compounds boiling below 200-250°C to stripping of the condensed liquid in the trap downstream of the reactor. The data of Figure 2-2 graphically illustrate that the products above this boiling point are dominated by a complex mixture of components, because the sharp peaks due to alkanes and alkenes are present but make up only a small part of the total products.

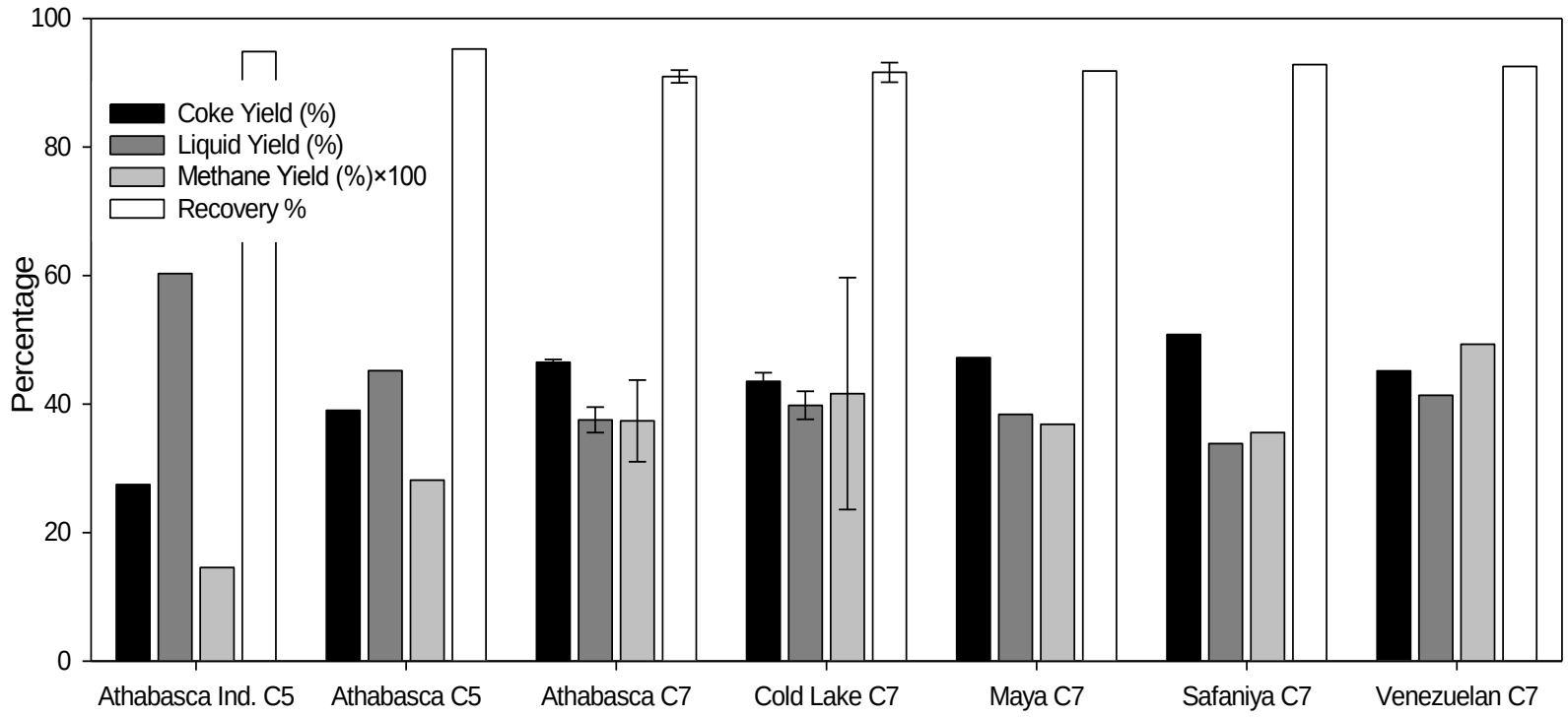

Figure 2-1. Yields of cracking products (ash-free basis) and recovery percentages of the products. All percentages are with respect to the mass of the feed. Error bars show the standard deviation from experiments conducted in triplicate; the remaining data are means of duplicate experiments.

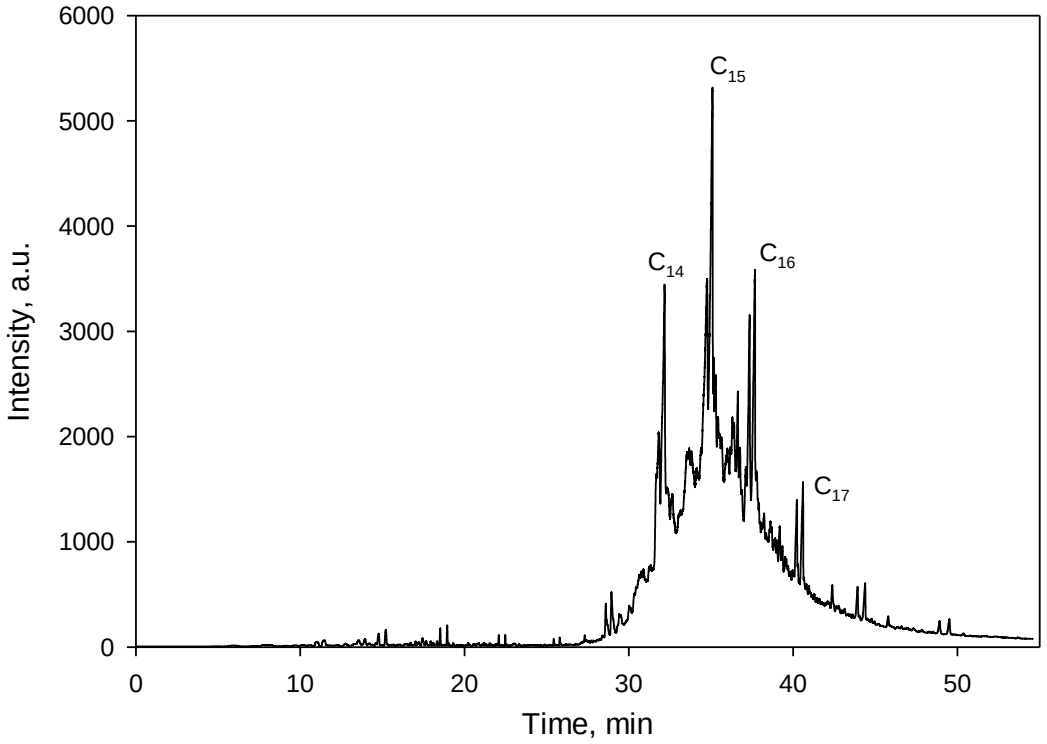

Figure 2-2. Chromatogram of volatile products of pyrolysis of Cold Lake C_7 asphaltenes analyzed by TD-GC-FID.

Light gases such as methane, ethane, ethylene, propane, butanes, and pentane were typically detected in the products. However, the concentration of some of these gases in the nitrogen-diluted sweep gas stream was not high enough for accurate quantification. Therefore, among the light gas products only the yields of methane are shown in Figure 2-1. For the same reason, these values have the largest error bars among all product groups. The total yield of gases was generally around 1% on a mass basis.

The yield of liquids of the Athabasca sample series followed the order industrial asphaltenes > C_5 asphaltenes > C_7 asphaltenes, consistent with their coke formation tendencies which increased in the reverse order. The yields of

liquid and coke products from the C_7 asphaltenes from the different sources were close, but based on the error bars for the Athabasca and Cold Lake samples, the higher coke yield and lower liquid yield of the Safaniya sample is statistically significant. The general similarity of the results is consistent with the narrow range in the quality of the feed materials, as pointed out in Elemental compositions of these asphaltenes are shown in Table 2-2, revealing a remarkable similarity between the samples. The low carbon content of the Cold Lake sample was due to the high ash content (Table 2-1). The samples show significant differences in nitrogen and sulfur content, but the range of values was relatively narrow (1.1-2.0% for nitrogen and 5.6 to 8.2% for sulfur).

Table 2-1 and Table 2-2. Boiling curves of the liquid products of the cracking of these asphaltenes obtained by simulated distillation also show a similar distribution of boiling points (Figure 2-3).

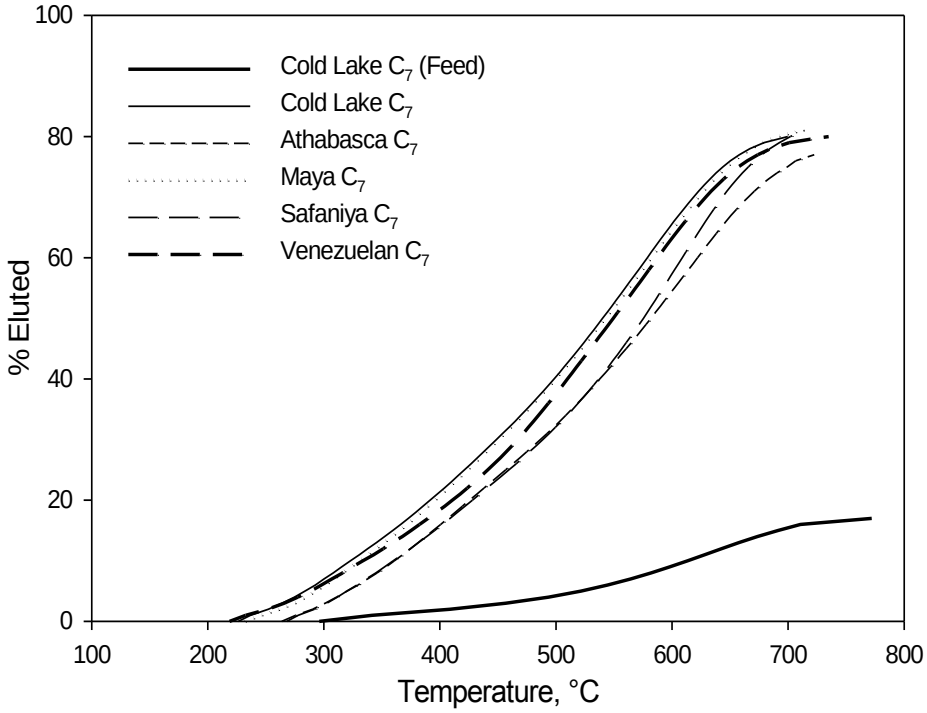

Figure 2-3. Boiling curves of the liquid products of the cracking of asphaltenes from various sources by simulated distillation. The boiling curve of a sample of unreacted Cold Lake C_7 asphaltenes has been included for comparison.

The liquid products of cracking appeared to become slightly heavier with reaction time as the reaction progressed (Figure 2-4). Nevertheless, a wide distribution of boiling points, corresponding to a wide range of molecular sizes, was produced in the later stages of the reaction. Consequently, the boiling points of the molecular fragments that are readily removed during the initial stages of thermal cracking are not significantly different from those liberated at later stages. In all cases, the products contained unconverted high-boiling components. The thin film reaction conditions were selected to minimize secondary reactions, but

this condition also enabled the evaporation of very high boiling components into the vapor phase, as indicated by the data of Figures 2-3 and 2-4.

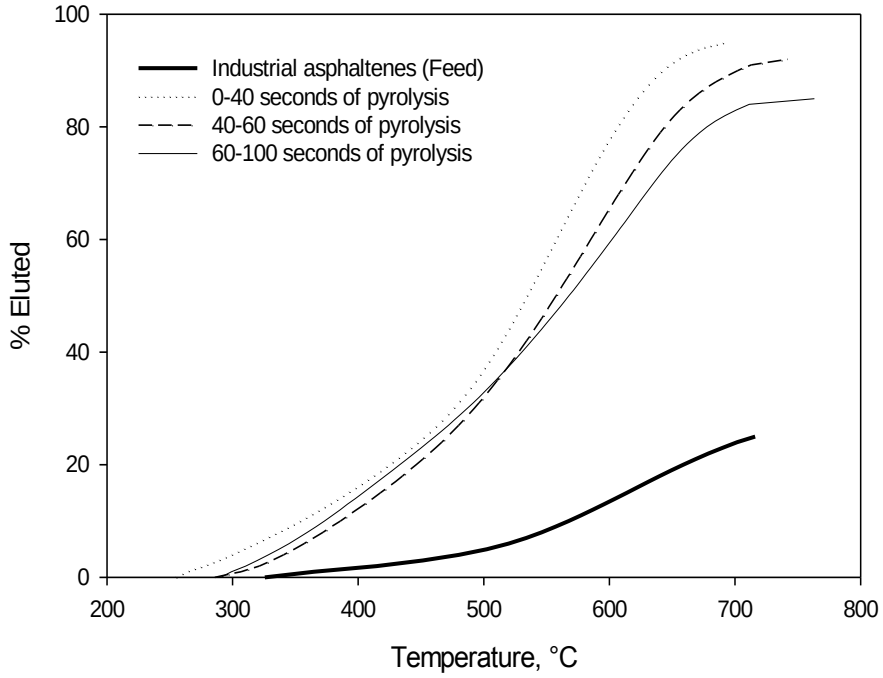

Figure 2-4. Simulated distillation boiling curves of raw industrial asphaltenes and the liquid products of three consecutive pyrolysis runs on the same sample.

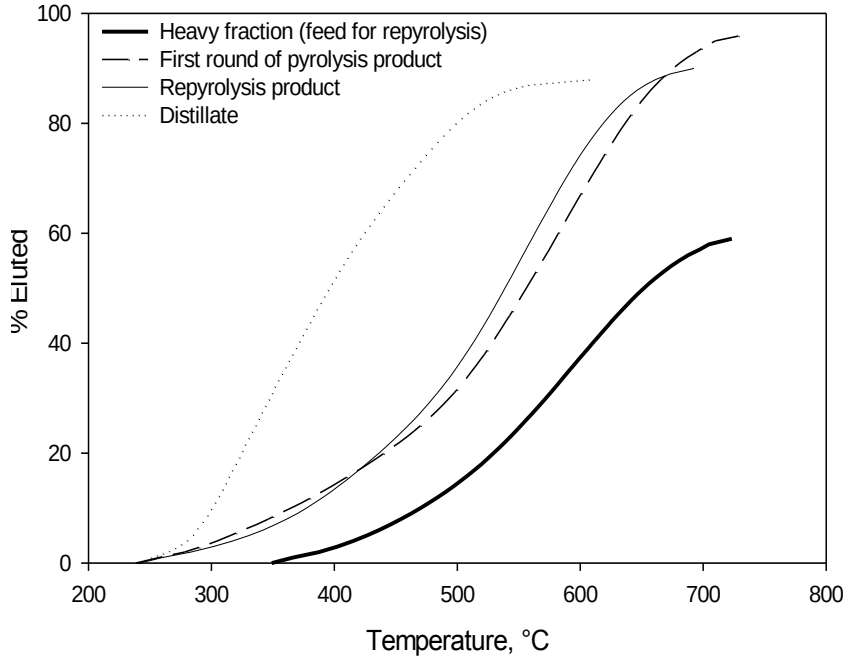

Figure 2-5. Simulated distillation curves for the products of the first and second rounds of pyrolysis of Athabasca industrial C_5 asphaltenes. The distillate and heavy (residue) fractions from the vacuum distillation of pyrolysis products are also shown. The latter was the feed for repyrolysis.

This result is consistent with previous observations of the carry over of such components in pyrolysis studies (25, 26). Indeed, the liquid products even contained asphaltenes (23.2% C_7 insolubles in the products of the pyrolysis of Athabasca industrial C_5 asphaltenes). Given that the C_7 asphaltenes were entirely comprised of vacuum residue components boiling over about 524°C, the conversion of this heavy material to distillates + gases was only about 15-20% of the original C_7 asphaltenes, and 35% of the Athabasca industrial C_5 asphaltene sample. Re-pyrolysis of the residue fraction of the products, separated by vacuum distillation, increased the conversion of the industrial C_5 asphaltenes further by

circa 10%. Simulated distillation of the repyrolysis product showed a similar distribution of boiling point as the first products of pyrolysis (Figure 2-5).

The ^{13}C-NMR analysis of the liquid products showed a narrow range of aromatic carbon content from the C_7 asphaltenes, from 43-51% (Table 2-3). Similarly, all of the coke material was in the range of 75-80% aromatic carbon content. These values are much lower than petroleum coke, which is typically in the range of 91-95%. The relatively high content of aliphatic carbon was consistent with the short reaction times of 2 min; i.e. the coke was still "green" and could be devolatilized further at longer reaction times. A material balance on the aromatic carbon content of the samples showed that the total mass of aromatic carbon in the recovered products from C_7 asphaltenes was 10-26% greater than the feed, with the Venezuelan asphaltene giving significantly greater formation of aromatic carbon than Athabasca and Safaniya. This result suggests significant differences between the asphaltene samples in the reactions of naphthenoaromatics (partly saturated polyaromatic groups), which are the most likely groups to form aromatics. The greatest portion of the increase in the aromaticity was likely in the coke, which was exposed to the highest temperatures for the longest period of time in comparison to the liquid products. The olefinic carbon content of the products was also included in the aromaticity value, which contributed to the increase. Japanwala et al. (26) observed an increase in the aromaticity of the products with respect to the feed in thermal cracking of Athabasca vacuum residue. However, they reported a fairly constant ratio of quaternary bridgehead carbons to total aromaticity for the liquid products of

different stages of pyrolysis and the feed, which suggests that the average number of aromatic rings per cluster in the products was the same as that in feed.

Table 2-3 Fraction of aromatic carbon (f_a) of feed and product samples and aromatic carbon balance. Increase in aromatic carbon is based on total mass of carbon.

Sample	Feed f_a	Liquid product f_a	Coke f_a	Increase in aromatic C, %
Athabasca C_5	0.47	0.46	nd[a]	nd
Athabasca C_7	0.50	0.44	0.78	10
Cold Lake C_7	0.46	0.39	0.75	20
Maya C_7	0.50	0.41	nd	nd
Safaniya C_7	0.51	0.41	0.79	11
Venezuelan C_7	0.43	0.40	0.79	26

[a] nd = not done

2.3.3 Structure of the molecular fragments

The high-resolution mass spectrometry data revealed that the majority of the products of the pyrolysis with boiling points below 538°C (in the range of 15-20% of the mass of the feed asphaltenes based on the boiling curves in Figure 2-3) consisted of structures containing of 1-4 saturated and/or aromatic rings (Figure 2-6). In refinery practice, components with boiling points below 538°C are termed distillates, because they are amenable to recovery by vacuum distillation, therefore, we use this designation for the 15-20% of the feed

asphaltenes that was analysed by GC-FI-TOF-HRMS. Paraffins comprised circa 7.3% of this fraction in the case of Cold Lake C_7 asphaltenes.

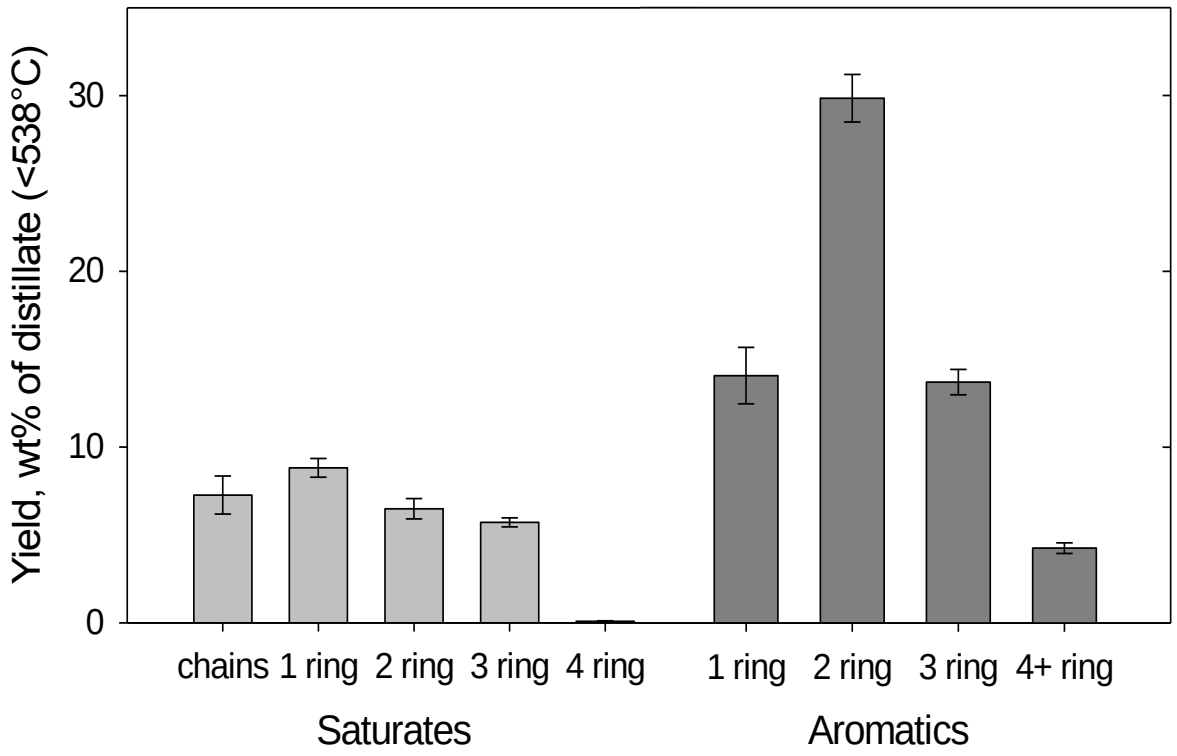

Figure 2-6. Distribution of the various classes of fragment structures in the distillate products of the pyrolysis of Cold Lake C_7 asphaltenes by GC-FI-TOF-HRMS analysis. Compounds with aromatic rings may also contain saturated rings. Error bars are the standard deviations of results from three replicate reactor experiments.

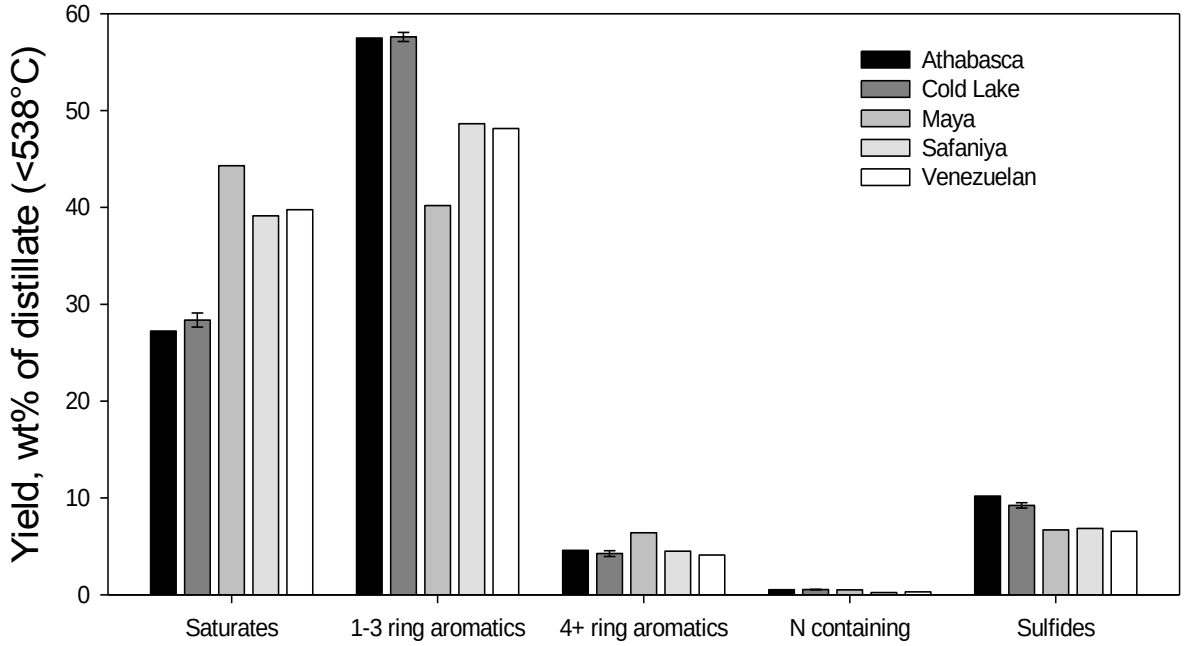

Figure 2-7. Comparison of the yields of compound classes in the distillate products of different C_7 asphaltenes by GC-FI-TOF-HRMS

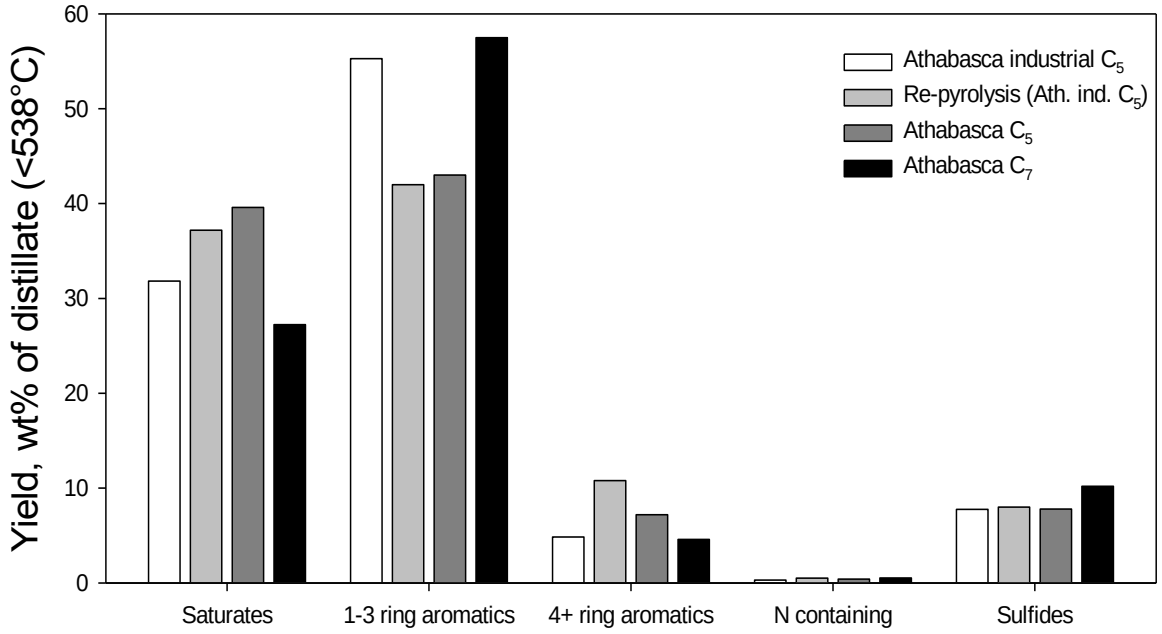

Figure 2-8. Comparison of the yields of compound classes in the distillate products of different Athabasca asphaltenes by GC-FI-TOF-HRMS

Figure 2-7 compares the yields of the main structural classes of the light liquid products from the C_7 asphaltenes. The Cold Lake and Athabasca asphaltenes gave significantly less saturates and more 1-3 ring aromatics than the other samples. The breakdown of these classes into selected major homologous series is given in Table 2-4. In most cases, the subclasses are additive to the totals; the exception is the alkyl benzenes which are a subset of the one-ring aromatics. The Maya sample gave a significantly higher yield of paraffins than the other samples, contributing to the high yield of saturates overall. The Athabasca and Cold Lake asphaltenes gave the highest yields of most of the aromatic classes.

Table 2-4. Composition of cracked liquid products from C_7 asphaltenes.

Error bounds on Cold Lake samples are standard deviations from three experiments.

Yield, wt% of distillate	Cold Lake	Athabasca	Maya	Safaniya	Venezuela
Total saturates	28.4±0.7	27.2	44.3	39.1	39.8
paraffins	7.3±1.1	6.0	17.0	11.7	11.4
1 ring naphthenes	8.8±0.5	8.1	11.8	12.4	14.3
2 ring naphthenes	6.5±0.6	7.1	8.2	9.3	8.7
3 ring naphthenes	5.7±0.3	5.9	6.2	5.7	5.3
4 ring naphthenes	0.1±0.0	0.1	1.1	0.1	0.1
Total 1 ring aromatics, olefins and thiophenes	14.1±1.6	12.4	13.4	13.4	13.4
one ring aromatics	11.7±0.4	11.3	10.3	10.0	10.0
alkyl benzenes	3.3±0.3	3.1	3.4	3.7	3.2
Total 2 ring aromatics	29.8±1.4	30.7	16.9	28.2	25.2
benzothiophenes	7.6±0.4	8.2	5.2	10.7	8.65
naphthenobenzo-thiophenes	6.1±0.4	6.7	3.8	8.6	6.20
naphthalenes	7.5±0.3	7.1	4.2	4.2	5.15
Total 3 ring aromatics	13.7±0.7	14.4	9.90	10.15	9.55
dibenzothiophenes	2.3±0.2	2.4	2.00	2.80	2.10
4+ ring aromatics	4.3±0.3	4.6	6.40	4.50	4.10
N containing molecules	0.5±0.0	0.5	0.50	0.23	0.30
Sulfides	9.2±0.3	10.2	6.70	6.85	6.55

The exceptions were the thiophenes (benzothiophenes, naphthenobenzo-thiophenes, and dibenzothiophenes) which were higher in Safaniya than in the other products. The concentration of sulfides in Safaniya was significantly lower, to balance the sulfur content.

As illustrated in Figure 2-8, the yields of various classes of compounds from the industrial C_5, C_5, and C_7 asphaltenes from Athabasca were surprisingly close, given the 62% difference in total pyrolysis liquid product yields of the Athabasca industrial C_5 and C_7 asphaltenes in Figure 2-1. This similarity suggests that the structural building blocks of the heptane soluble fraction of the industrial asphaltene sample (54.5% by weight) must be very similar to those of the heptane insoluble portion. However, there must be factors other than structural building blocks that determine the solubility of some of the molecules in heptane while they remain insoluble in pentane. These factors may include the size of the molecule as well as the arrangement of the building blocks in the molecule, both of which could not be identified in the present study.

Consistent with the simulated distillation data (Figure 2-5), the yields of the products of the re-pyrolysis of the heavy products of the Athabasca industrial C_5 sample were also in the same range as the other samples (Figure 2-8). This result suggests that the heavier portion of the pyrolysis products, which could not be directly analyzed by mass spectrometry, is largely comprised of similar building blocks to the distillate products.

Figure 2-9 illustrates the distribution of three example series of compound types with molecular weight. The size distribution of the cyclohexanes, for

example, suggests that these fragments generally contain side chains of various sizes, which can make their molecular weights as high as 600. While the molecular weight distributions of the other two groups shown containing aromatic rings seem very similar, it should be noted that the latter groups may contain saturated rings in addition to side chains. These distributions emphasize that the building blocks cover a wide range of molecular weight, and can exhibit a significant degree of alkyl substitution. Given the loss of low boiling material apparent in Figure 2-2, these distributions are biased toward higher molecular weight product components, for example, by the loss of monoaromatics such as toluene.

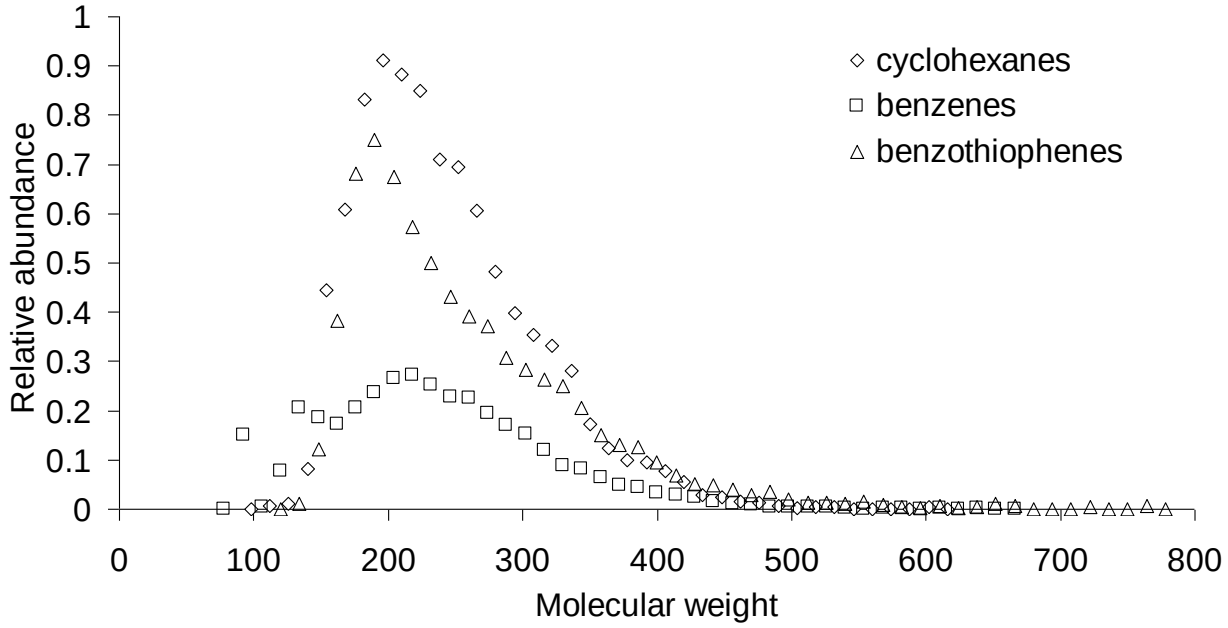

Figure 2-9. Examples of the size distribution of compounds with similar structures identified by the GC-FI-TOF-HRMS technique. Compounds with aromatic rings may also contain saturated rings, for example, tetrahydronaphthalene would appear in the "benzene" series.

2.3.4 Implications for molecular architecture of asphaltenes

The data demonstrate that the distillates from thermal cracking of asphaltenes are comprised of an extraordinarily complex mixture of paraffins, saturated rings, and aromatic groups, which is entirely consistent with refinery experience in processing vacuum residue fractions. The yields of cyclic saturated series, aromatics, nitrogen compounds, and sulfides were in the range of 13-17% of the initial asphaltenes, in contrast to only 1-2% paraffins derived from alkyl side chains. The repeat pyrolysis of unconverted vacuum residue (Figure 2-5) demonstrated that these yields were limited by the low conversion in the thin film experimental method, rather than the intrinsic structure of the asphaltene molecules. These reaction conditions were selected such that breakage of single bonds (carbon-carbon, carbon-sulfur, and carbon-oxygen) would predominate; breakage of polycyclic aromatic compounds or naphthenic rings would not be significant under these conditions based on prior work with model compounds (10, 27, 28).

The only possible conclusion from this study is that bridges between clusters of ring groups (aromatic, naphthenoaromatic, or saturated) are abundant in the petroleum asphaltene samples in this study. As illustrated in Figure 2-10, the asphaltenes must be viewed as being randomly built from blocks of ring and paraffin groups to give a distribution of molecular weights. This result confirms the earlier work of Strausz et al. (20) that characterized petroleum asphaltenes as complex mixtures of bridged structures.

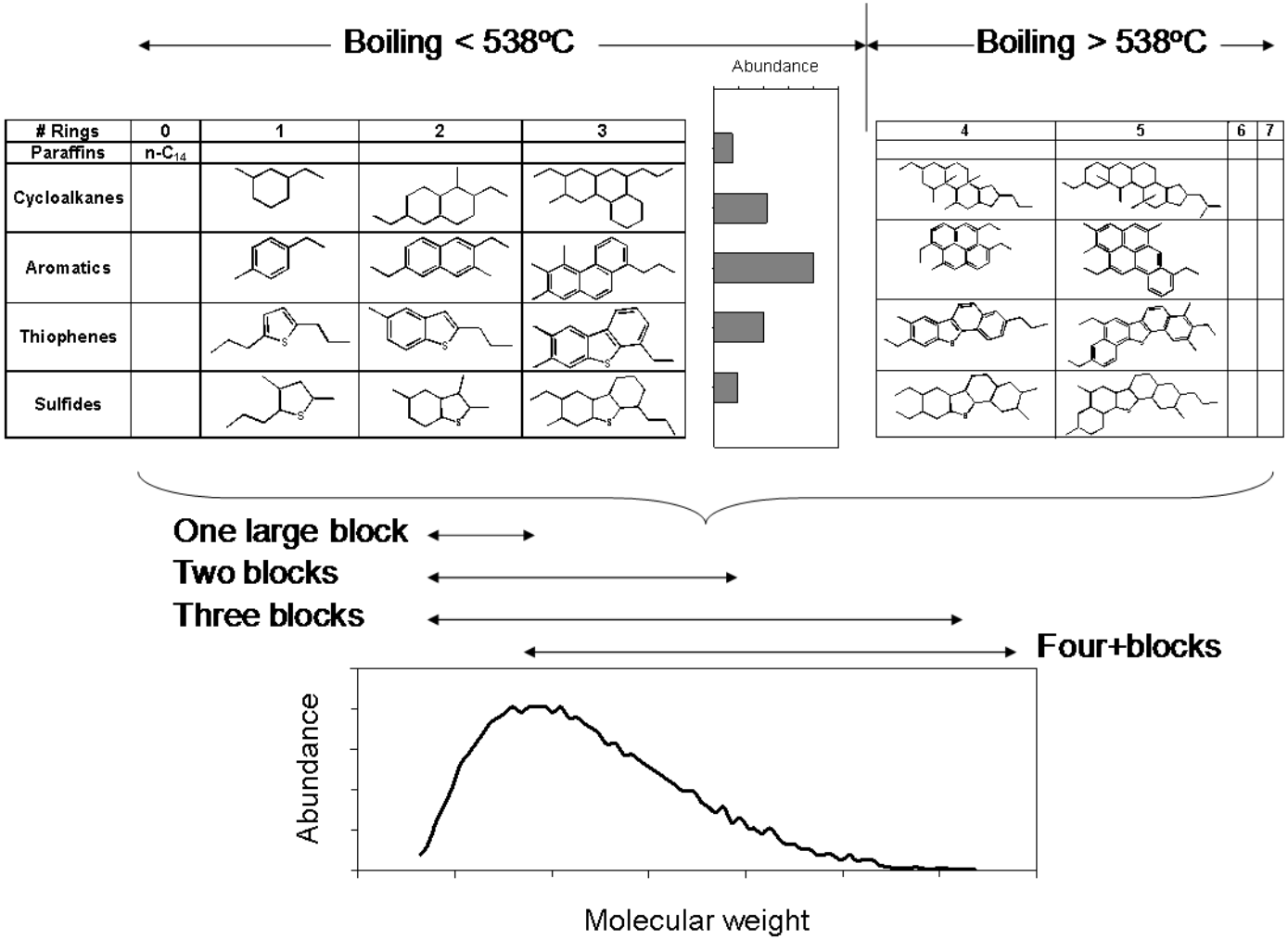

Figure 2-10. Schematic representation of petroleum asphaltene construction based on building blocks. Small building blocks (ca. 200 Da) were detected in the product fraction boiling < 538°C. Larger building blocks (> 400-500 Da) and multi-block structures occur in the range > 538°C. Bridging groups include carbon, sulfide, and ester bridges. Nitrogen, metal, and oxygen compounds are omitted for clarity. The distribution of sizes of large ring groups in the vacuum residue range (T_b > 538°C) are not defined in this study.

The similar data for asphaltenes from crude oils and bitumens from distinct geological basins in North and South America and the Middle East suggest that this conclusion is widely applicable to petroleum asphaltenes, but we cannot rule out the existence of a naturally occurring material with different structural features. The experimental results are utterly at odds with attempts to characterize the asphaltenes as predominantly simple alkyl aromatics and alkyl-napthenoaromatics.

The thin-film thermal cracking method suffers from several drawbacks as a tool for quantitative analysis of the constituent groups in asphaltenes. A considerable amount of coke was produced in these reactions, which makes it impossible to define the maximal size of the aromatic ring groups or to rule out the presence of large alkyaromatics. The use of a large volume of sweep gas was designed to quench the vapor products, but it apparently gave very low recovery of C_5-C_{12} products from cracking. Finally, the conversions were limited by the residence time of components in the liquid film, based on the results from the re-reaction of recovered heavy product.

2.4 Conclusions

Cracking of thin films of asphaltenes at 500°C gave significant yields of a diverse set of chemical structures, dominated by cyclic saturates and 1-3 ring aromatics. The significant yield of complex ring products can only be explained by the presence of significant mass of bridged compounds in the original asphaltene samples. The source of the asphaltene sample did not have a significant impact on the general nature of the building blocks, although small

quantitative differences were noted depending on the geographic origin of the sample. Athabasca asphaltenes precipitated using different solvents showed similar structures in terms of the constituent building blocks. The boiling curves of the cracked products did not change significantly with reaction time, suggesting that the molecular fragments that are readily removable in the early stages of reaction are not significantly different from those separated at higher conversions. A similar boiling curve was obtained when heavy material was subjected to a second round of reaction.

2.5 References

1. Yen, T. F. *Prepr.-Am. Chem. Soc., Div. Pet. Chem.* **1972**, *17*, F102.
2. Speight, J.G. Handbook of Petroleum Analysis, John Wiley & Sons Inc., New York, 2001.
3. Speight, J.G. *Oil & Gas Science and Technology – Rev. IFP* **2004**, *59*, 467-477.
4. Calemma, V.; Iwanski, P.; Nali, M.; Scotti, R.; Montanari, L. *Energy Fuels* **1995**, *9*, 225.
5. Groenzin, H.; Mullins, O. C. *Energy Fuels* **2000**, *14*, 677-684.
6. Strausz, O. P.; Safarik, I.; Lown, E. M. ; Morales-Izquierdo, A. *Energy & Fuels* **2008,** *22*, 1156–1166.
7. Payzant J. D.; Lown, E. M.; Strausz, O. P. *Energy & Fuels* 1991, 5 , 445-453.
8. Savage, P. E.; Klein, M. T.; Kukes, S. G. *Ind. Eng. Chem. Process Des. Dev.* **1985**, *24*, 1169-1 174

9. Gray, M. R. *Energy & Fuels* 2003, 17, 1566-1569.
10. Smith, C. M.; Savage P. E. *AIChE Journal* 1991, 37, 1613-1624.
11. Wiehe, I. A. *Energy & Fuels* **1994**, *8*, 536-544.
12. Jaffe, S. B.; Freund, H.; Olmstead, W. N. *Ind. Eng. Chem. Res.* **2005,** *44*, 9840-9852.
13. Behar, F.; Lorant, F.; Lewan, M. *Organic Geochemistry* **2008**, *39*, 1–22.
14. Strausz, O. P.; Mojelsky, T. W.; Lown, E. M.; Kowalewski, I.; Behar, F. *Energy & Fuels* **1999**, *13*, 228-247.
15. Rubinstein I., Spyckerelle C., and Strausz O. P. *Geochimica et Cosmochimica Acta* **1979**, *43*, 1-6.
16. Peters, K. E.; Scheuerman, G . L.; Lee, C. Y.; Moldowan, J . M.; Reynolds, R. N.; Peña, M. M. *Energy & Fuels* **1992**, *6*, 560-577.
17. Strausz, O. P.; Mojelsky, T. W.; Faraji, F.; Lown, E. M. *Energy & Fuels* **1999**, *13*, 207-227.
18. Peng, P.; Morales-Izquierdo, A.; Hogg, A.; Strausz, O. P. *Energy & Fuels* **1997,** *11*, 1171-1187.
19. Dutta, R. P.; McCaffrey, W. C.; Gray, M. R.; Muehlenbachs, K., Use of 13C Tracers to Determine Mass-Transfer Limitations on Thermal Cracking of Thin Films of Bitumen. *Energy Fuels* **2001,** *15*, 1087-1093.
20. Strausz, O. P.; Mojelsky, T. W.; Lown, E. M. *Fuel* **1992**, *71*, 1355-1363.
21. Gray, M. R.; Le, T.; McCaffrey, W. C.; Berruti, F.; Soundararajan, S.; Chan, E. et al. *Ind. Eng. Chem. Res.* **2001**, *40*, 3317-3324.
22. Qian, K.; Dechert, G. J. *Analytical Chemistry* **2002**, *74*, 3977-3983.

23. Speight, J. G.; Pancirov, R. J. *Liquid Fuels Technology* **1984**, *2*, 287-305.
24. Philp, R. P.; Bakel, A.; Galvez-Sinibaldi, A.; Lin, L H. *Org. Geochem*. **1988**, *13*, 915-926.
25. Gray, M. R.; McCaffrey, W. C.; Huq, I.; Le, T. *Ind. Eng. Chem. Res.* **2004,** *43*, 5438-5445.
26. Japanwala, S.; Chung, K. H.; Dettman, H. D.; Gray, M. R. *Energy & Fuels* **2002,** *16*, 477-484.
27. Kissin, Y. V. *Org. Geochem.* **1990**, *15*, 575-594.
28. Savage, P. E.; Klein, M. T. *Ind. Eng. Chem. Res.* **1988**, *27***,** 1348-1356.

3 Effectiveness and Mobility of Catalysts for Gasification of Bitumen Coke[1]

3.1 Introduction

Coke is one of the by-products of oil sands upgrading in Alberta, Canada, and from the refining of heavy oil at many refineries world wide. Due to the high cost of transportation of coke from remote locations in Canada, over 64 million tons have accumulated by the end of 2009, which shows a 12.3% increase from the previous year (1). Gasification is a well-established technology for the conversion of carbonaceous materials to hydrogen or synthesis gas. However, the high temperature and pressure required in modern gasification technologies increases the capital and operating costs of the process considerably (2). Addition of catalysts to promote the gasification reactions is a promising means of reducing the reaction temperature significantly (3, 4), thereby reducing the severity of the reactor conditions and the cost of the process.

Salts and oxides of alkali metals and alkaline earth metals, as well as some transition metals can catalyze the gasification reactions of a range of carbon materials (3). High sulfur content, as in petroleum cokes, eliminates the possible application of transition metals. In low rank coals and biomass, the open structure and surface functional groups enable the addition of catalysts by aqueous

[1] The contents of this paper have been published as: Karimi, A.; Gray, M. R. *Fuel* **2011**, *90*, 120-125

impregnation and ion exchange (5). In lower rank coals, the combination of lower surface area and significant ash content makes the use of catalyst less attractive. In contrast, petroleum cokes offer very low porosity, but offer the potential to add catalysts or precursors to the liquid vacuum residue fraction prior to coking. This alternate mode of addition, coupled with the low ash content of petroleum cokes, may make catalysis more attractive. Some evidence suggests, however, that alkali metal compounds may be mobile enough at gasification temperatures that the mode of catalyst addition may not be significant (3, 6, 7).

In this study we examine the catalytic steam gasification of coke prepared from the vacuum residue fraction of bitumen from Alberta's oil sands. Hydrogen production by steam gasification as well as availability of industrial steam make this gas attractive for industrial implementation of gasification processes. Therefore, gasification with other reactant gases was not considered in this research. Based on a number of criteria including cost and availability for industrial-scale application, physical and chemical stability at high temperatures, and non-corrosiveness, several compounds were selected to test for catalytic activity for the steam gasification of bitumen coke. The effectiveness of a range of alkali metal and alkaline earth metal compounds and the potential benefit of adding the catalyst to liquid bitumen fractions prior to coke formation are investigated. This study allows a comparison of the performance of catalytic additives that are well known from prior work on gasification of coal, to a high-sulfur petroleum coke derived from bitumen.

3.2 Materials and Methods

3.2.1 Bitumen fractions

The vacuum residue fraction of Athabasca bitumen (542°C+ fraction, referred to as Athabasca vacuum residue, or AVR hereafter) was used as received from Syncrude Canada Ltd. for the preparation of the coke samples. Table 3-1 shows the data on composition of AVR and the coke. The elemental analysis was performed by a Vario MICRO cube elemental analyzer (Elementar Analysensysteme, GmbH, Hanau, Germany). The ash mainly consisted of silicon and aluminum (remaining solid particles from extraction of bitumen from oil sands), as well as iron (most likely from the corrosion of processing and transfer equipment) and vanadium (from bitumen) as detected by EDX.

Table 3-1. Ultimate analysis of AVR and coke.

	C	H	N	S	Balance*
AVR	81.7 ± 0.2	9.2 ± 0.1	0.7 ± 0.1	6.3 ± 0.1	2.1
Coke	81.4 ± 2.5	4.0 ± 0.2	1.8 ± 0.1	6.8 ± 0.1	6.1

* Includes ash, moisture, and oxygen content.

3.2.2 Alkali metal and Alkaline earth metal compounds

The catalytic materials used were as-received reagent grade (≥ 99.0%) sodium and potassium carbonates (Sigma-Aldrich), potassium chloride (BDH Chemicals), calcium carbonate (ACP Chemicals), calcium oxide (Anachemica), and magnesium oxide (GPR, BDHG).

3.2.3 Preparation of coke

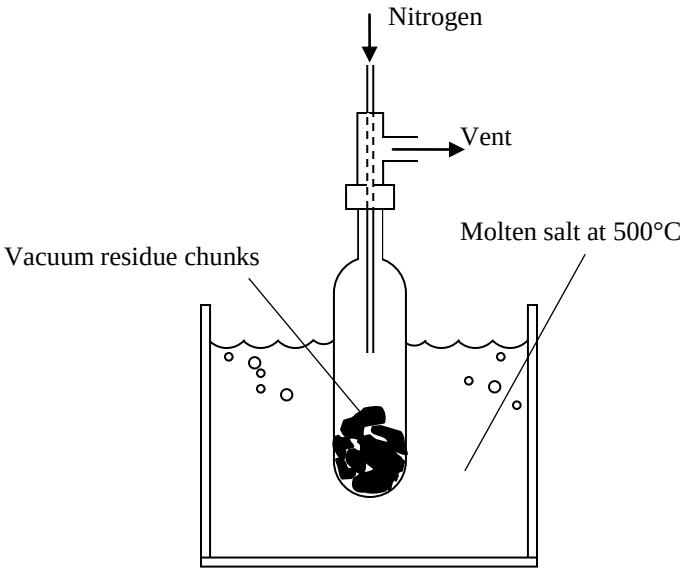

Figure 3-1. Schematic diagram of the apparatus used for the pyrolysis of vacuum residue into coke

A 50 ml quartz flask was loaded with 5-7 g of vacuum residue. A 500 ml/min nitrogen flow through a 1/8" stainless steel tube inserted half way into the flask through the ½" neck was used to purge the air from the flask and carry the pyrolysis products away through the union junction connected to the flask by a Swagelok Ultra-Torr vacuum fitting. The flask was immersed into a molten salt bath[2] maintained at 500°C for 15 min (Figure 3-1). The apparatus allowed for some recycling of the thermal cracking product vapors by condensing back to flask upon contact with the upper part of the flask which remained cold. The coke was then washed with excess toluene to remove any remaining lighter products of

[2] The application of molten salts must be under a ventilated area (fume hood) as a safety precaution. Proper protective outfit (temperature-resistant gloves, face shields, etc.) must be used.

the cracking reactions (tars). The toluene was removed by decanting and the coke was left under a fume hood overnight to let the residual toluene evaporate.

When the catalyst was premixed with the vacuum residue, the vacuum residue was melted at 70-100°C, then the catalyst powder was added at a ratio of 0.7 mol of cation per kg AVR followed by stirring vigorously using a spatula as the mixture cooled down. The sample was subsequently left in a freezer at –18°C to solidify. The brittle frozen mixture was then broken into small pieces (< 5 mm).

The obtained coke was ground into a fine powder by a mortar and pestle. In the case of premixed coke and catalyst samples, 2-3 batches of the coke were mixed to maximize uniformity. In the case of samples of coke admixed with catalyst, the catalyst was added to the coke before grinding at a ratio of 2.4 mol of cation per kg coke to achieve an equivalent concentration in both the premixed and admixed cases, considering a 30% coke yield from AVR. The measured coke yields varied between 29-37%, as complete recovery of the coke from the flasks was not possible.

3.2.4 Gasification of coke samples

The gasification experiments were conducted at near atmospheric pressure in a tubular (¾" x 2') quartz reaction chamber, which was placed horizontally in a tubular furnace (Trans-Temp Furnace, Thermcraft Inc., Winston-Salem, NC) at 600-800 °C. The chamber was purged for 10 min with a nitrogen flow (0.35 sL/min), which also served as the carrier gas for steam during the experiment. The steam was generated by injecting deionized water by a peristaltic pump (at ~2.5

mL/min) into a heated coil maintained at 400°C. The partial pressure of steam thus produced was ca. 90 kPa. Coke samples of 30-40 mg were loaded in ceramic combustion boats and covered with a thin layer of quartz wool to protect the coke particles from entrainment with the gas flow. The mass loss of the sample after reaction was used to determine the conversion, according to the following relationship:

$$\text{coke conversion\%} = \frac{\text{mass loss}}{\text{coke content of the sample}} \times 100\% \qquad (3.2\text{-}1)$$

This equation assumed no conversion of the catalyst during the reaction. The length of all gasification reactions was 30 minutes.

The evolved gases were collected in gas bags after the excess steam was condensed. The gas bag was then connected to a gas chromatograph for analysis of the product mixture (SRI Instruments 8610C GC equipped with two 6-ft columns of silica gel and molecular sieve 13X packings and a thermal conductivity detector). The GC had a sample loop volume of 1 ml with a flow of helium at 32 psi. The temperature was initially held constant at 40 °C for 4 min followed by ramping to 220 °C at 10 °C/min. The sequence of the columns was switched after 7 min to allow for the elution of CO_2.

3.2.5 Leaching experiments

To quantify the extent of diffusion of potassium and sodium species in the coke particles, a series of leaching experiments were performed. A measured mass of 2.4 (mol cation)/(kg coke) coke-catalyst mixtures was added to 50 g of deionized water and stirred to make a 2.9 mN solution of the salt. The

conductivity of the solution was measured after at least 24 h using a conductivity meter (Jenway 470, Bibby Scientific, Staffordshire, UK) with a meter coefficient of K = 0.90. Deionized water was added to make up for evaporation. The conductivity was constant after one day. Standard solutions were prepared by adding the same amount of salt present in the corresponding coke-catalyst sample to 50 g of water to calibrate the conductivity measurements. The difference between the conductivity of the coke-catalyst in water solutions and the corresponding standard solution (i.e. the amount of missing salt) was a direct measure of the amount of salt within the coke particles that could not be redissolved in water, assuming linear relationship between the concentration and the conductivity.

3.2.6 Characterization of catalyst-coke samples

Scanning electron microscopy (SEM) images (Hitachi S-2700 SEM, Hitachi High-Technologies, Toronto) as well as energy dispersive x-ray (EDX) spectra (Princeton Gamma-Tech PRISM IG EDX spectrometer, Princeton, NJ) were obtained from the samples to analyze the dispersion of the catalysts in the coke. The particles were coated with carbon before analysis. The semi-quantitative EDX analyses were conducted at relatively flat areas on the particles, where back-scattered electron SEM images showed less impurity present. TEM images and diffraction patterns (JEOL 2010 TEM at 200 kV, JEOL Ltd., Tokyo), as well as X-ray diffraction spectra (Geigerflex 2173 with Co Kα incident beam, Rigaku Americas, The Woodlands, TX) were obtained from the samples to identify any possible crystalline structures in the samples.

3.3 Results and Discussion

3.3.1 Gasification results

Table 3-2 lists the conversions of various coke-catalyst samples from gasification with steam. Standard deviations are based on triplicate experiments.

Table 3-2. Comparison of the activity of alkali metal and alkaline earth metal compounds as catalysts for gasification at 800°C for 30 min with ca. 90 kPa partial pressure of steam; Each compound was premixed with AVR at a ratio of 0.7 mol cation/kg AVR

Catalyst	Weight% in Coke	Conversion %
No catalyst	NA	35 ± 8
MgO	8.8	29.7 ± 3.0
CaO	11.8	27.0 ± 7.7
$CaCO_3$	19.4	35.6 ± 2.1
KCl	15.3	81.3 ± 1.8 (77)*
Na_2CO_3	11.2	95.6 ± 5.4
K_2CO_3	14.2	99.3 ± 1.4

* Corrected conversion of coke was 77 ± 1.7% based on complete hydrolysis of KCl into KOH. Mass loss due to possible evaporation of KOH could not be distinguished from the mass loss by gasification of the coke.

Potassium and sodium carbonates gave very high conversions. The differences in conversions with $CaCO_3$, CaO, and MgO catalysts as well as the uncatalyzed reaction at 800°C after 30 min of reaction time were insignificant.

Based on the observations of hydrolysis of halide salts, Wood and Sancier (1984) proposed the likelihood of inactivity of halides as catalysts for gasification and commented further that catalytic compounds for gasification require oxygen atoms in their anions (3). Veraa and Bell (1978) reported that alkali metal chlorides inhibited the reaction at early stages, but weakly promoted it in later stages (8). In the current study, the conversion with KCl at 700°C was negligible (9.9 %) and no chlorine was detected in the remaining sample using EDX. The absence of chlorine was consistent with hydrolysis (3) as a result of the contact with steam:

$$KCl + H_2O\ (g) \rightarrow KOH + HCl\ (g) \qquad (3.3\text{-}1)$$

A portion of the mass loss for this sample at 800°C could be due to vaporization of KOH, as the temperature is much higher than the melting point of KOH (420°C). Hence the real conversion due to gasification with KCl at 800°C must be smaller than the reported conversions in Table 3-2, which are based on mass of sample plus catalyst.

Analysis of gases from the gasification experiments by GC confirmed the production of hydrogen as well as CO_2 (Table 3-3). Carbon monoxide was present only in trace amounts, which suggests that the water-gas shift reaction (reaction (1.2-4)) was strongly promoted by the catalysts. Therefore, the following reaction scheme would be expected:

$$C + H_2O \rightarrow CO + H_2 \qquad (3.3\text{-}2)$$

$$CO + H_2O \leftrightarrows CO_2 + H_2 \qquad (3.3\text{-}3)$$

from which the hydrogen to CO_2 ratio should be 2. However, the ratio was typically greater than 2 (on average ca. 2.5). The difference was likely due to the absorption of a portion of the produced CO_2 in the steam condensates present in the path of the gases as they exited the reaction chamber. Small amounts of methane were also present in the gases. The concentration of methane was higher in the cases with less conversion, which was consistent with methane evolving from further pyrolysis of the coke prior to gasification reactions. Higher yields of methane would require higher reaction pressures (9).

Table 3-3. Normalized average concentrations of reaction product gases in mol percent over the first 20 min of steam gasification

Catalyst:	K_2CO_3		Na_2CO_3	
Temperature:	600°C	700°C	600°C	700°C
Hydrogen	70.3 ± 1.4	68.3 ± 0.4	63.9	71.5 ± 0.7
Carbon dioxide	27.2 ± 1.8	29.5 ± 0.3	29.0	25.9 ± 0.5
Carbon monoxide	ND*	1.9 ± 0.1	1.0	1.8 ± 0.1
Methane	2.5 ± 0.4	0.4 ± 0.1	6.1	0.7 ± 0.2

* ND: Not Detected (< 1ppm in the gas sample)

To examine the effect of adding the catalytic salts before (premixing) or after coking (admixing), a series of gasification experiments were performed. Figure 3-2 compares the effect of mixing method on the conversion of K_2CO_3-coke samples. The difference in conversion between the two sets of samples at a given temperature was insignificant. The error was larger for the premixed

samples due to the variability in the yield of coke from the AVR, which could alter catalyst loading by up to 25%.

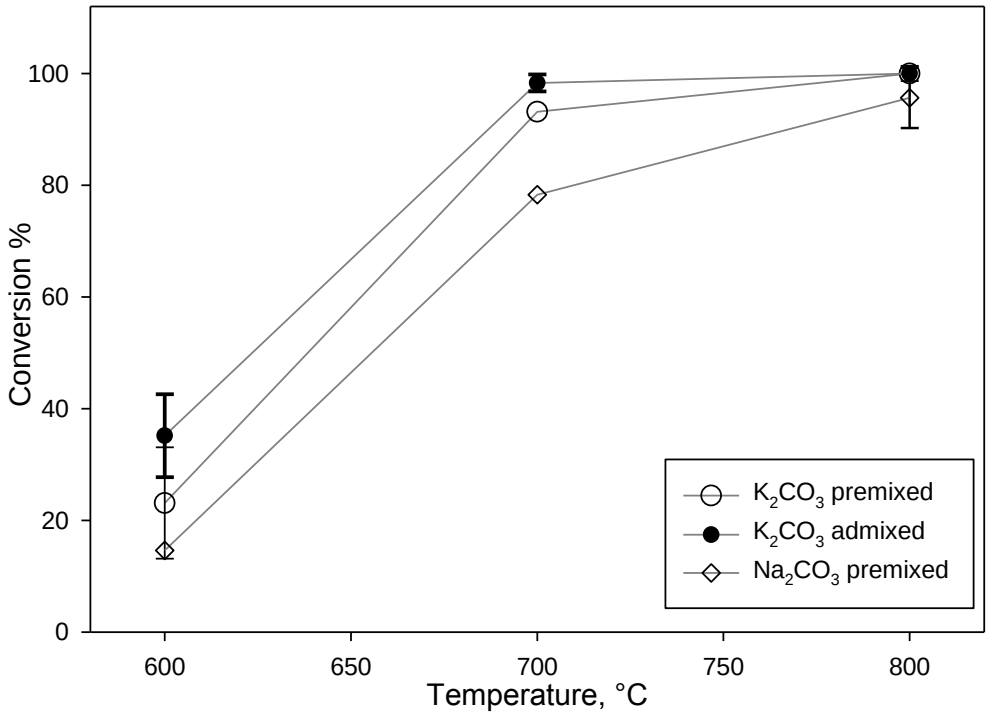

Figure 3-2. Conversions of coke by steam gasification for 30 min with ca. 90 kPa partial pressure of steam and a catalyst loading of 0.7 mol cation/kg AVR precursor (equivalent to 14.3% wt in coke for K_2CO_3 and 11.2%wt for Na_2CO_3); Error bars for experiments with K_2CO_3 are standard deviation from triplicate experiments

3.3.2 Characterization of coke materials

EDX spectra from the samples confirmed that potassium and sodium salts were highly mobile at 500°C and higher temperatures. Figure 3-3 shows the SEM image of a region of glossy non-porous surface on a particle of coke from bitumen

that had been premixed with K_2CO_3. The EDX line scan for potassium along the particle confirms that potassium was relatively uniformly spread over the coke particle. A similar trend was seen with the coke sample from AVR that had been premixed with KCl. In the case of addition of Na_2CO_3, the intensity of the spectrum for Na was weaker, due to its smaller atomic mass, but the line scan confirmed that Na was uniformly distributed in this sample.

In contrast, the SEM/EDX analysis of coke from AVR premixed with $CaCO_3$, CaO, and MgO showed that Ca and Mg were present in the coke particles only as relatively large distinct crystals with little contact with the coke or trapped inside it. Almost no calcium or magnesium could be detected by EDX away from the crystals in the coke (Figure 3-4). These observations explain the differences observed in the gasification rates with different catalysts; potassium and sodium carbonates which maintain a very good contact with the coke provided the highest gasification rates, whereas with Ca and Mg compounds – which showed no mobility and hence poor contact with the coke – the conversions were similar to uncatalyzed reaction.

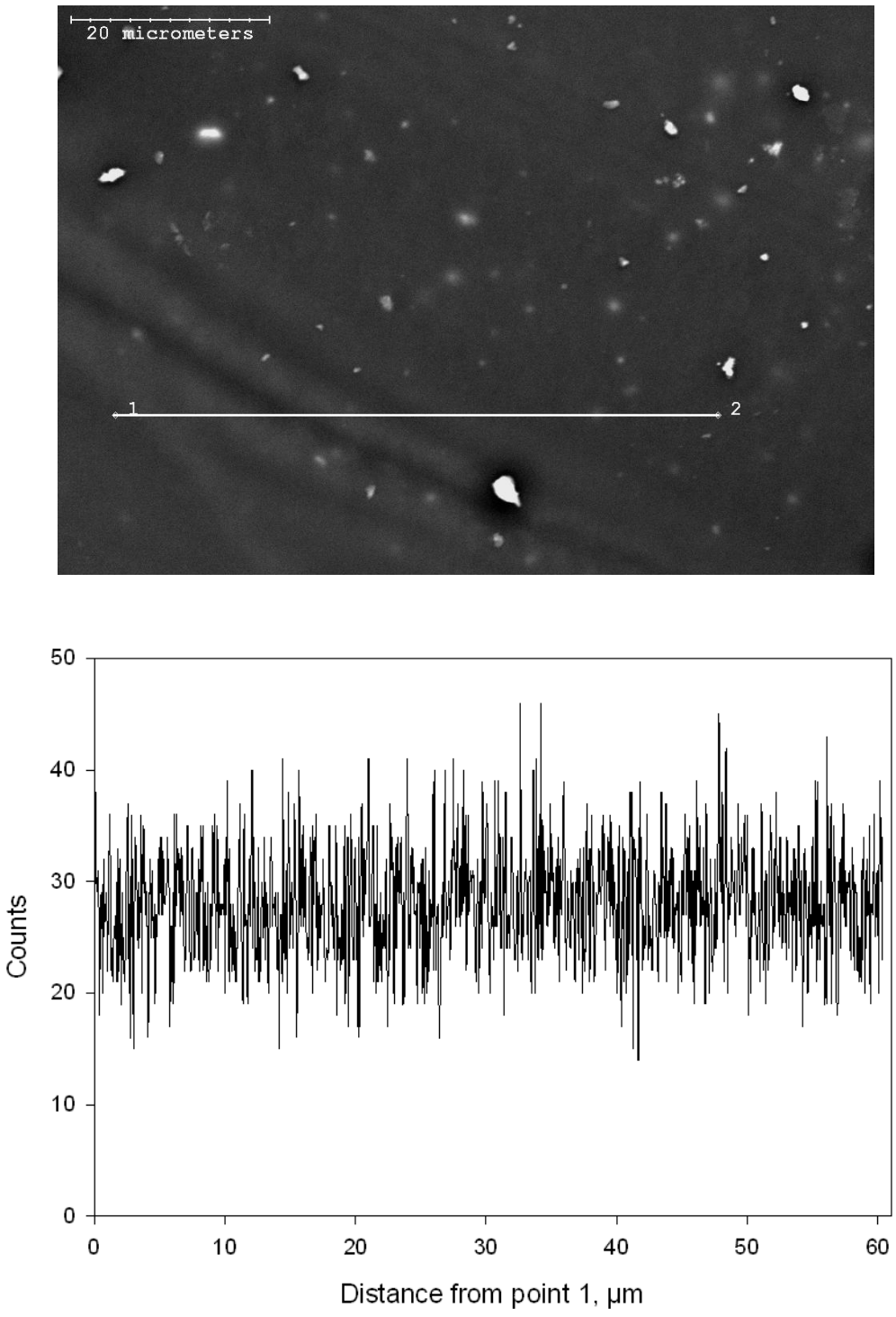

Figure 3-3. Top: Back-scattered electron SEM micrograph of the surface of a K_2CO_3 premixed coke particle; Bottom: EDX line scan profile for potassium along the line between points 1 and 2 on the micrograph

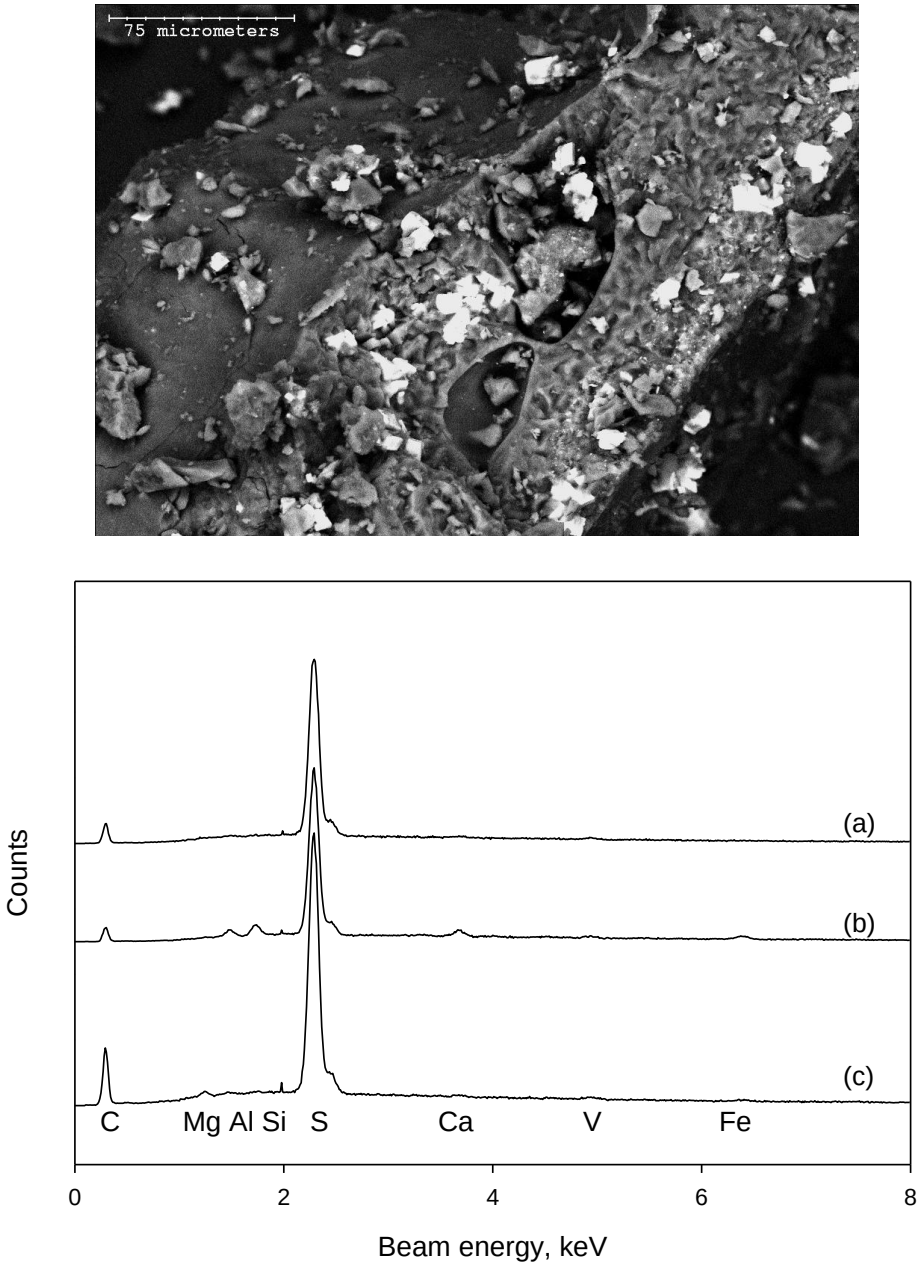

Figure 3-4. SEM/EDX analysis of alkaline earth metal compounds premixed coke samples.

Top: back-scattered electron micrograph of a $CaCO_3$ premixed coke particle. Bottom: (a) EDX spectra at points on the surface of the coke particle (dark areas) in the same sample, (b) a similar point on a CaO premixed coke particle, (c) a similar point on a MgO premixed coke particle.

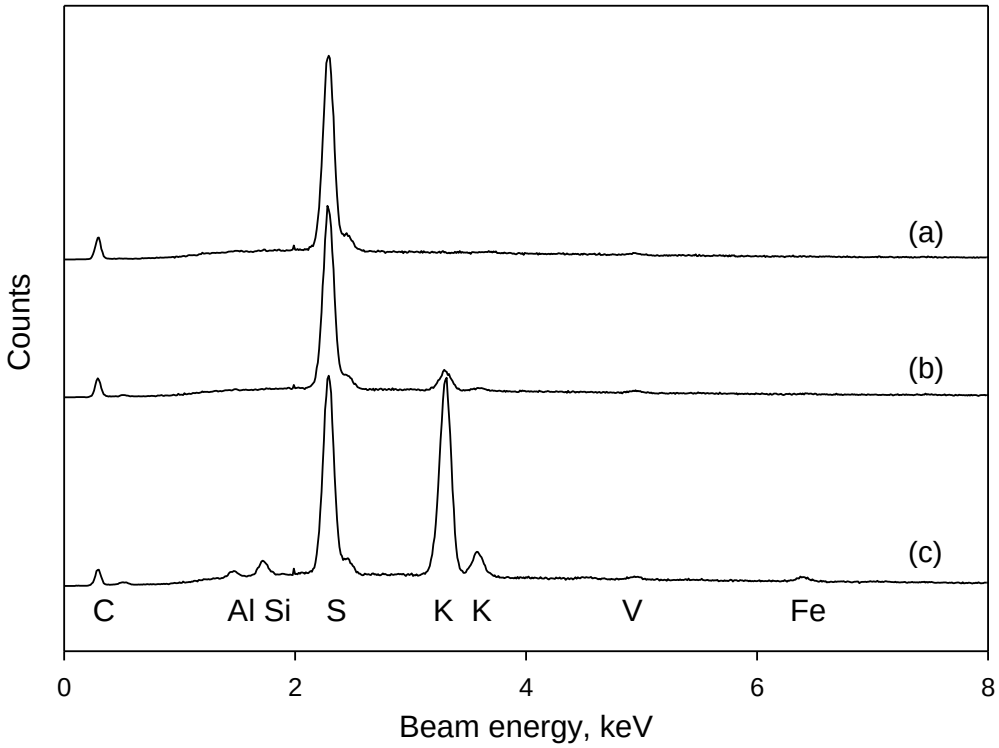

Figure 3-5. EDX spectra at points on the surface of coke particles with no visible particles of catalyst. K_2CO_3 was admixed with coke and analyzed: (a) before heating, (b) heated at 500°C for 15 min, (c) heated at 600°C for 15 min.

When the salt was premixed with the vacuum residue precursor prior to coking the salt was well distributed in the resulting coke. At temperatures of 500-600°C under nitrogen the alkali metals were mobile in the coke particles. As illustrated in Figure 3-3, zones of coke that had no visible salt particles developed a significant concentration of potassium upon heat treatment. When alkali metal salts were mixed with coke particles (after coking of AVR), spreading of the salts was observed at a sufficiently high temperature (Figure 3-5).

The mobility of the alkali metals was further tested by leaching coke samples with water to dissolve external salts. EDX spectra of samples of coke premixed and admixed with K_2CO_3, heated up to 600°C, then thoroughly washed with water still showed considerable amounts of potassium in the coke (Figure 3-6). Given the non-porous morphology of the coke particles, the latter observation could only be explained by the migration of potassium species into the coke particles. Not only did the alkali metal salts spread on the surface of the coke, but the metal also diffused into the coke. Yokoyama et al. (1980) studied samples of K_2CO_3-doped amorphous carbon heated under vacuum at 650°C by XPS (10). They noted that part of the K_2CO_3 decomposed into K_2O and CO_2, while the former reduced in contact with carbon to metallic K, which "sank" into bulk carbon. Among the mechanisms suggested for the interaction of alkali metal salts with carbon to describe their catalytic activity in gasification (3), intercalation of the alkali metal in the carbon structure may be a reasonable explanation for the diffusion of the K_2CO_3 into the coke, as observed in the present study.

Based on semi-quantitative EDX analyses of several samples of K_2CO_3 admixed with coke then heated for different times, the diffusion phenomenon appeared to be faster than gasification. Figure 3-6 illustrates a semi-quantitative measure of the heating-time dependence of the diffusion of potassium species into coke. The concentration of carbon, hydrogen, and other light elements in coke could not be reasonably measured by EDX. Therefore, since the concentration of sulfur in the coke is expected to be relatively constant, the ratio of the

concentrations of potassium to sulfur (K/S) by EDX was used as a measure of the concentration of potassium in the coke near the surface. The concentration of potassium reached a final value within 2-3min.

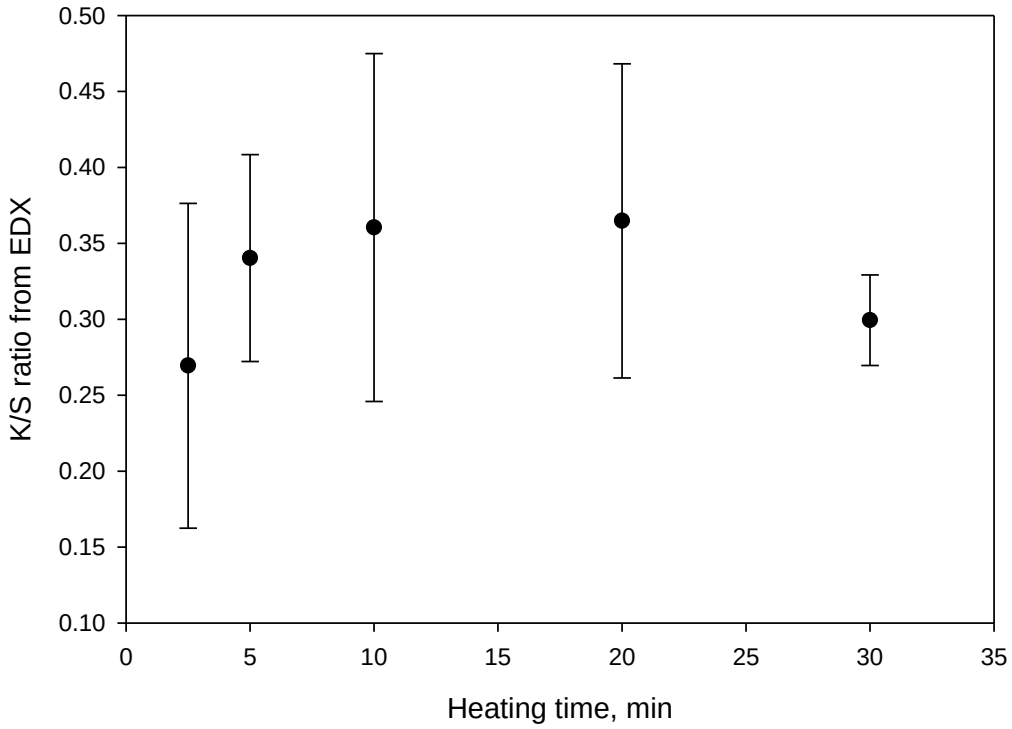

Figure 3-6. Semi-quantitative potassium to sulfur ratios by EDX in samples of coke admixed with K_2CO_3 and washed after heating at 600°C.

Table 3-4 shows the results of the leaching experiments of salt-coke mixtures. When the salts were mixed with the AVR prior to coking, the amount of salt retained after leaching was in the series K_2CO_3 > Na_2CO_3 > KCl, which was the same as the sequence of activities of these compounds as catalysts for gasification (Table 3-2). The salt retained in the coke would include salt particles within the impermeable coke matrix as well as any alkali metal that diffused into

the coke. The significant difference between these premixed samples was likely due to a larger amount potassium diffused into the coke from potassium carbonate. Therefore, these results once again confirm the importance of the intrinsic mobility of the compounds for a successful catalytic activity in gasification, as noted by previous researchers (3, 11, 12).

Table 3-4. Amounts of alkali metal salt retained in the coke after leaching with water using the conductivities of 2.4 mol cation/kg coke samples added to 50 g of water to make a 2.9 mN solution equivalent to complete dissolution of the salt compared to the standard solution of the same salt.

Description	% salt retained by coke
KCl premixed in with AVR then coked at 500°C for 15 min	11
Na_2CO_3 premixed in AVR then coked at 500°C for 15 min	27
K_2CO_3 premixed in AVR then coked at 500°C for 15 min	46
K_2CO_3 admixed with coke without heating	12
K_2CO_3 admixed with coke then heated at 500°C for 15 min	20
K_2CO_3 admixed with coke then heated at 600°C for 15 min	33

The amount of salt retained in the coke after heating the admixed samples was lower than premixed samples, but both types of samples gave similar catalytic activity (Figure 3-2), indicating that the effective concentration of the catalyst on the surface of the coke was equivalent.

Although the analyses mentioned above confirmed the existence of potassium and sodium species in the coke particles from premixed and

admixed/heated samples after washing, the chemical structure and composition of the diffused portion was not determined. The X-ray diffraction pattern (Figure 3-7) of the K_2CO_3 premixed sample did show some of the bands corresponding to K_2CO_3 which disappeared after washing the solution with water (Figure 3-7). The patterns were otherwise similar to that of the sample without the catalyst. Therefore, the K_2CO_3 material in the premixed sample which gave a crystal diffraction in the XRD pattern was the undiffused portion of the salt. The portion of the salt material that diffused into the coke either had no crystal structure or did not have a sufficient concentration for the XRD analysis. Similarly, TEM images and diffraction patterns (Figure 3-8 shows an example of the TEM images) of the washed sample did not show any indication of any observable crystalline structure due to potassium species residing in the coke particles.

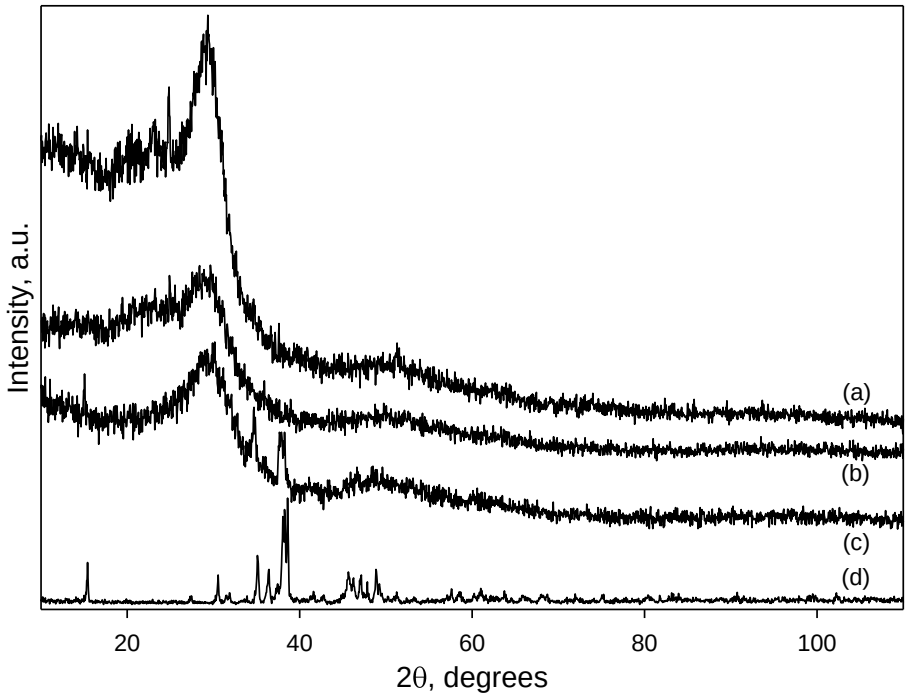

Figure 3-7. XRD patterns of: Plain coke (a); K_2CO_3 premixed coke after leaching (b); K_2CO_3 premixed coke before leaching showing bands due to the salt (c); K_2CO_3 powder(d)

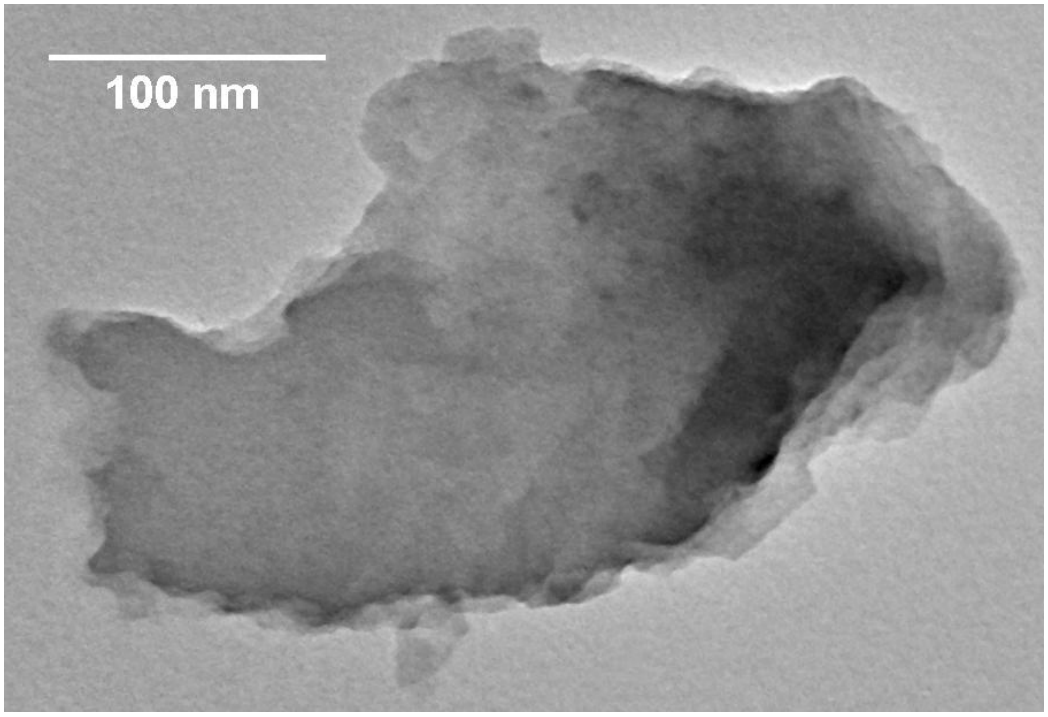

Figure 3-8. TEM micrograph of a K_2CO_3 premixed coke particle after leaching;

Localized EDX spectra on different regions of the particle confirmed the existence of potassium all over the particle with no apparent crystalline structure

Alkali metals can also form intercalation complexes with many (poly-) aromatic compounds as well (13) Therefore, a possible explanation for the migration of the K species into the coke is by formation of potassium intercalate-like structures in condensed aromatic layers of carbon in coke. Wigmans et al. (1983) attributed an observation of no catalytic activity at very low catalyst loadings to the inaccessibility of the catalyst to the reactant gas as a result of the formation of potassium intercalate compounds (14).

3.4 Conclusions

Potassium and sodium carbonates showed the highest activities among the compounds tested as steam gasification catalysts for coke from oil sands bitumen. KCl also showed a high catalytic activity at 800°C, but no activity at 700°C. Chlorine had disappeared from the EDX spectrum after the latter test, likely by hydrolysis. $CaCO_3$, CaO, and MgO did not show any catalytic activity. Further investigation revealed that these compounds were incapable of providing sufficient contact with the coke and steam due to lack of mobility. The metals from K_2CO_3, Na_2CO_3, and KCl were highly mobile in the coke material, which was consistent with their high activities as gasification catalysts relative to the alkaline earth metals. Due to the high mobility of the catalytic species on the coke, a significant difference was not observed in the gasification rate of the samples in which the salt was mixed with the vacuum residue prior to pyrolysis (premixed samples) with those in which the coke was mixed with salt after the coking (admixed samples). A portion of the alkali metal species migrated into the non-porous coke particles, but gave no evident crystalline structure.

3.5 References

1. Energy Resources Conservation Board. Report on Alberta's Energy Reserves 2009 and Supply/Demand Outlook 2010-2019 (Document #St98-2010). Retrieved from http://www.ercb.ca/docs/products/STs/st98_current.pdf on 13/7/2010
2. Higman, C.; van der Burgt, M. Gasification. 2nd ed., Amsterdam: Elsevier; 2008.

3. Wood, B. J.; Sancier, K. M. *Cat Rev Sci Eng* **1984**, *26*, 233-279.
4. Sheth, A. C.; Sastry, C.; Yeboah, Y. D.; Xu, Y.; Agarwal, P. *Fuel* **2004**, *83*, 557-572.
5. Tomita A. *Catal. Surv. Jpn.* **2001**, *5*, 17-24.
6. Mims, C. A.; Chludzinski Jr., J. J.; Pabst, J. K.; Baker, R. T. K. *J. Catal.*, **1984**, *88*, 97-106.
7. Spiro, C. L.; McKee, D. W.; Kosky, P. G.; Lamby, E. J. *Fuel* **1984**, *63*, 686-691.
8. Veraa, M. J.; Bell, A. T. *Fuel* **1978**, *57*, 194-200.
9. Epperly, W. R.; Siegel, H. M. Catalytic coal gasification for SNG production. In: Proceedings of the 11th intersociety energy conversion conference, New York: AIChE, **1976**, 249-253.
10. Yokoyama, S.; Tanaka, K.; Toyoshima, I.; Mihyahara, K.; Yoshida, K.; Tashiro, J. *Chem. Lett.* **1980**, *5*, 599-602.
11. Otto, K.; Bartosiewicz, L.; Shelef, M. *Fuel* **1979**, *2*, 565-572.
12. Sharma, A.; Saito, I.; Takanohashi, T. *Energ. Fuel* **2008**, *22*, 3561-3565.
13. Wen, W. Y. *Cataly. Rev.* **1980**, *22*, 1-28.
14. Wigmans, T.; Elfring, R.; Moulijn, J. A. *Carbon* **1983**, *21*, 1-12.

4 Kinetics of Catalytic Steam Gasification of Bitumen Coke[1]

4.1 Introduction

Large quantities of coke from the upgrading of oil sands bitumen are being stockpiled in northern Alberta (1). Therefore, gasification is of interest for utilizing this resource. Gasification reactivities of coals and chars are a function of the porosity (hence the surface area), crystal structure of the fixed carbon, as well as the catalytic effect of the ash (2). Petroleum cokes, including bitumen coke, are relatively non-porous, in contrast to most coals and active carbons, which have been predominant in studies of gasification kinetics. This low porosity may explain the generally lower reactivity of petroleum cokes (2). Therefore, extreme gasification conditions are needed to achieve a high conversion of coke from oil sands coke bitumen (3).

Addition of a range of alkali and alkaline earth metals to carbonaceous materials is known to enhance gasification reactions (4), but the high ash content of coal renders the recovery of such additives difficult. In contrast, petroleum coke has low ash content, and a greater potential for rate enhancement than coals and chars. Despite the known capacity of catalysis for increasing the rate of gasification (4, 5), making relatively low temperature operation possible, few published studies have addressed the catalytic gasification of coke from bitumen.

[1] The contents of this chapter have been published as: Karimi, A.; Semagina, N.; Gray, M. R. *Fuel*, *Article In Press* (2010), doi:10.1016/j.fuel.2010.12.006.

Ueda et al. (6) investigated the catalytic effect of alkaline earth metal compounds on gasification of bitumen coke in a fluidized bed reactor. Furimsky and Palmer (7) used a lignite ash containing Ca, Mg, Ba, Fe, and Ni oxides as catalyst with both delayed and fluid cokes from Alberta oil sands in a fixed bed reactor. They found the ash to affect the gasification at 930°C, but not at 830°C. Watkinson et al. (8) studied the addition of potassium carbonate to coke in a fluidized bed gasifier at temperatures above 869°C. The highest conversion that they achieved in their catalytic experiments was 92.6%, apparently including burn off with oxygen. The residence time of the cokes in the reactor was not stated.

The kinetics of catalytic gasification reactions have been widely studied (9), although the mechanism of gasification reactions is still a subject of ongoing studies (2). While some researchers believe that the catalyst only increases the number of active sites on the carbon surface rather than altering the kinetic path (10), it has also been suggested that the catalyst changes the identity and reactivity of the surface intermediates (11). Several mechanisms have been proposed to explain the catalytic action of alkali metals towards gasification reactions (3), ranging from oxygen transfer mechanisms such as reduction-oxidation cycles (12) to electrochemical schemes and mechanisms involving free radicals. Wen (13) suggested a variation of the original reduction-oxidation cycle proposed by McKee and Chatterji (12), which required the formation and participation of alkali metal intercalation compounds as an essential step for the cycle. A modification of the oxidation-reduction cycle mechanism was introduced by Wigmans et al. (14) which involved the participation of metallic potassium and

the formation of an oxygen-carbon intermediate compound in the cycle. More recently, Wang et al. (15) suggested an alternative form of this scheme which postulated that potassium would participate only in oxidized form based on the work of Saber et al. (16).

In Chapter 3 (17) the catalytic effect of several compounds on steam gasification of bitumen coke was compared. As in studies of coal gasification, both potassium carbonate and sodium carbonate were effective catalysts. In both cases, the alkali metal rapidly diffused through the coke, so that the catalytic benefit was insensitive to the mode of addition of the catalyst (either premixed with vacuum residue or admixed to the coke). In this chapter, the kinetic behavior of bitumen coke during catalytic steam gasification using potassium and sodium carbonates in the temperature range of 650-800°C is examined. The originally non-porous coke material facilitated the determination of reaction rates in the absence of mass transfer limitations induced by pore diffusion restrictions or clogging of the pores by the mobile catalysts.

4.2 Materials and Methods

4.2.1 Characteristics of the raw materials

Vacuum distillation tower bottoms (524°C+ boiling cut) of Athabasca bitumen (referred to as Athabasca vacuum residue, or AVR) were provided by Syncrude Canada Ltd. Table 4-1 shows the composition of the AVR. Reagent

grade (≥ 99.0%) sodium and potassium carbonates (Sigma-Aldrich) were used as catalyst as received.

Table 4-1. Ultimate analysis of AVR and coke

	C	H	N	S	Balance*
AVR	81.7	9.2	0.7	6.3	2.1
Coke	81.4	4.0	1.8	6.8	6.1

* Includes ash, moisture, and oxygen content.

4.2.2 Sample preparation

The coke samples were prepared as described earlier (17). In brief, a 50 ml quartz bottle was loaded with 5-7 g of vacuum residue and air was purged from the bottle by a flow of nitrogen gas (ca. 500 ml/min). The bottle was then immersed in a molten salt bath maintained at 500°C for 15 minutes. The resulting coke was subsequently washed with toluene to remove any remaining lighter products of the cracking reactions. After drying the coke, it was ground by a pestle and mortar and sieved (Fisher Scientific W. S. Tyler 100, 170, 270, and 400 mesh standard test sieves complying with ASTM E-11 standard) into 5 size ranges: < 38 µm, 38–53 µm, 53–90 µm, 90–120 µm, and > 120 µm. Sodium carbonate was premixed with the AVR prior to coking in the case of the samples used for the tests to verify the absence of mass transfer limitations. In all other experiments the appropriate proportion of the catalytic salt was added to the sieved coke particles followed by the addition of a few droplets of water to evenly distribute the catalyst in the subsamples. The water was then evaporated at circa 150°C.

4.2.3 Gasification experiments

A Thermo Cahn Thermax 300 thermogravimetric analyzer (TGA) was used to carry out the gasification experiments at atmospheric pressure. A flow of argon gas (Praxair grade 5.0) was used as sweep gas. The steam generator consisted of a 300W rod heater inserted into an insulated ½" stainless steel tube at the gas inlet of the TGA. Deionized water was pumped onto the heating rod which was controlled at a temperature circa 300°C. The flow of argon gas then carried the steam to the reaction chamber of the TGA, through heat-traced tubing to avoid condensation. The carrier gas and water flow rates were chosen between 69-150 ml/min and 0.170-0.303 ml/min respectively, to produce steam partial pressures between 60-85 kPa. Steam flow was started after the desired isothermal temperature was reached and the mass loss due to devolatilization of the coke became negligible. The specific rates of gasification ($r = \frac{-1}{m}\frac{dm}{dt}$) were calculated based on the mass of ash and catalyst-free devolatilized coke.

The output gases were continuously analyzed by a Thermo Scientific Nicolet 6700 FTIR spectrometer and intermittently by a SRI Instruments 8610C gas chromatograph (GC, equipped with two 6 ft silica gel and molecular sieve columns and a thermal conductivity detector). The temperature of the columns was held constant at 75 °C for 3 min to allow for elution of H_2 at ca. 1.6 min followed by ramping to 220 °C at 75 °C/min for fast elution of all other gases from the columns. The carrier gas for GC analyses was nitrogen (Praxair grade 5.0).

4.2.4 Characterization of the samples

BET measurements were performed using an Autosorb-1 physisorption station (Quantachrome Instruments). Samples were degassed at 200°C until an out gas pressure rise rate of less than 10 μm Hg min^{-1} (typically 1-3 μm Hg min^{-1}) was achieved. The 7-point BET equation was used for the calculation of the specific surface areas. Krypton and nitrogen gas flows were used for low and high surface area samples, respectively. The tests were carried out at liquid nitrogen temperature. The partially gasified samples were washed with distilled water and dried at room temperature overnight to remove the catalyst.

Scanning electron microscopy was performed using a Hitachi S-2700 SEM (Hitachi High-Technologies, Toronto). The particles were carbon-coated prior to analysis.

Secondary Ion Mass Spectrometry (SIMS) was performed on flakes of coke heated in a furnace under nitrogen atmosphere with an excess amount of K_2CO_3 at 600°C for 15 min. Depth profiling of a coke-catalyst sample was performed using a time-of-flight secondary ion mass spectrometer (TOF-SIMS IV – 100, ION-TOF GmbH) with an O_2 sputtering ion source and a liquid metal Ga analysis ion source at 25 keV.

4.3 Results and Discussions

4.3.1 Verification of kinetic control of coke conversion

A typical mass loss curve is illustrated in Figure 4-1, where reaction time was counted from the introduction of steam to the TGA. The initial rate was

determined by linear regression of the data points between 2-5 minutes of gasification, leaving out the fluctuations due to starting the steam flow in the first minute. Experiments showed that up to at least 10 mg of initial sample mass there was no gas-solid mass transfer limitation (Table 4-2). Initial mass of the samples for all subsequent tests were therefore maintained in the range of 7.0-7.5 mg to avoid gas-solid mass transfer limitations in the sample pan. The initial gasification rate was also not affected by the gas flow rate in the studied range. The internal diffusion limitations are excluded due to the non-porous nature of the bitumen coke.

Table 4-2. Initial rates of gasification as a function of sample mass and gas flow rate to confirm independence of rates on heat and mass transfer limitations. All experiments used 13% Na_2CO_3 premixed coke samples gasified at 800°C. Steam concentration was 77.1%.

Total Gas Flow, $ml \cdot min^{-1}$	Initial Mass, mg	Initial Rate, min^{-1}
1586	5.7	0.14
1586*	10.4	0.14
1586	16.3	0.12
1192	10.5	0.15
1269	10.7	0.14
1586*	10.4	0.14
2379	10.9	0.15

* Table line repeated to show the trend for alteration of gas flow rate.

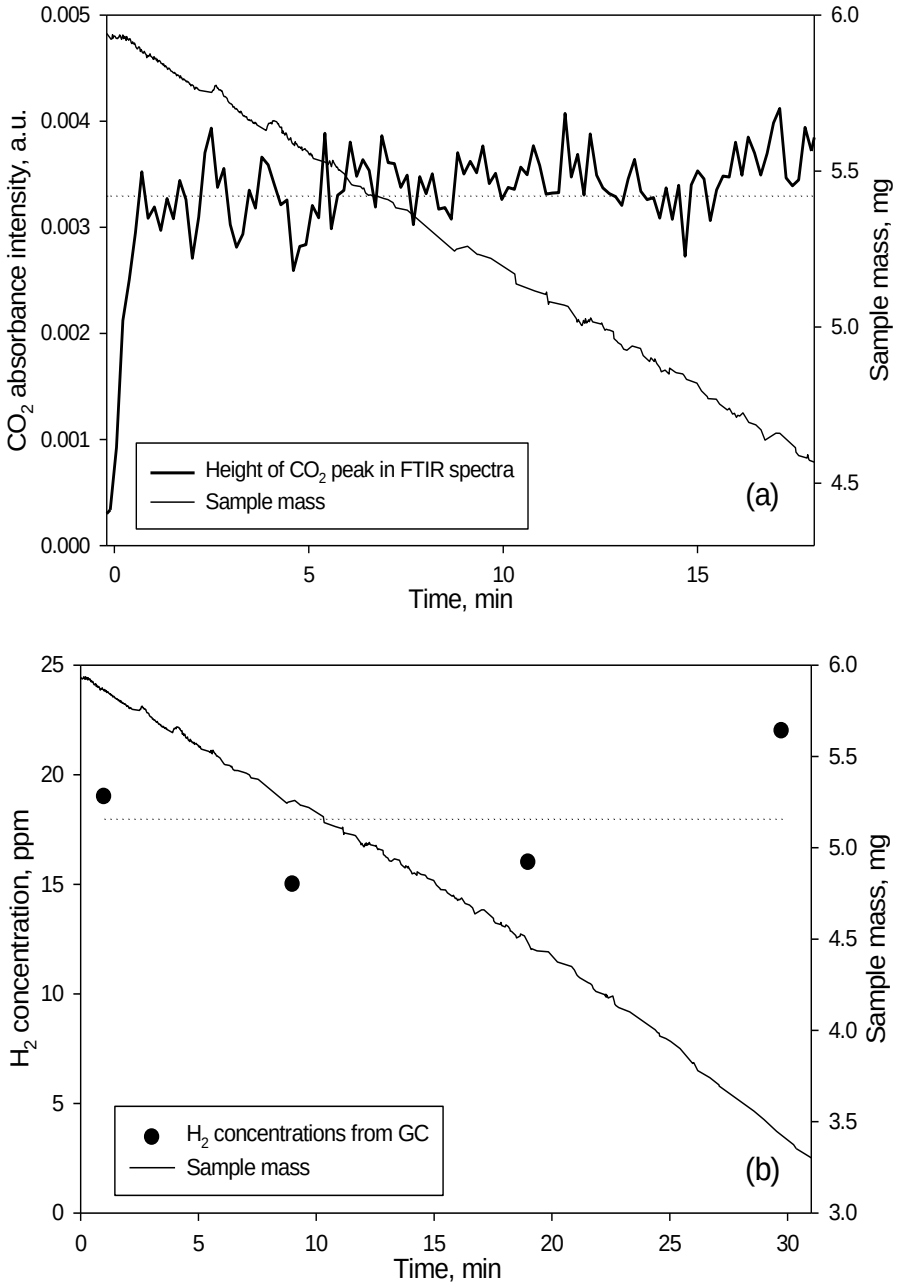

Figure 4-1. Comparison of variations in mass in TGA with the CO_2 production trend as measured by the FTIR spectrometer (a); and the H_2 production trend as measured by GC (b) in the early stages of a catalytic gasification test at 750 °C with p_{H2O} = 0.77 atm, K_2CO_3 loading of 0.6 (mol potassium)/kg, and a gas flow rate of 1200 ml min^{-1}.

4.3.2 Gas production

A constant rate of CO_2 and H_2 production was confirmed by continuous FTIR spectrometry and intermittent GC sampling, respectively, during the initial constant mass loss rate period (Figure 4-1). CO was absent from the evolved gases during gasification according to both FTIR and GC analyses, consistent with its conversion to CO_2 by the water-gas shift reaction (WGSR):

$$CO + H_2O \leftrightarrows CO_2 + H_2 \quad (4.3\text{-}1)$$

4.3.3 Activation energies of catalytic and non-catalytic reactions

Figure 4-2 compares the Arrhenius plots of the reactions catalyzed by Na_2CO_3 and K_2CO_3 with the non-catalytic reaction. Apparent activation energies were reduced from 2.1×10^5 J/mol in the non-catalytic reaction to 1.3×10^5 J/mol and 1.2×10^5 J/mol in the cases of Na_2CO_3 and K_2CO_3 catalysts, respectively. Based on the data of Wigmans et al. (14) the difference in the catalyst loadings in this range of concentrations is not expected to affect the activation energies significantly. The considerable decrease in the activation energy of the reaction by catalysis is consistent with a change in the reaction pathway, rather than solely increasing the number of active sites (10).

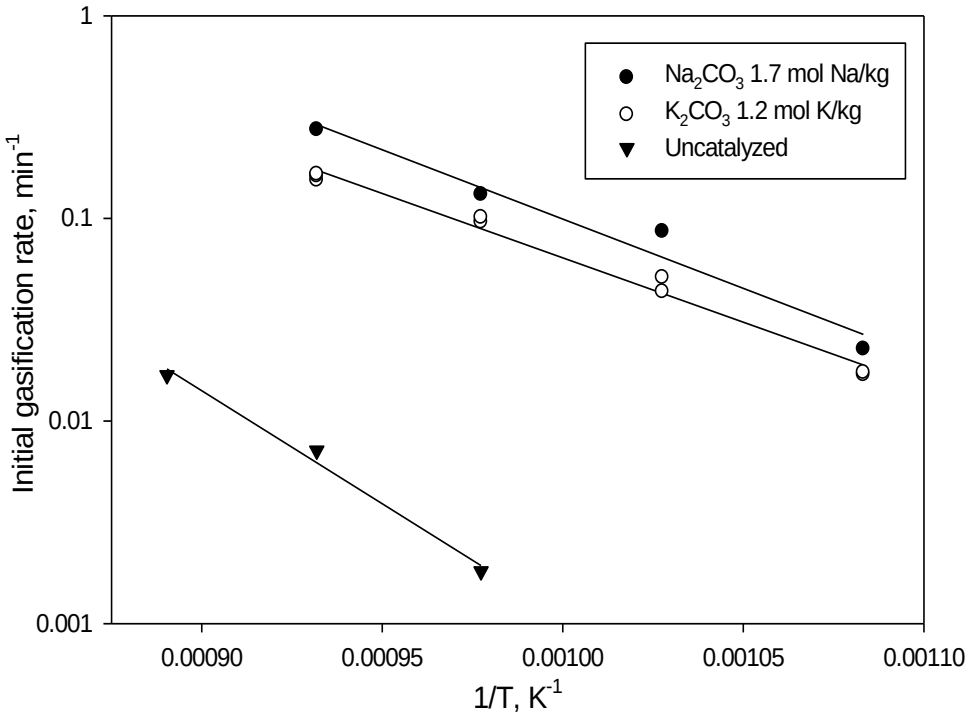

Figure 4-2. Arrhenius plot of the two catalytic cases compared with non-catalytic gasification of 53-90 µm coke particles at p_{H2O} = 0.77 atm.

4.3.4 Effect of partial pressure of steam

In the present study, the concentration of hydrogen in the gas phase was negligible in the gas phase due to the small sample quantity (7-7.5 mg) and high sweep gas flow. A Langmuir-Hinshelwood (L-H) type rate equation of the following form has been reported to fit the kinetics of the gasification reactions under these conditions (5, 9):

$$r = \frac{k_1 p_{H_2O}}{1 + K_2 p_{H_2O}} \qquad (4.3\text{-}2)$$

Figure 4-3 shows the initial specific rate of gasification (r) as a function of the partial pressure of steam (p_{H_2O}). The values of k_1 and K_2 obtained from the non-linear regression of the L-H equation on the data were 2.0×10^{-3} and 6.5×10^{-3}, respectively. While the F-test on the regression gives a p-value of 0.0981 (which is within 90% significance level), the t-test on K_2 for this fitted curve results in a p-value of 0.5178 which suggests that parameter K_2 is insignificant. In other words, as the experiments were performed at low pressure and rate data were scattered, the term $K_2 p_{H_2O}$ can be avoided. Therefore, a first order rate expression could sufficiently fit the data in the range of partial pressures of steam studied ($k_1 = 1.3\times10^{-3}$). Regression of rate-temperature data (considering the temperature dependence of the rate constants) on Na_2CO_3-catalyzed reactions at p_{H_2O} = 78 kPa confirmed the equivalence of equation (4.3-2) to a first order rate equation with respect to p_{H_2O} for this salt also.

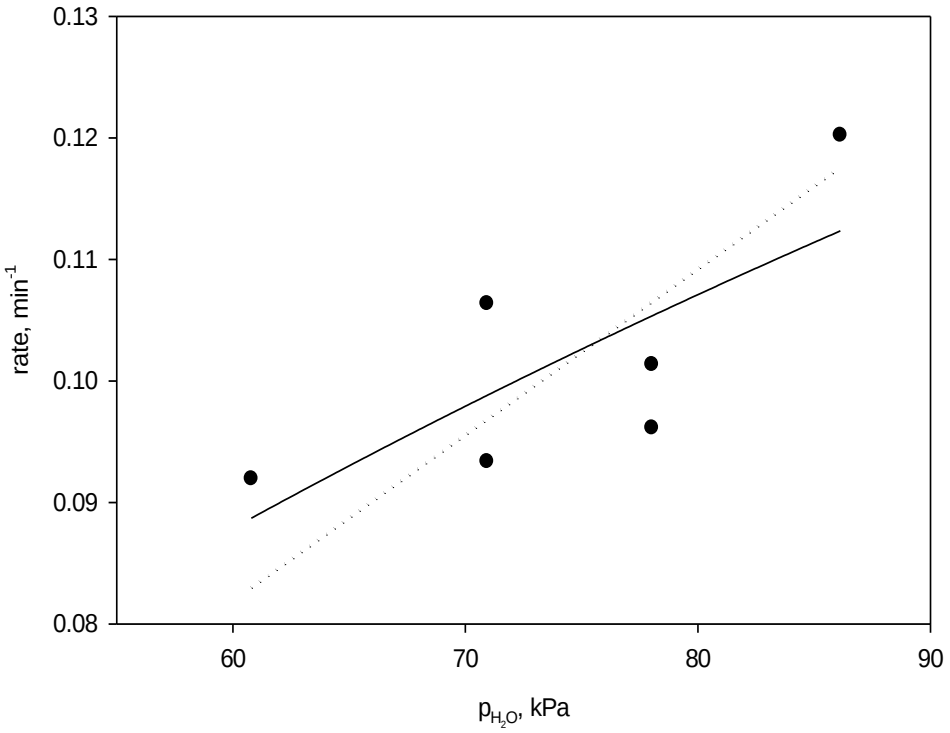

Figure 4-3. Plot of initial gasification rates versus partial pressures of steam. Solid line: Langmuir-Hinshelwood model fit. Dotted line: First order rate equation. Gasification conditions: 750 °C, 53–90 µm particles, and K_2CO_3 loading of 1.2 mol potassium/kg with a gas flow rate of 1200 ml min^{-1}.

4.3.5 Effect of surface area

The initial rates of steam gasification were linearly dependent on the calculated external surface area of coke particles of different sizes (Figure 4-4), consistent with the non-porous properties of the initial coke, with BET surface area less than 1 m^2/g (Table 4-3). The partially converted samples showed a significant increase in the specific area (Table 4-3), which increased further after the partially converted coke had been washed with water to remove the catalyst.

Table 4-3. BET specific surface area measurements on samples of unconverted and partially converted (X = 35-40% , K_2CO_3 loading of 1.2 (mol potassium)/kg) Athabasca coke ($m^2\ g^{-1}$)

Particle size range	External area estimate	unconverted coke (w/o catalyst)	Partially gasified sample w/catalyst	Partially gasified and washed
38-53 μm	0.06-0.09	<1	98	129
90-150 μm	0.02-0.04	<1	23	83

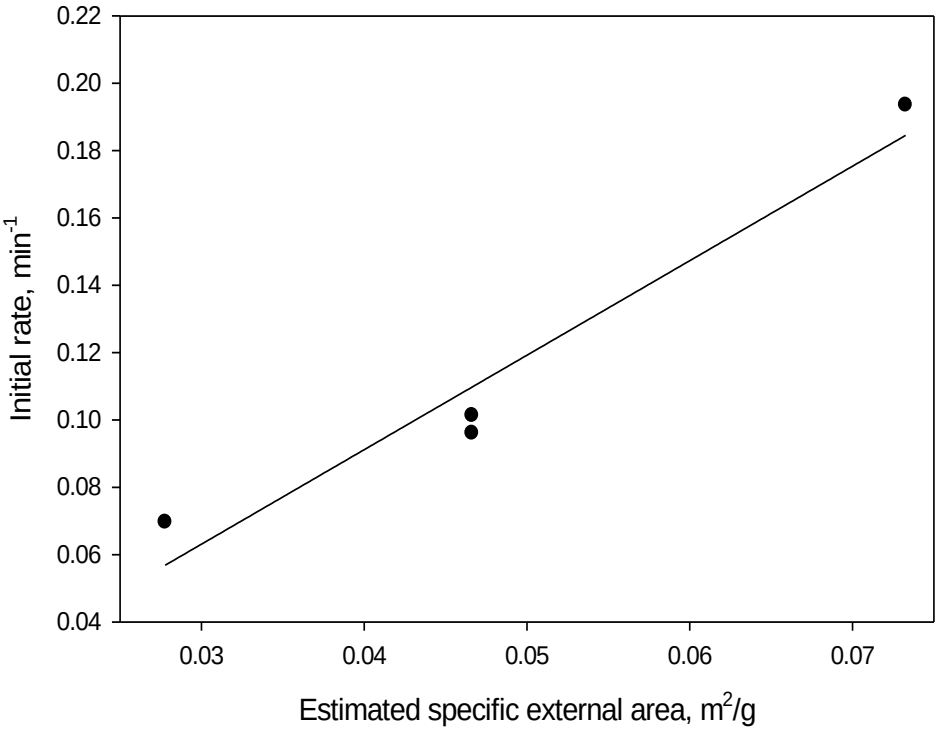

Figure 4-4. Variations of the initial gasification rate at 750 °C, p_{H2O} = 0.77 atm, gas flow rate of 1200 ml min^{-1}, and a K_2CO_3 loading of 1.2 (mol potassium)/kg with the estimated external area of the coke particles.

This observation is consistent with the liquid-like behavior of the catalyst at the reaction temperatures (17). The SEM image of the surface of an unwashed partially gasified coke particle clearly shows relatively large (ca. 300 nm) K-containing agglomerates on the surface of the particles, which could block the pores during the BET analysis (Figure 4-5).

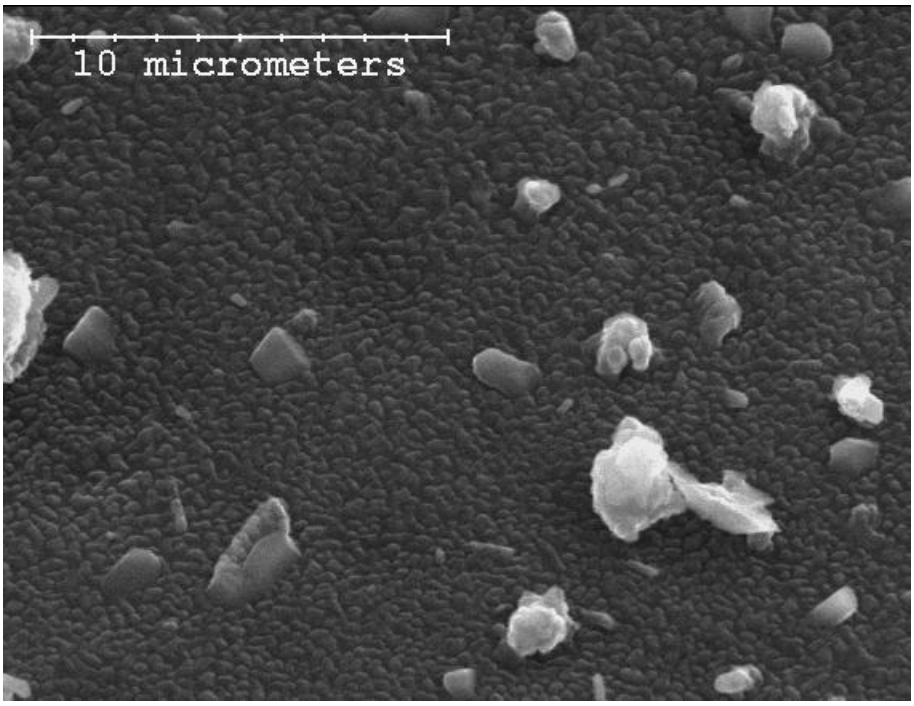

Figure 4-5. Secondary electron SEM micrograph of the surface of a partially reacted coke particle (X = 40%) covered with K-containing agglomerates.

4.3.6 Catalyst loading

The initial rate of gasification was directly affected by the concentration of the catalyst (Figure 4-6). At the same molar loading of the cation, which is believed to be the active part of the catalyst in the reaction (4), potassium carbonate was slightly superior to sodium carbonate. However, considering the

lower molecular weight of Na_2CO_3 (ca. 106.0 g/mol) than K_2CO_3 (ca. 138.2 g/mol), the latter would be inferior at equal weight percents.

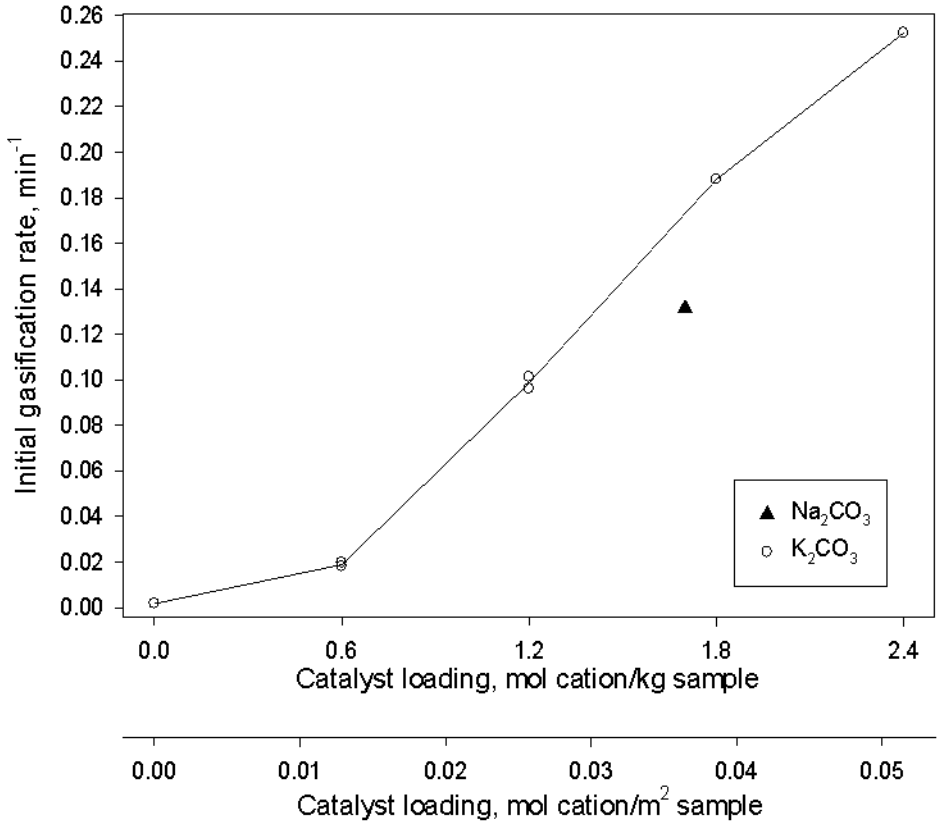

Figure 4-6. Effect of catalyst loading on the initial rate of gasification of 53-90 μm coke particles at 750°C, p_{H2O} = 0.77 atm, and gas flow rate of 1200 ml min^{-1}. The lower horizontal axis shows the corresponding catalyst loading per unit area of coke particles.

The lowest catalyst loading (0.6 mol potassium/kg corresponding to 5 wt%) increased the initial rate ca. 11-fold from the uncatalyzed reaction, whereas the next portions of the catalyst improved the rate much more (57-fold in the case of 1.2 mol K/kg loading). In addition, at the low initial catalyst loading an unexpected acceleration of the rate at moderate conversions was observed, which

can be justified by assuming a gradual increase in the surface concentration of the catalyst due to release of the diffused potassium species, as the surrounding coke is consumed during the reaction (Figure 4-7). Wigmans et al. (14) attributed these trends to the formation of intercalate-like compounds, making the catalyst inaccessible to the gaseous reactant. They considered an observed enlargement of the surface area during gasification (18) as an indication of the destruction of intercalate-like structures.

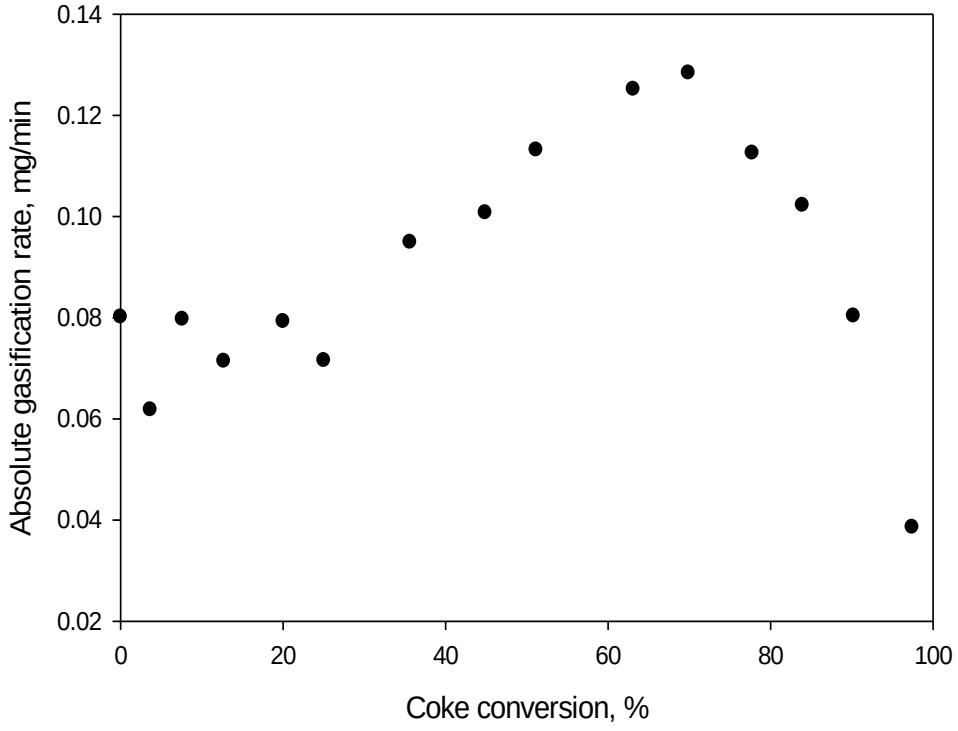

Figure 4-7. Acceleration of gasification at moderate conversions observed at low initial catalyst loading (0.6 mol potassium/kg, 53-90 µm coke particles at 750°C and p_{H2O} = 0.77 atm).

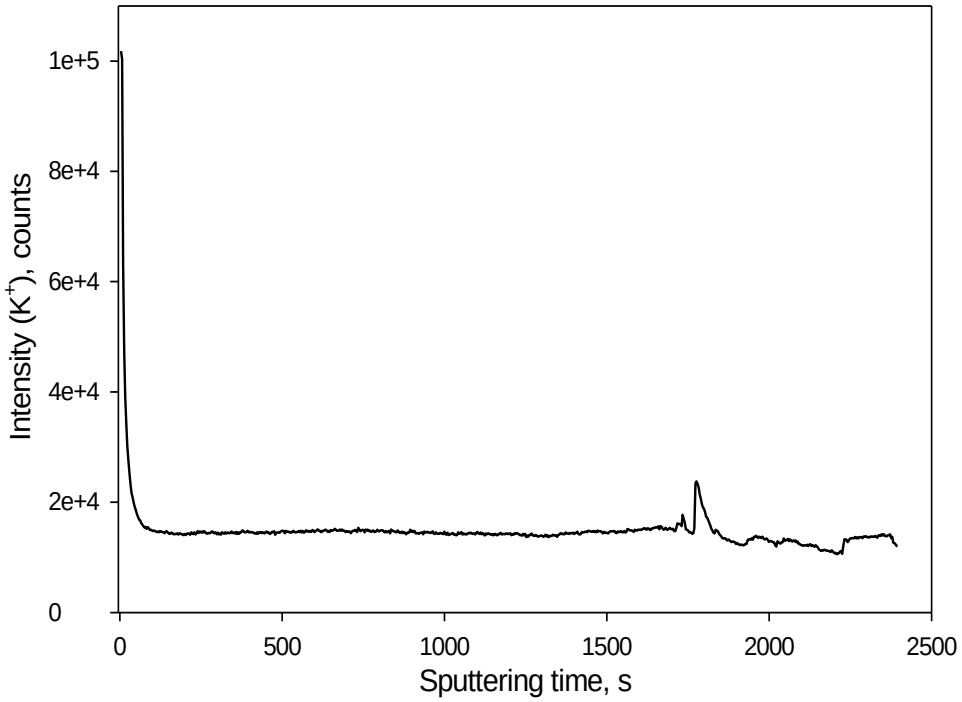

Figure 4-8. Depth profile of potassium concentration in a heated coke particle by ToF-SIMS. The entire sputtering experiment corresponded to a depth of roughly 2 μm.

Wen (13) first suggested that the catalytic action of alkali metal carbonates requires the formation of intercalate-like structures, which then participate in the gasification reaction through a reduction-oxidation cycle. Evidence for the diffusion of potassium into coke upon heating is given in Figure 4-8. The sharp drop in the concentration during the first few seconds of sputtering reflects the high concentration of potassium at the surface of the sample. Thereafter, the almost constant concentration of a significant level of potassium inside the coke particle was consistent with the rapid diffusion of the alkali metal into the coke upon heating, up to a saturation concentration. Consequently, the trend of Figure

4-6 reflects saturation of the coke phase at below 0.6 mol potassium/kg, followed by increases in surface concentration at higher loading of catalyst. Similarly, the data of Figure 4-7 show acceleration of the rate as the loading of potassium increases due to carbon removal. If intercalates were the key reaction intermediate, as suggested by Wen (13), then the dependence of reaction on catalyst loading would cease once the coke phase were saturated, and not continue to increase beyond 0.6 mol potassium/kg.

4.3.7 Reaction kinetics as a function of area and catalyst loading

Wigmans et al. (14) divided the general trend of gasification rates of a high surface area activated carbon into three sections: (A) 0-50% conversion in which the absolute rate (*-dm/dt*) increased constantly; (B) 40-80% conversion in which the absolute rate remained relatively constant; and (C) above 80% conversion in which the absolute rate decreased sharply, likely due to carbon limitations. Based on previous reports of binding of potassium to the carbonaceous substrate by forming K-O-C complexes (19) they hypothesized that these structures need to be broken up in order the catalyst to achieve mobility. Therefore they suggested that during period (A) the K-O-C structures gradually break up as the conversion increases, and once this phase is completed, a constant activity per active site is established (region B).

In the present study, the change in reaction rate with conversion was similar, except that region (A) was so short that it was excluded from the calculation of initial rates. The relatively constant mass loss rate (constant

absolute gasification rate, region B) corresponding to an apparent reaction order of zero with respect to the remaining coke mass was established within less than 10% conversion (Figure 4-9). Although the catalyst loadings are reported on a mass basis, from the kinetic point of view a more accurate form of expressing the catalyst loading would be the number of moles of catalyst (cation) per unit area of the substrate (surface loading). In the case of char combustion, specific internal surface area increases with the carbon burn-off due to more new pores opening, but at high conversions the pores collapse, causing a decrease in specific surface area. The critical carbon burn-off point, after which the area ceased to increase, was at 35-50% conversion (20). If a catalyst is present, as in the current study, a surface area decrease after a certain conversion implies that the catalyst loading per unit area increases. Therefore, at higher conversions an increasing trend for the specific rates would be expected as a function of conversion.

In order to verify a potential occurrence of a shift in the reaction mechanism, a series of calculations were performed to predict the rates at higher conversions using the initial rate as follows. We assumed that in the absence of any interfering phenomena, such as mass transfer limitations, the rate at any given conversion X would be only a function of the surface loading of the catalyst (w) at that conversion:

$$r(X) = r(w(X)) \tag{4.3-3}$$

Assuming that the loss of the catalyst by evaporation, decomposition, etc. during the reaction, as well as the increase in the surface loading by the release of the diffused catalyst to the surface as the carbon is consumed are negligible, the

surface loading is only a function of the change in the surface area of the coke. The latter can be expressed as a geometric factor *y*, which is a function of the conversion:

$$w(X) = w_0 \cdot y(X) \tag{4.3-4}$$

The geometric factor of the change in the surface area of ideal spherical (or cubic) particles can be calculated assuming a shrinking core model. For char gasification, typically three models are considered (21), either a volumetric model, a grain (shrinking core) model or a random pore model. The volumetric model, assuming a homogeneous reaction throughout a particle, predicts a constant decrease of reactivity with conversion, which contradicts the observed kinetics (Figure 4-9). The random pore model, considering growth of pores along with their destruction, predicts a maximum for the reactivity with conversion increase. In the current study this model could be suitable for low catalyst loadings (Figure 4-7), but it would not be representative for higher loadings. A shrinking core model, proposed for the reactions of a porous solid and gas with a moving boundary, assumes that a porous particle consists of spherical nonporous grains and the reaction takes place on their surface (21). The shrinking core model can be applied to each of these grains during the reaction. Despite the formation of internal pore area with conversion (Table 4-3), we found that the specific rates can be predicted over a wide range of conversion based only on the external surface area of the particles, assuming a non-porous shrinking core model as follows:

$$y(X) = \frac{A_0}{A} = \left(\frac{d_0}{d}\right)^2 = \left(\frac{V_0}{V}\right)^{2/3} = \left(\frac{m_0\rho}{m\rho}\right)^{2/3} = \left(\frac{m_0}{m_0(1-X)}\right)^{2/3} = (1-X)^{-2/3}$$

(4.3-5)

At any level of conversion, the effective catalyst loading *w(X)*, was calculated according to equation (4.3-4) by multiplying the initial catalyst loading w_0 by the geometric factor *y(X)* from equation (4.3-5). Following equation (4.3-3), the predicted rate of reaction *r(X)* was interpolated from the data of Figure 4-6 for the calculated value of *w(X)*.

The data of Figure 4-9 compare the experimental rate data with the rates predicted from the initial rates as described above. The specific rate at X = 0.5 was approximately doubled (i.e. $r \cong 2r_0$) with the ca. 59% increase in the catalyst surface loading (y = 1.59), as illustrated in Figure 4-9(b). Over this range of conversion the absolute rate was relatively constant (Figure 4-9(a)), because the increase in catalyst loading was approximately cancelled by the loss of mass of coke:

$$r_{a,x=0.5} = \{r \cdot m\}_{x=0.5} = \{r \cdot m_0(1-x)\}_{x=0.5} = \left\{\frac{1}{2} r \cdot m_0\right\}_{x=0.5} \cong \left\{\frac{1}{2}(2r_0)m_0\right\}_{x=0.5} \cong r_0 \cdot m_0 \qquad (4.3\text{-}6)$$

In contrast, specific rate based on the measured BET areas (Table 4-3) would exhibit a dramatic decrease with extent of conversion. The match between the model and the data diminishes at the final conversions, either due to contributions from the developing pore area, or to mass transfer limitations as a result of the coverage of the remaining small coke particles with the catalyst.

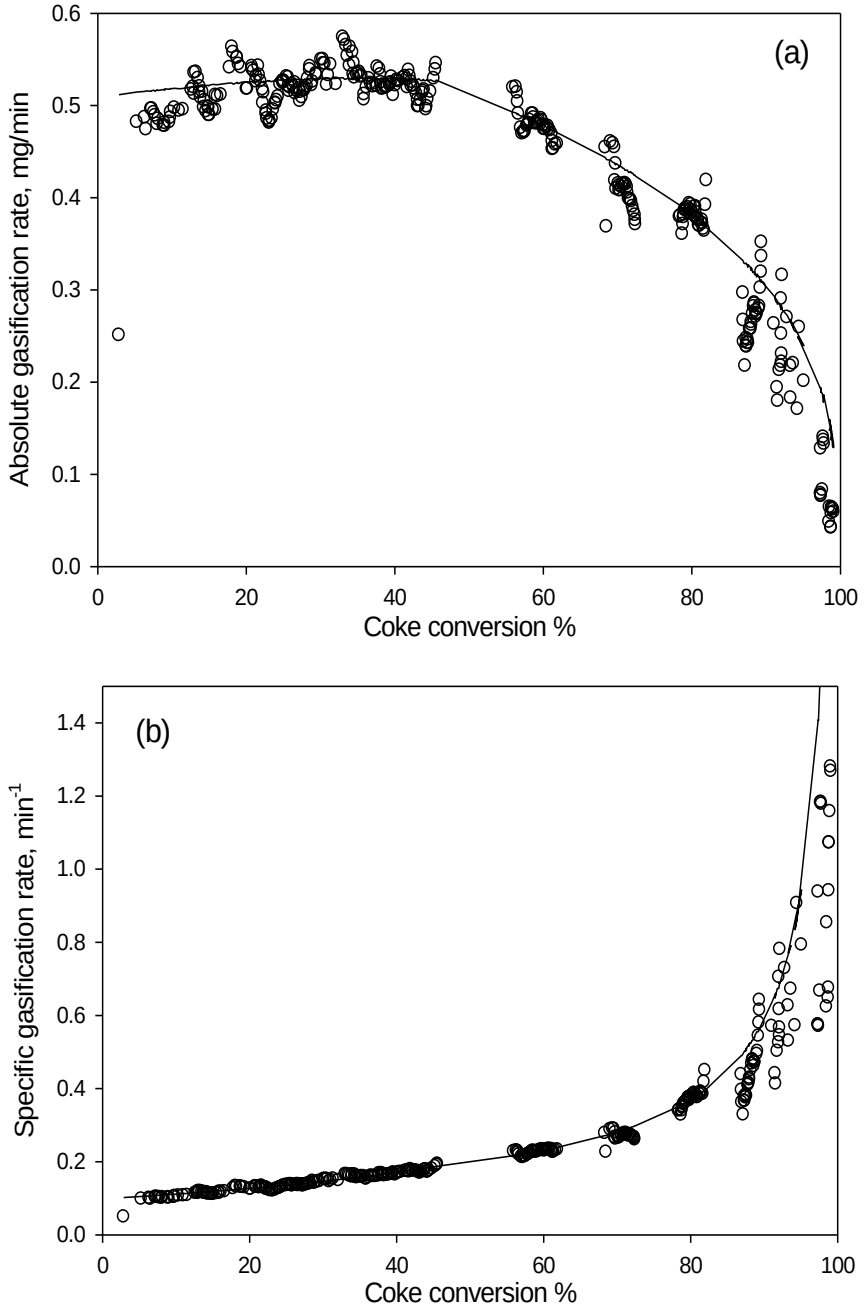

Figure 4-9. Gasification rates at 750°C and p_{H2O} = 0.77 atm with respect to coke conversion for an initial catalyst loading of 1.2 mol K/kg and initial particle size range of 53-90 µm: Circles: measured data points for (a) absolute rate as mg/min and (b) specific rate as mg reacted/mg sample/min; Solid lines: calculated as described in text.

The presence of a catalyst layer could partly account for the lack of correlation between the internal area (from BET measurement) and the rate. Further study is required to fully reconcile the respective roles of pore surface area, catalyst layer, and external particle surface in the observed reaction rates.

The predictability of the rates at later stages of gasification from the initial rate data suggests that the rate of gasification at different stages of the reaction varies proportionally to the instantaneous surface loading of catalyst in the sample at the given conversion. This observation suggests that a shift in the mechanism during the course of the reaction did not occur in the present work. Therefore, the conclusion made by Wigmans et al. (14) – that the gradual increase in absolute rates is caused by the gradual release of the potassium atoms from the K-O-C structures in order to obtain mobility and equal activity to other potassium atoms – is not consistent with the results of this study. Even if such K-O-C structures are indeed impeding the activity of the catalyst, their concentration must have been very small in bitumen coke samples, as the warm-up region (A) was very short in our experiments. Note that potassium and sodium are very mobile on coke even at temperatures lower than catalytic gasification temperatures and in the absence of a gaseous reactant (17). Furthermore, since Wigmans et al. (14) had used a highly porous high surface area activated carbon as substrate, other factors such as internal mass transfer limitations may have affected their rate measurements. In the event of severe pore diffusion limitation in gasification of a porous substrate, mostly the external area would be active for gasification. On the other hand, a portion of the catalyst which has been trapped in the pores would gradually

become available to the external surface as the carbon is consumed (a possible explanation for the prolonged region A in their results). Note that the amount of this portion of the catalyst can be much more than the amount that normally diffuses into the carbon structure itself. Therefore, the catalyst loading per unit *external* area would increase at a faster rate but starting from a lower initial rate than it would for a non-porous substrate.

4.4 Conclusions

Both sodium and potassium carbonates reduced the apparent activation energy of the reaction, which suggests that the reaction path was altered by the catalysts.

A Langmuir-Hinshelwood (L-H) type rate equation was used to describe the dependency of rate on the partial pressure of steam. Because of the low pressures used and the scatter in the rate data, a simple first order rate equation could also fit the data (i.e. the K_2 parameter of the L-H equation was statistically insignificant for the range studied).

A fraction of the alkali metals diffused into the coke until it was saturated, as revealed by SIMS depth profiling. This result explained the lower activity of the catalyst at low catalyst loadings, as the diffused portion was not accessible to the gaseous reactant. This observation contradicts proposed reaction mechanisms requiring the participation of intercalation compounds in the reaction, as these mechanisms fail to explain the increase in the rate with further catalyst loading when the already-saturated coke cannot promote the formation of new intercalation compounds by diffusion.

Rates of gasification of coke during the reaction matched the prediction based on initial rate vs. catalyst loading data, despite the increase in the internal pore are as determined by BET surface area measurement.

4.5 References

1. Energy Resources Conservation Board. Report on Alberta's Energy Reserves 2009 and Supply/Demand Outlook 2010-2019 (Document #St98-2010). Retrieved from http://www.ercb.ca/docs/products/STs/st98_current.pdf on 13/7/2010
2. Higman, C.; van der Burgt, M. Gasification. 2nd ed. Amsterdam: Elsevier; 2008: 37–38.
3. Furimsky, E. *Fuel Process. Technol.* **1998**, *56*, 263–290.
4. Wood, B. J.; Sancier, K. M. *Cat Rev Sci Eng* **1984**, *26*, 233-279.
5. Sheth, A. C.; Yeboah, Y. D.; Godavarty, A.; Xu, Y.; Agarwal, P. K. *Fuel* **2003**, *82*, 305–317.
6. Ueda, M.; Yoshitake, M.; Sumi, S.; Mikami, K.; Matsuo, K. *Mitsui Zosen Giho* **1981**, *112*, 37–48.
7. Furimsky, E.; Palmer, A. *Appl. Catal.* **1986**, *23*, 355−365.
8. Watkinson, A. P.; Cheng, G.; Fung, D. P. C. *Fuel* **1989**, *68*, 4–10.
9. Van Heek, K. H.; Mühlen, H. J.; Jüntgen, H. *Chem. Eng. Technol.* **1987**, *10*, 411–419.
10. Moulijn, J. A.; Kapteijn, F. *Carbon* **1995**, *33*, 1155–1165.
11. Mims, C. A.; Pabst J. K. *J. Catal.* **1987**, *107*, 209–220.

12. McKee, D. W.; Chatterji, D. *Carbon* **1975**, *13*, 381–390.

13. Wen, W. Y. *Cataly. Rev.* **1980**, *22*, 1–28.

14. Wigmans, T.; Elfring, R.; Moulijn, J. A. *Carbon* **1983**, *21*, 1-12.

15. Wang, J.; Jiang, M.; Yao, Y.; Zhang, Y.; Cao, J. *Fuel* **2009**, *88*, 1572–1579.

16. Saber, J. M.; Kester, K. B.; Falconer, J. L.; Brown, L. F. *J Catal* **1988**, *109*, 329–346.

17. Karimi, A.; Gray, M. R. *Fuel* **2011**, *90*, 120-125 (Chapter 3 of this thesis).

18. Wigmans, T.; Hoogland, A.; Tromp, P.; Moulijn, J. A. *Carbon* **1983**, *21*, 13–22.

19. Mims, C. A.; Pabst, J. K. *Prepr. Am. Chem. Soc. Div. Fuel. Chem.* **1980**, *25*, 258–262.

20. Sadhukhan, A.K.; Gupta, P.; Saha, R.K. *Fuel Proc. Techn.* **2009**, *90*, 692-700.

21. Fermoso, J.; Arias, B.; Pevida, C.; Plaza, M. G.; Rubiera, F.; Pis, J. J. *J. Therm. Anal. Cal.* **2008**, *91*, 779-786.

5 General Discussion and Conclusions

5.1 Structure of asphaltene molecules

5.1.1 Discussion

The present study on the structure of asphaltenes (Chapter 2) reconfirmed the existence of molecules consisting of bridged small (1-4) ring groups, also known as the archipelago structure, in considerable quantities in the asphaltenes from various sources around the world. As mentioned in Chapter 1, the main feature of the present work was to overcome some of the limitations and weaknesses of the previous studies to provide stronger evidence for the existence of these structures.

The results confirmed that the fraction of the samples of asphaltenes from around the world that could be identified by this method were very similar in terms of their building blocks. There are, however, some differences in the relative abundance of the various chemical classes of the building blocks. Another important finding of this work was that the identified building blocks of the Athabasca C_7 asphaltenes sample and the Athabasca industrial C_5 asphaltenes sample (which contained 45.5% heptane-solubles and 28.2% pentane-solubles) were strikingly similar in terms of the relative abundances of the various chemical

classes in the products of pyrolysis. This suggests that the C_7-, C_5-, and even lower alkanes-insoluble asphaltenes were very similar in terms of the building blocks. They may, however, be different in other structural aspects such as the molecular size, i.e. the average number of building blocks per molecule.

Figure 5-1 illustrates the understanding of the structure of asphaltenes arising from the present study. It shows hypothetical molecular structures of asphaltenes consisting of various building blocks that can range from alkane chains to aromatic and saturated ring systems, rarely exceeding four rings per block. This representation is principally similar to the pendant-core model proposed by Wiehe (1). However, in the model depicted in Figure 5-1 differentiation between pendant and cores have been intentionally avoided for the reasons discussed in Section 1.1.3. In short, a solid difference in chemical composition of the pendants and cores was not defined by Wiehe (1) other than that the cores do not volatilize upon thermal cracking until they join to each other to form coke. He also mentioned an example of a small group consisting of a single aromatic ring that would normally be classified as a pendant, but which can become a core, if bound with multiple bonds. The model in Figure 5-1 uses this concept to suggest that asphaltene molecules without large ring systems (> 4 rings per block) may exist that can still form coke upon thermal cracking by condensation of several groups such those marked by the dashed box.

On the other hand, as the possibility of the existence of larger ring systems cannot be ruled out by the present study, another plausible structural form for the asphaltenes might include one or more such groups with smaller blocks attached

to it (Figure 5-2). This form is consistent with the hypothetical structure proposed by Strausz et al. (2).

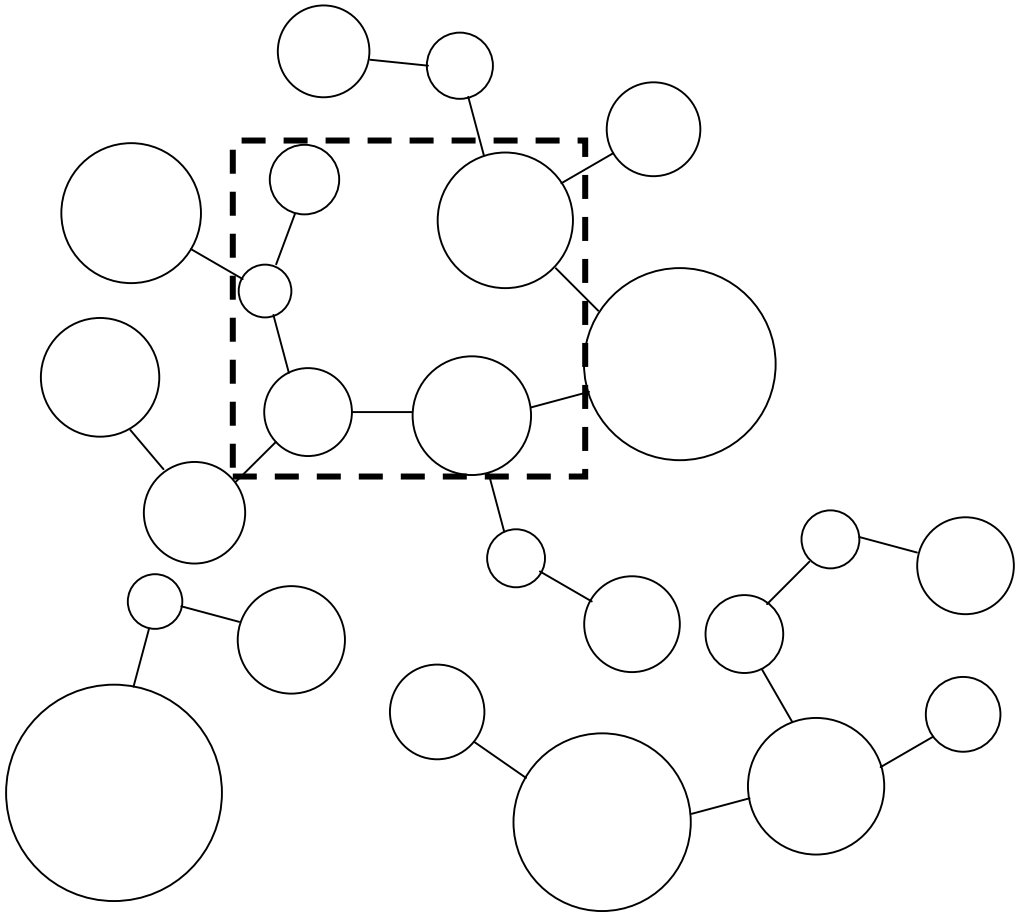

Figure 5-1. Schematic drawing depicting three hypothetical asphaltene molecules.

Each circle represents a building block which can be substituted by a wide range of species including straight or branched paraffinic chains, aromatic and/or saturated ring clusters with various sizes (typically 1-5 rings), and heteroatomic species. The solid lines represent single covalent bonds between any two building blocks. The area marked by the dashed box shows some groups prone to coke formation.

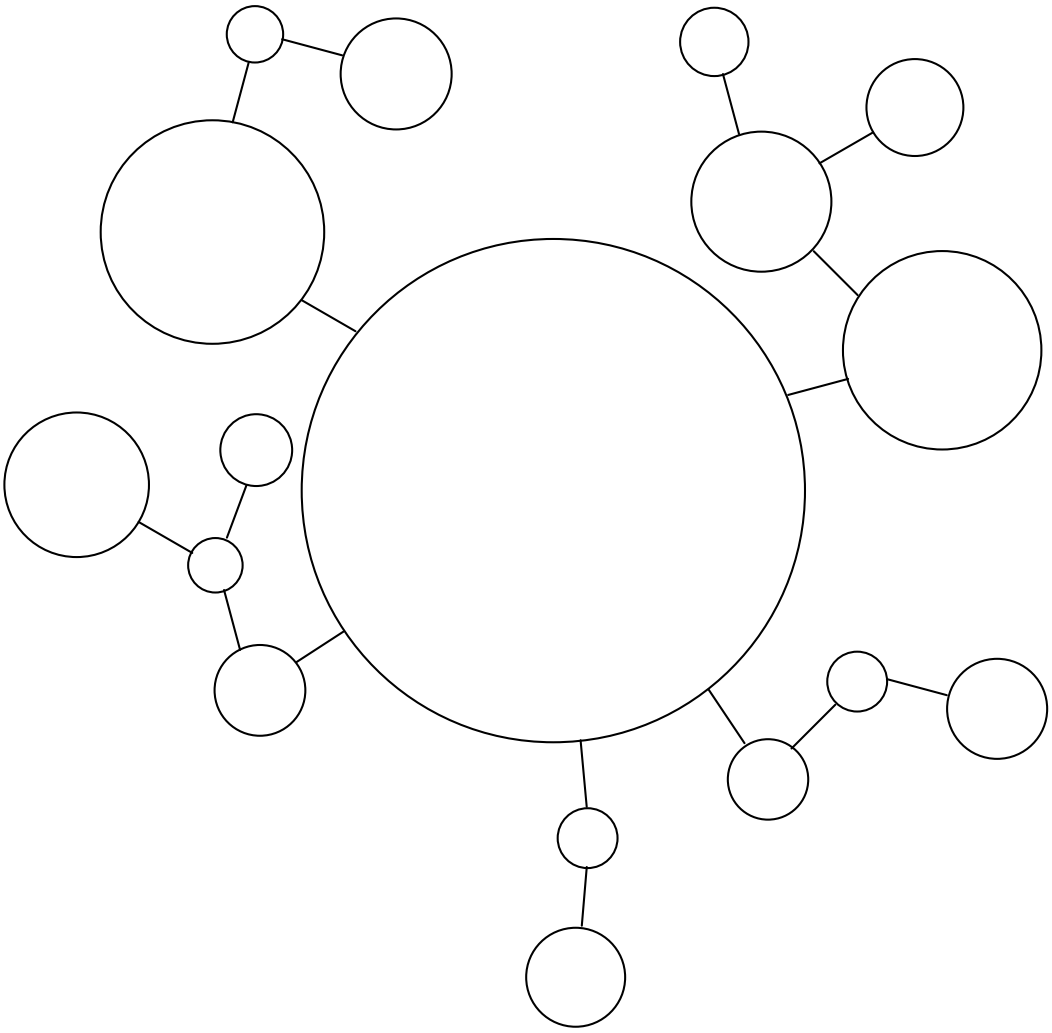

Figure 5-2. Hypothetical structure of an asphaltene molecule with a relatively large aromatic/saturated ring cluster (5-10 rings).

Although, the existence of such structures were not supported by the results of the present work, as any such groups would end up in the coke in these experiments, the possibility of the existence of such structures in asphaltenes cannot be ruled out at this point. Application of a different technique is required to confirm or reject the existence of such structures.

5.1.2 Summary of conclusions

A considerable amount of archipelago-structured molecules were found in the asphaltene samples. Asphaltene samples with different origins were generally similar in terms of the building blocks. However, some differences in the yields of various classes of the building blocks were evident. Asphaltenes precipitated by different solvents showed remarkable structural similarity in terms of the building blocks.

5.1.3 Recommendations for future work

The main limitation of this study was the high yield of coke as a result of the thermal cracking reactions. No structural information can be obtained from the portion of the samples turned into coke. Therefore, it is desirable to perform these tests in such a way to reduce the coke formation. Application of a hydrogenating environment is a promising technique to this end. Minimizing the evaporation loss of the products and/or a quantitative analysis of the vapors is another issue to be considered in future experiments of this type.

The experiments done with samples of Athabasca asphaltenes precipitated using different solvent suggested that these asphaltenes consist of similar building blocks. The tested samples were Athabasca C_7, C_5, and industrial C_5 asphaltenes. The latter sample contained 28.2 % of C_5 solubles, which implies that lower-alkane insolubles also have similar structural units. It is recommended to repeat these experiments using C_3 and C_9 asphaltenes for further confirmation of this conclusion. It may also be worthwhile to perform the tests on solvent-fractionated

samples (e.g. C_3-insoluble C_5-soluble asphaltenes, C_5-insoluble C_7-soluble asphaltenes, etc.).

5.2 Catalytic gasification of bitumen coke

A series of alkali metal and alkaline earth metal compounds were tested as catalysts for gasification. The investigated alkaline earth metal compounds (i.e. $CaCO_3$, CaO, and MgO) did not catalyze the reaction. SEM/EDX analysis revealed that these compounds were immobile upon heating and the level of dispersion obtained by physical mixing of these compounds was not sufficient to trigger any interaction between the catalyst particles and the coke.

In contrast, the tested alkali metal compounds (K_2CO_3, Na_2CO_3, and KCl) showed substantial mobility on the coke particles after heating. The high dispersion of the catalyst in these cases was certainly an important factor in the high catalytic activity observed from these compounds. Nonetheless, it appears that the catalytic activity also requires the aid of oxygen; KCl did not show any activity at 700°C, but it showed remarkable activity at 800°C. Chlorine was absent in the EDX spectra of the sample after exposure to gasification conditions at 700°C for 30 min, likely due to hydrolysis to gaseous HCl. The oxygenation of potassium to KOH as a result of the hydrolysis apparently plays a critical role in its catalytic activity. On the other hand, the carbonate cation of K_2CO_3 oxidizes the cokes surface upon heating as revealed by SIMS and XPS analyses (Appendix 3). This is consistent with previous studies that suggest such oxidized sites are required for the catalytic action.

The method of the addition of the catalyst, i.e. mixing with the coke after the coke formation vs. mixing with the vacuum residue precursor, did not affect the catalytic activity as a result of the high mobility of the alkali metal species. A portion of the alkali metal species diffused into the coke particles. Washing the samples of coke heated to 500°C or higher in the presence of potassium carbonate effectively removed all of the potassium species from the surface as shown by the XPS analysis (Figure A3-2 in Appendix 3). However, the existence of potassium inside the coke particles even after washing was confirmed by EDX, due to the higher depth of penetration of the X-rays employed by this technique. Moreover, the depth profile by SIMS showed a constant concentration of potassium inside the coke particle. No crystalline structure of the penetrated potassium species could be observed inside the coke particles by TEM microscopy. A possible mechanism for the diffusion phenomenon may be by intercalation of potassium atoms between aromatic sheets in the coke's structure as suggested by Wigmans et al. (3). The diffusion of alkali metals into the coke was quantified by the measurement of the thermal conductivity of water solutions from washing the heated coke-catalyst samples.

Both sodium and potassium carbonates decreased the activation energy of the gasification of bitumen coke. At an equal molar catalyst loading (i.e. mol cation/kg sample) both catalysts showed remarkable activity, with potassium carbonate being superior. However, since sodium has a lower atomic mass, at an equal mass loading (i.e. kg cation/kg sample) sodium carbonate showed higher activity. Therefore, from an economic standpoint, sodium carbonate maybe a

more viable solution. But it should be taken into account that the loss of catalyst due to evaporation maybe more pronounced in the case of sodium.

The initial rate of the reaction at various partial pressures of water fitted reasonably with a Langmuir-Hinshelwood (L-H) type rate equation. A first order rate equation with respect to partial pressure of water could also fit the data, given the low pressures employed and the scattered data.

The rate of the reaction at higher conversions was successfully predicted using the initial rates by a shrinking core model. This suggests that a shift in the mechanism of the reaction as proposed by Moulijn and coworkers (4) did not exist in the catalytic gasification of bitumen coke. They postulated that the C-O-M bonds had to be broken up to achieve mobility at higher conversions; whereas the mobility of the alkali metal salts on coke upon heating was evident in our work even without gasification.

Unexpectedly low catalytic activity of potassium carbonate observed at low catalyst loading can be explained by the diffusion of the catalyst into the coke, where it is not accessible to the reactant gas (i.e. steam). Upon the consumption of the coke, the diffused portion of the catalyst is released to the surface at moderate conversions. The reaction accelerates as a result (Figure 4-7). A modification of the shrinking core model based on this hypothesis successfully accounted for the acceleration phenomenon (Appendix 2). Therefore, the inhibition of the catalysis at low catalyst loading by diffusion of the catalyst seems to be a reasonable explanation.

In contrast, the explanation of the same phenomenon (lack of activity at low catalyst loading) by the formation of low activity single metal C-O-M complexes at low catalyst loadings (suggested by Yang and coworkers (5) and supported later by Moulijn and Kapteijn (6)) does not seem to be valid. It is re-emphasized here that enough evidence to support the low catalytic activity of the single metal C-O-M complexes in comparison to clustered groups was not provided.

Another conclusion from the inactivity of the potassium species in the penetrated form is that it contradicts the proposed mechanisms of catalytic gasification involving the active participation of intercalation compounds in the reaction as a necessary step. In other words, the potassium species need to be exposed to show catalytic activity. As mentioned before, they also appear to need the aid of oxygen atoms to perform their role as a catalyst for this reaction. Furthermore, the mechanisms involving intercalates fail to explain the increased reaction rate at increasing the catalyst loading. The constant concentration of potassium within the coke as shown in Figure 4-8 implies that the coke has a saturation limit, beyond which potassium cannot penetrate into the coke anymore. Therefore, at higher catalyst loadings the reaction rate would not increase, given the requirement of the formation of new intercalates for increased reactivity.

5.2.1 Summary of conclusions

Potassium and sodium carbonates were highly active as catalysts for the steam gasification of oil sands bitumen coke. They both reduced the activation energy significantly, suggesting that the reaction path was altered. KCl was also

an active catalyst at higher temperature; however, there were evidences suggesting that it required to be hydrolyzed before catalyzing the reaction.

These alkali metal salts were highly mobile in the sample at the reaction conditions. In contrast, the alkaline earth metal compounds $CaCO_3$, CaO, and MgO did not show mobility and were inactive as catalysts.

The rate of the reaction using K_2CO_3 could be fit to a Langmuir-Hinshelwood (L-H) type rate equation with respect to the partial pressure of steam. At the low pressures used in this study, a simple first order rate equation could also fit the data (i.e. the K_2 parameter of the L-H equation was statistically insignificant for the range studied due to the scatter in the rate data).

A fraction of the alkali metals diffused into the coke where it was not accessible to the gaseous reactant and could not promote the reaction. Further addition of the catalyst did, however, increase the rate, which is in contradiction with the proposed reaction mechanisms requiring the participation of intercalation compounds.

Only the external surface area of the particles appeared to be active in the reaction. The rates could be predicted at higher conversions by a shrinking core model using initial rate data, which suggests that the reaction mechanism did not change.

5.2.2 Recommendations for future work

As mentioned before, an obstacle towards the large-scale application of the catalytic gasification processes has been the deactivation of the catalyst as a result of the irreversible reaction of the alkali metals with the mineral impurities

in the sample. In the case of bitumen coke, therefore, a low ash containing type of coke is desirable for this process. Yet, the recycling of the catalyst needs to be studied before scaling up the process. Catalyst losses by evaporation over time during a continuous process should also be evaluated.

This study was carried out by low pressure (atmospheric) experiments. Nevertheless, commercial gasifiers usually operate at high pressures to save in compression energy and reduce the equipment size (7). Thus, the reaction is recommended to be studied at elevated pressures. Given the relatively low temperatures required for catalytic gasification, a considerable yield of methane from the high pressure operation of the process would be expected, which provides an opportunity for the production of synthetic natural gas (SNG) from the coke piles of Alberta.

Development of high surface area during the catalytic gasification of coke was observed in this experiment. Although only the external surface of the particles appeared to be active in the reaction, an analysis of the surface area changes during the gasification and its impact on the surface loading of the catalyst and other kinetic parameters seems to be essential.

5.3 References

1. Wiehe, I. A. *Energy & Fuels* **1994**, *8*, 536-544.
2. Strausz, O. P.; Mojelsky, T. W.; Lown, E. M. *Fuel* **1992**, *71*, 1355-1363.
3. Wigmans, T.; Hoogland, A.; Tromp, P.; Moulijn J. A. *Carbon* **1983**, *21*, 13-22.

4. Wigmans, T.; Elfring, R.; Moulijn, J. A. *Carbon* **1983**, *21*, 1–12.
5. Chen, S. G.; Yang, R. T. *J. Catal*. **1993**, *141*, 102-113.
6. Moulijn, J.A.; Kapteijn, F. *Carbon* **1995** *33*, 1155-1165.
7. Higman, C.; van der Burgt, M. Gasification. 2nd ed. Amsterdam: Elsevier; **2008**.

Appendix 1: Analysis of Gudao asphaltenes

Heptane insoluble asphaltenes from Gudao crude (China) were studied to investigate possible differences with asphaltenes from other sources. Gudao is a waxy crude. Therefore, the separation of the asphaltenes from this crude oil requires avoiding the precipitation of waxes. The method used in this case was a hot extraction technique equivalent to the method described in ASTM D 6560. Heptane was added to the crude sample at a ratio of 40:1. The solution was heated to boil under reflux. The sample was subsequently filtered followed by washing the asphaltenes with hot heptane to remove the remaining waxes. The rest of the procedures were the same as those described in Section 2.2.

Figure A1-1 shows the recovery percentage and the yields of the products of the pyrolysis of Gudao asphaltenes. The recovery was more than 100% likely due to reduced losses during solvent evaporation (i.e. lower yield of volatile compounds) as well as residual solvent used to separate the coke from the remaining toluene soluble materials. The coke and liquid yields (56.9% and 42.8%, respectively) were fairly higher than those of the other asphaltenes, as shown in Figure 2-1. On the contrary, the gas yield was lower (0.3% methane). These values suggest that the Gudao asphaltenes have structural differences with the other studied asphaltenes in terms of the yield of certain types of fragments. The same point is seen in the boiling curve of the products of reaction (Figure A1-2).

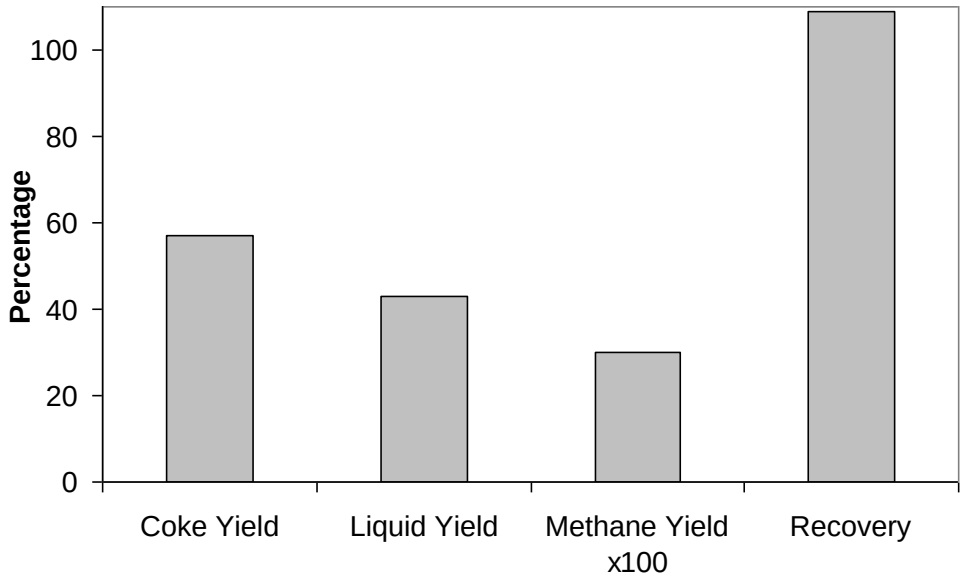

Figure A1-1. Recovery % and the yield of pyrolysis product of Gudao C_7 asphaltenes

While the observed offset in the boiling curve depicts the different size distribution of the product molecules, the chromatogram used to calculate the simulated boiling curves of this figure shows the differences in more detail (Figure A1-3). The chromatogram shows that, in contrast to the Cold Lake asphaltenes which showed a trend more similar to the typical trend in the other cases studied, the height of the two humps resembling a bimodal distribution of the products are relatively equal. Hence the resulting calculated boiling curve of the Gudao asphaltenes was linear for the most part (Figure A1-2). The other important feature of the chromatogram is the higher amount of homologous alkane/alkene series. This observation suggests the waxy nature of this crude apparently extends to the asphaltenes, i.e. the Gudao asphaltenes are richer in long alkane side chains than the other asphaltenes.

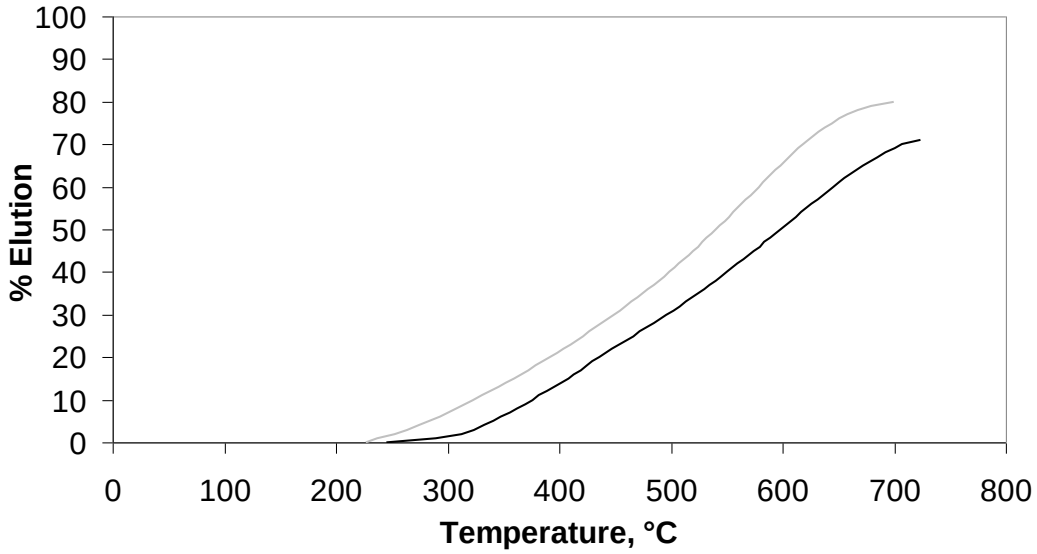

Figure A1-2. Comparison of the simulated distillation boiling curves of the liquid products of the pyrolysis of Gudao (black) and Cold Lake (grey) C_7 asphaltenes

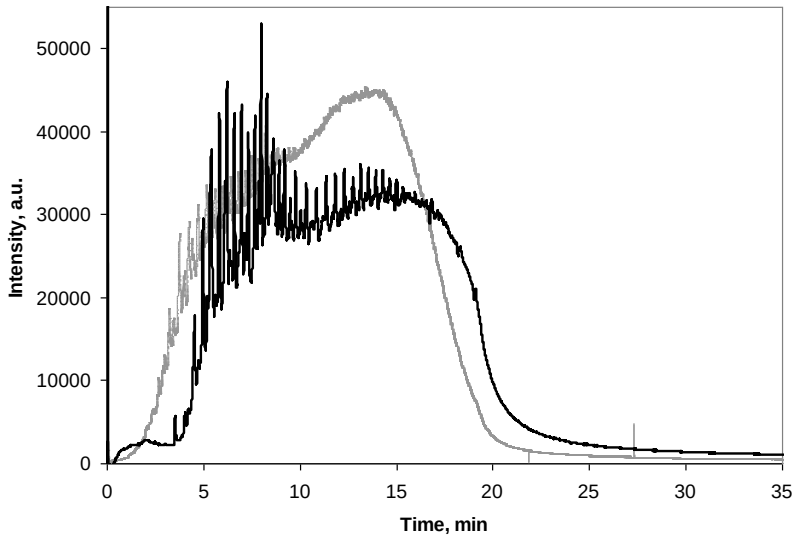

Figure A1-3. Comparison of the GC-FID chromatograms of the liquid products of the pyrolysis of Gudao (black) and Cold Lake (grey) C_7 asphaltenes

Nevertheless, the broad range of the thermal cracking products of the Gudao crude asphaltenes suggests that the archipelago-type structures do exist abundantly in this sample as in the other samples.

Appendix 2: Modified shrinking core model for catalytic gasification of coke

As was mentioned before, it was observed that a portion of the catalyst penetrated into the coke upon heating. Therefore, as the gasification reaction proceeds and the coke particle is consumed, the portion of the catalyst trapped in the consumed coke will be exposed. This amount of the catalyst which was previously inaccessible to the steam will then become available and participate in the reaction. Therefore, the reaction is expected to experience acceleration due to this factor, which was unaccounted for in the previous form of the shrinking core model discussed in Section 4.3.7. The model assumes that the entire catalyst is on the surface of the coke particle. This assumption is valid only at higher initial catalyst loadings where either:

- the fraction of the catalyst penetrated into the coke particle compared to the amount remaining on the surface is negligible, or
- the acceleration of the reaction due to the increased surface concentration by the gradual exposure of the penetrated catalyst is negligible.

However, at low initial catalyst loadings the ratio of the penetrated portion of the catalyst to the remaining portion can be significant even at higher conversions when the surface loading naturally increases due the decreased total surface area of the particles as they shrink. Thus, an acceleration of the reaction is

clearly observed in this case (Figure 4-7). Therefore, a modified version of the model will be provided in this section, which will consider a correction to take the gradual liberation of the penetrated catalyst into account.

In order to consider the penetrated portion of the catalyst loading it is necessary to apply a correction to the surface loadings, since the initial surface loading will be less without the assumption of negligible penetration:

$$w_0' = w_0 - w_{p0} \tag{A2-1}$$

w_{p0} is the initial surface loading of the catalyst (mol cation/m^2) which is lost due to penetration. The corrected instantaneous surface loading at any given conversion with the consideration of the gradual release of the penetrated catalyst can then be calculated as:

$$w'(X) = (w_0' + w_{p0} \cdot X) \cdot y(X) = (w_0 + w_{p0} \cdot (X - 1)) \cdot y(X) \tag{A2-2}$$

The above equation assumes that there is a uniform concentration of the catalyst in the coke (Figure 4-8) and therefore, the amount of catalyst released to the surface is proportional to the conversion of the coke (hence the term $w_{p0} \cdot X$). $y(X)$ is calculated the same way as in Chapter 4 (Equation (4.3-5)). The corrected surface loading ($w'(X)$) can then be used to look up the rate value in the initial rate (r_0) vs. corrected surface loading (w'_0) data by interpolation and extrapolation between the data points as necessary. The value of w_{p0} which is necessary for these calculations should be obtained either by a proper method of measurement or numerically by minimizing the difference between the measured and calculated rates (i.e. minimizing the sum of squared residuals - SSR).

Figure A2-1 shows an example of the application of the modified model for a case of low initial catalyst loading (0.6 mol K/kg sample = 0.013 mol K/m^2). As the graph suggests, the original model under predicts the rates at moderate conversions. The modified model, however, makes a better fit in this range of conversions (30-75%). At higher conversions the difference between the two models diminishes as the significance of the release of the penetrated catalyst species gets smaller compared to the large amount of catalyst available on the surface. However, both models over predict the rate at final conversions, as the severe mass transfer limitation due to the congestion of the surface of the remaining tiny coke particles with the catalyst has not been accounted for. Also, between ca. 77% and 93% of conversion, the rate measurement was disturbed due to fluctuations in the measured mass losses making the calculation of derivatives inaccurate. The optimum value of w_{p0} obtained arithmetically for this experiment, by minimizing the SSR of the rates over the moderate conversions, was 0.019 mol K/m^2 = 0.9 mol K/kg. However, since this value is higher than the initial catalyst loading, for the calculated rates illustrated in Figure A2-1 a value of $w_{p0} = w_0 =$ 0.013 mol K/m^2 was used.

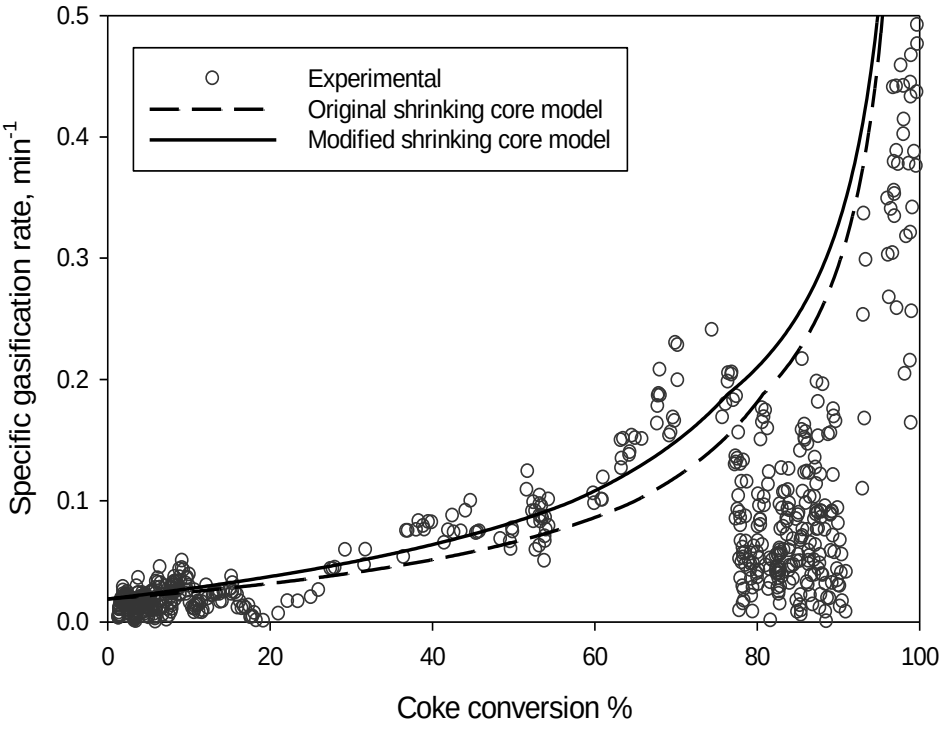

Figure A2-1. Comparison of measured and calculated gasification rates at 750°C and p_{H2O} = 0.77 atm with respect to coke conversion for an initial catalyst loading of 0.6 mol K/kg and initial particle size range of 53-90 µm using the modified shrinking core model.

Appendix 3: Additional analysis of the interactions of potassium and coke by XPS and SIMS

In order to achieve a better understanding of the interactions of potassium with coke, a series of qualitative analyses were performed using an Axis 165 X-ray Photoelectron Spectrometer (Kratos Analytical) with a monochromatic Al source. Three coke samples were tested as follows:

- Sample 1: Cold Lake Coke (Devolatilized at 600°C for 15 min)
- Sample 2: Cold Lake Coke admixed with K_2CO_3 and heated at 600°C for 15 min and washed with deionized water
- Sample 3: Cold Lake Coke admixed with K_2CO_3 and heated at 600°C for 15 min

The samples were not ground into powder to assist with the surface analysis. The obtained XPS spectra are illustrated in Figures A3-1 to 4. Table A3-1 summarized the major identified peaks. Some of the concentration profiles obtained from the SIMS analysis performed on Sample 3 as described in Section 4.2.4 are shown in Figure A3-5.

The relative peak heights of oxygen and carbon in the samples in Figure A3-1 show that, as expected, the addition of K_2CO_3 increases the oxygen content of the sample significantly due to the oxygen content of the carbonate (c.f. Samples 1 and 3). Although much of the oxygen is removed from the sample after washing, the surface of the washed sample still contains a considerable amount of

oxygen (Sample 2). The oxygen content of the fresh surfaces evolved after etching the sample with an argon beam showed little oxygen corresponding to low oxygen content in the coke particle away from the surface. This is consistent with the SIMS profile for oxygen shown in Figure A3-5.

The formation of oxygenated functional groups on the surface as seen in Figure A3-2 as well as Figure A3-3 is consistent with the mechanisms of catalytic gasification proposed in the literature that consider the oxygenated groups as a requirement for the catalytic activity. Another indication of this matter is the activity pattern of KCl, as reported in this study earlier (see Section 3.3.1).

The behavior of sulfur species is another noteworthy point. The SIMS profiles of the sulfur species indicate that their concentration is considerably high at the surface. As the sulfur is expected to be uniformly distributed within the coke particles, its elevated concentration on and near the surface in the sample heated with K_2CO_3, together with the monotonously decreasing trend of the concentration with increasing distance from the surface, resembles some form of migration of the sulfur to the surface. On the other hand, formation of sulfates on the surface of Sample 3 is evident from the XPS spectra (Figure A3-3 and Figure A3-4). This is consistent with the SIMS concentration profile of oxygen-bearing sulfur species in Figure A3-5. This was previously suggested by another study (Wood and Sancier, 1984). Alkali metal sulfates, however, are also known to be active for gasification (ibid). Therefore, the high sulfur content of bitumen coke does not appear to be a threat for the catalytic activity of alkali metal compounds.

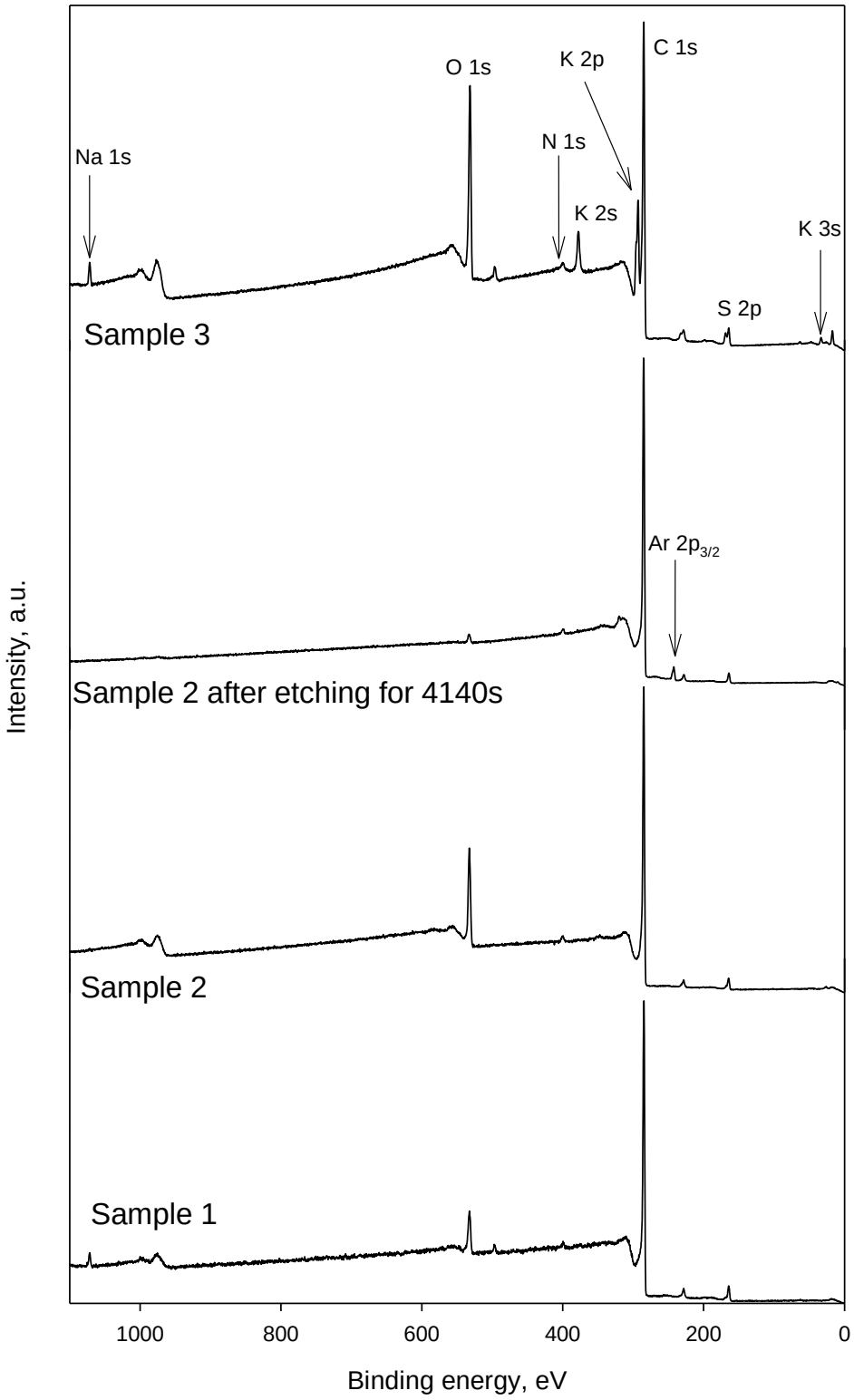

Figure A3-1. XPS overall survey spectra of the coke samples

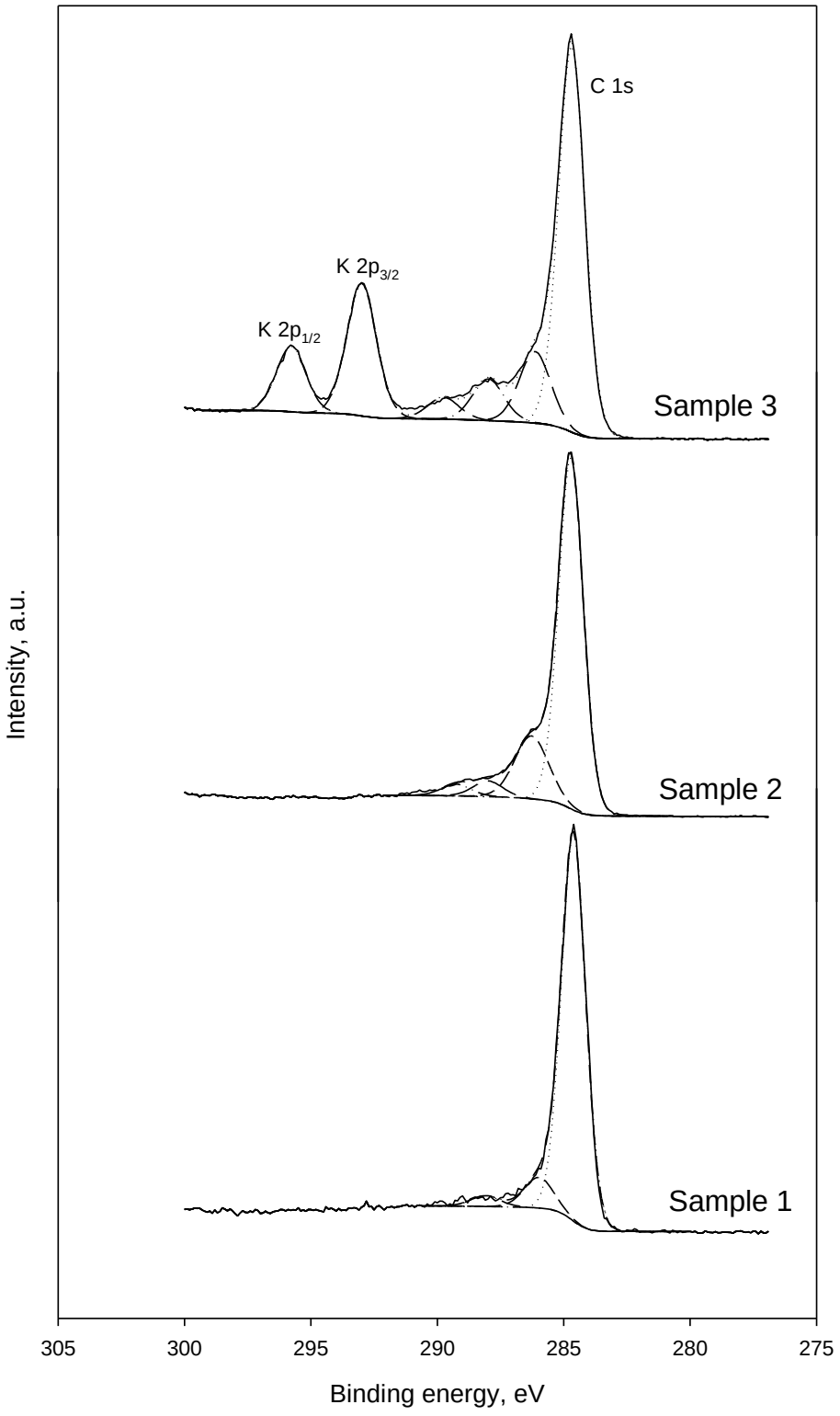

Figure A3-2. High resolution XPS spectra of the coke samples featuring C 1s and K 2p peaks. Dotted and dashed lines denote the deconvoluted curves.

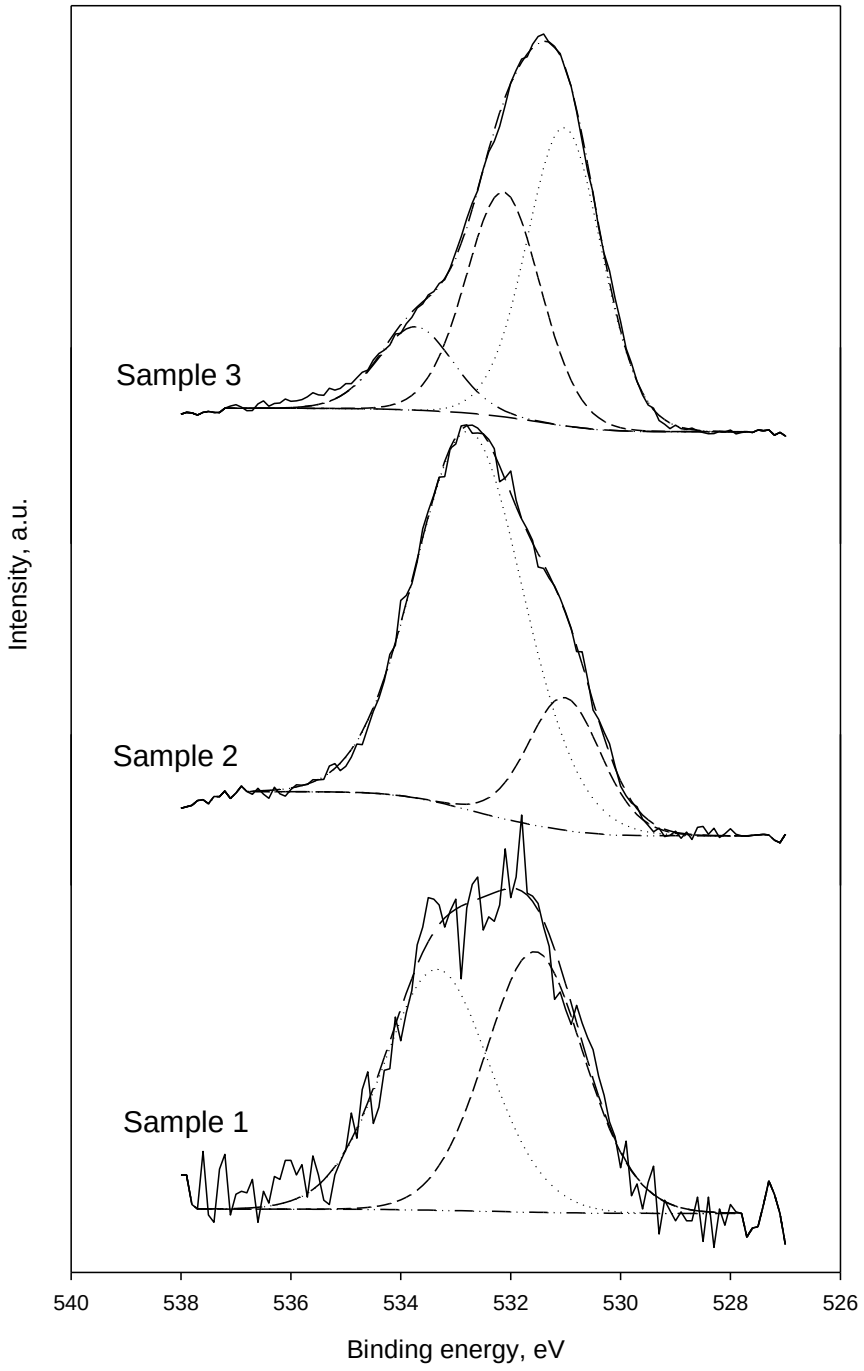

Figure A3-3. High resolution XPS spectra of the coke samples featuring O 1s peaks. Dotted and dashed lines denote the deconvoluted curves. Peak heights do not reflect quantities (use C:O peak ratios from Figure A3-1 for quantities).

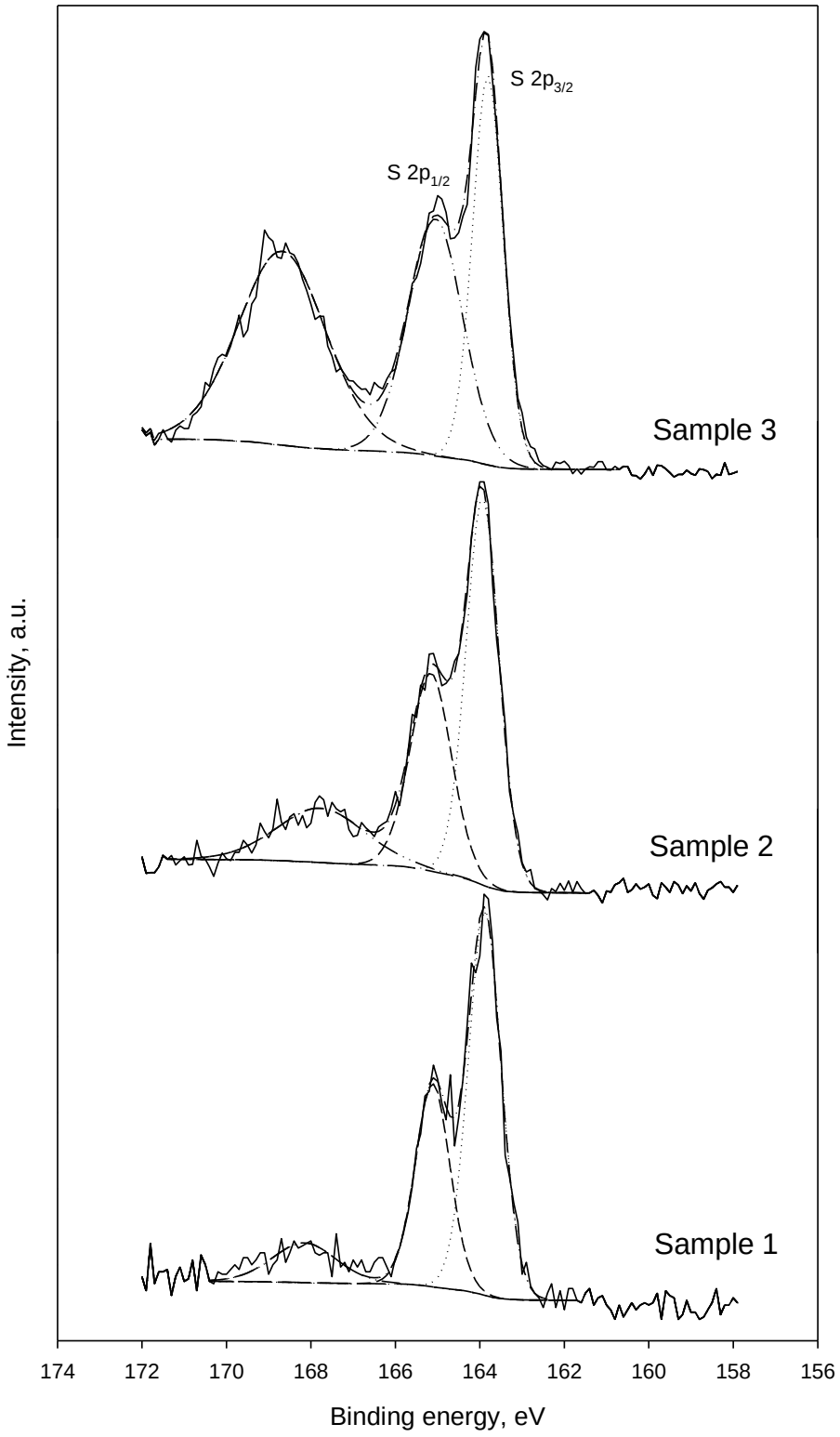

Figure A3-4. High resolution XPS spectra of the coke samples featuring S 2p peaks. Dotted and dashed lines denote the deconvoluted curves.

Table A3-1. Identification of the major peaks from the XPS spectra

Sample	B.E. (eV)	Assignment	Most probable type	Ref
1	163.9	S 2p3/2	Sulfide/Thiophenic	1
1	165.1	S 2p1/2	Sulfide/Thiophenic	1
1	168.2	S 2p	Sulfates/Sulfones	1
1	284.6	C 1s	C-C bonds	2
1	286.0	C 1s	Aliphatic/Oxygenated functional groups	2
1	288.1	C 1s	Oxygenated functional groups in polymers	2
1	531.6	O 1s	Oxygenated functional groups in polymers, Al2O3, etc.	2
1	533.3	O 1s	Oxygenated functional groups in polymers, SiO2, etc.	2
2	163.9	S 2p3/2	Sulfide/Thiophenic	1
2	165.2	S 2p1/2	Sulfide/Thiophenic	1
2	167.8	S 2p	Sulfates/Sulfones	1
2	284.7	C 1s	C-C bonds	2
2	286.3	C 1s	Aliphatic/Oxygenated functional groups	2
2	288.0	C 1s	Oxygenated functional groups in polymers	2
2	289.3	C 1s	Carbonates/Carboxylic	1
2	531.0	O 1s	Carbonates/Hydroxides	1
2	532.8	O 1s	Sulfates	1
3	163.8	S 2p3/2	Sulfide/Thiophenic	1
3	165.1	S 2p1/2	Sulfide/Thiophenic	1
3	168.7	S 2p	Sulfates/Sulfones	1
3	284.7	C 1s	C-C bonds	2
3	286.1	C 1s	Aliphatic/Oxygenated functional groups	2
3	288.0	C 1s	Oxygenated functional groups in polymers	2
3	289.8	C 1s	Carbonates/Carboxylic	1&2
3	293.0	K 2p3/2	Oxydized K (non-metalic/not intercalated)	1&2
3	295.8	K 2p1/2	Oxydized K (non-metalic/not intercalated)	1&2
3	377.8	K 2s	Oxydized K (non-metalic)	1&2
3	531.0	O 1s	Carbonates/Hydroxides	1
3	532.1	O 1s	Sulfates	1
3	533.7	O 1s	Oxygenated functional groups in polymers	2

References: 1. Moulder, J. F.; Stickle, W. F.; Sobol, P. E.; Bomben K. D. Handbook of X- ray Photoelectron Spectroscopy, Eden Prairie, MN:Perkin-Elmer Co. (1992).
2. Wagner, C. D.; Naumkin, A. V.; Kraut-Vass, A.; Allison, J. W.; Powell, C. J.; Rumble Jr., J. R. NIST X-ray Photoelectron Spectroscopy Standard Reference Database, Version 3.5. Accessed online from: http://srdata.nist.gov/xps on 17/4/2009.

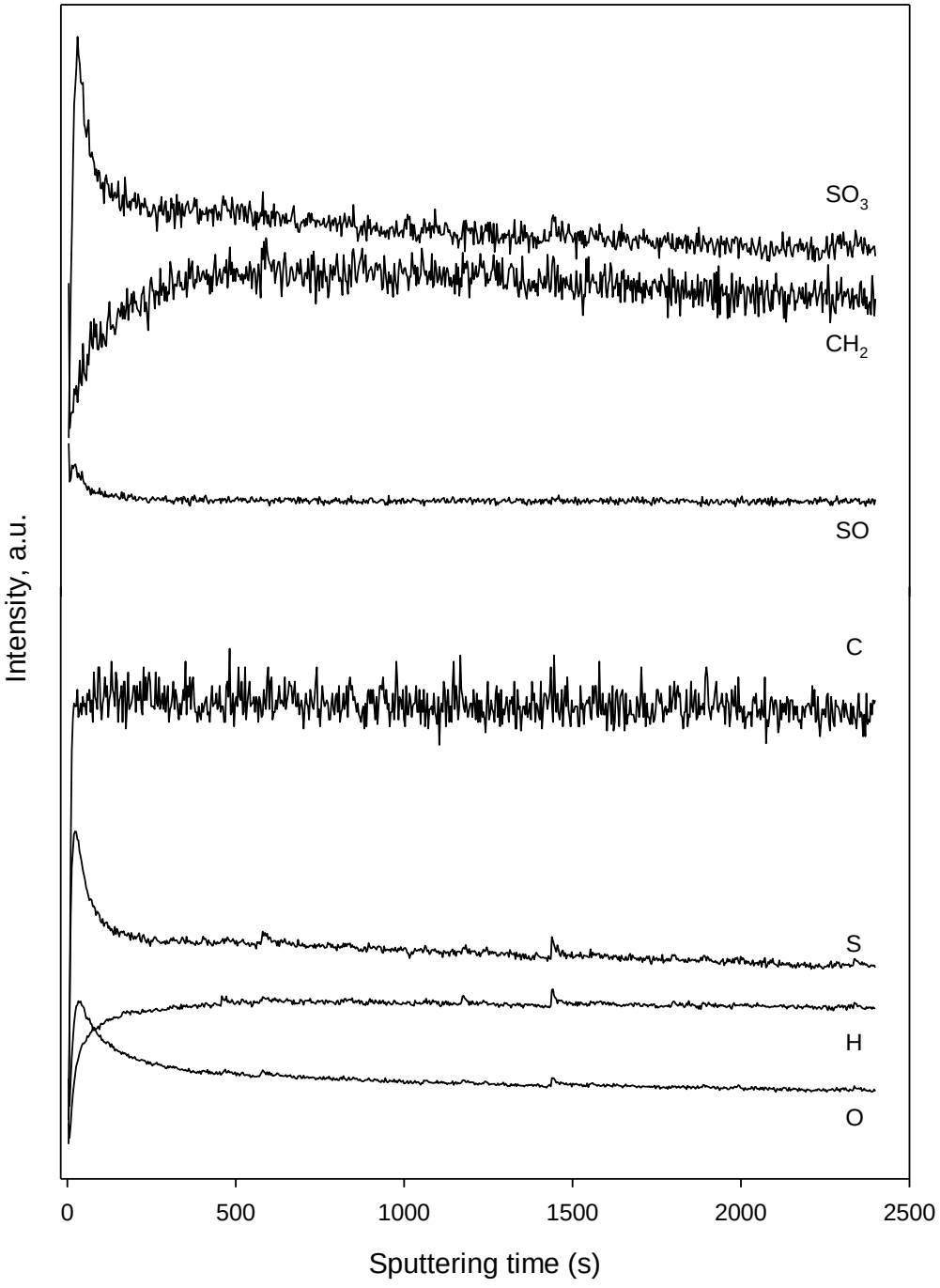

Figure A3-5. Depth profiles of various secondary ions by ToF-SIMS.